GRAPHENE OXIDE FUNCTIONALIZATION AS FRICTION MODIFIER ADDITIVES FOR LUBE OIL

NURUL ATHIRAH BINTI ISMAIL

INSTITUTE OF GRADUATE STUDIES
UNIVERSITY OF MALAYA
KUALA LUMPUR

2017

GRAPHENE OXIDE FUNCTIONALIZATION AS FRICTION MODIFIER ADDITIVES FOR LUBE OIL

NURUL ATHIRAH BINTI ISMAIL

DISSERTATION SUBMITTED IN FULFILMENT OF THE REQUIREMENTS FOR THE DEGREE OF MASTER OF PHILOSOPHY

INSTITUTE OF GRADUATE STUDIES
UNIVERSITY OF MALAYA
KUALA LUMPUR

2017

UNIVERSITY OF MALAYA

ORIGINAL LITERARY WORK DECLARATION

Name of Candidate: NURUL ATHIRAH BINTI ISMAIL

Matric No: HGA140022

Name of Degree: Master of Philosophy

Title of Dissertation ("this Work"): Graphene Oxide Functionalization as Friction Modifier Additives for Lube Oil

Field of Study: Chemistry

I do solemnly and sincerely declare that:

(1) I am the sole author/writer of this Work;
(2) This Work is original;
(3) Any use of any work in which copyright exists was done by way of fair dealing and for permitted purposes and any excerpt or extract from, or reference to or reproduction of any copyright work has been disclosed expressly and sufficiently and the title of the Work and its authorship have been acknowledged in this Work;
(4) I do not have any actual knowledge nor do I ought reasonably to know that the making of this work constitutes an infringement of any copyright work;
(5) I hereby assign all and every rights in the copyright to this Work to the University of Malaya ("UM"), who henceforth shall be owner of the copyright in this Work and that any reproduction or use in any form or by any means whatsoever is prohibited without the written consent of UM having been first had and obtained;
(6) I am fully aware that if in the course of making this Work I have infringed any copyright whether intentionally or otherwise, I may be subject to legal action or any other action as may be determined by UM.

Candidate's Signature Date: 19 June 2017

Subscribed and solemnly declared before,

Witness's Signature Date: 20 June 2017

Name:

Designation:

ABSTRACT

Nowadays, increasing transportation activities have consumed much of our energy resources day by day, and a significant portion of the energy produced is spent on overcoming friction in moving mechanical systems. Lubricant additive is one of the technologies that can be used to reduce friction. Therefore, it is expected that the demand and consumption of additives will increase. To lubricate moving mechanical systems, lube oil is required. However, base oil itself is not good enough to act as a lubricant in reducing friction. Addition of additives to base oil are required to provide excellent lubrication. The modification of graphene oxide (GO) as a friction modifier additive is proposed to improve lube oil lubrication in moving mechanical systems. In recent studies, graphene is indicated as a two-dimensional material which offer unique friction and wear properties that are not typically seen in conventional materials. According to its structure, GO consists of several oxygen functional groups. In general, the hydroxyl (OH) group can be found on the surface of GO and carboxylic (COOH) group found at the edges. However, inorganic nanoparticles can agglomerate easily, hence their dispersive ability is very poor in organic solvents and oil. The agglomeration of GO in the base oil will occur especially at high temperatures. Therefore, various chemical modifications of GO has been studied, to change its surface properties in order to have a well-dispersed GO in the base oil. The introduction of organic moiety on the surface of the GO is expected to increase its dispersibility in oil. Therefore, this study focuses on the synthesis of GO materials through the oxidation of graphite powder. This step was continued with the functionalization of GO that has been carried out by introducing alkyne-functionalized GO, GO_f and azide-functionalized alkyl, N_3R via click chemistry as a dispersing agent. The modified GO was then introduced into base oil at different compositions. The

obtained reduced functionalized graphene oxide (rGO_f) materials were then further studied in terms of its properties as lubricating oil in moving mechanical systems.

ABSTRAK

Pada masa kini, peningkatan aktiviti pengangkutan telah menggunakan banyak sumber tenaga dari sehari ke sehari, dan sebahagian besar tenaga tersebut digunakan untuk mengatasi geseran di dalam sistem mekanikal yang bergerak. Untuk melincirkan sistem mekanikal yang bergerak, minyak pelincir diperlukan. Tetapi, minyak asas sendiri sebagai minyak pelincir tidak dapat memberikan kesan yang terbaik dalam mengurangkan geseran. Pengubahsuaian grafena oksida (GO) sebagai bahan tambahan anti-geseran dicadangkan untuk penambahbaikan sifat mekanikal minyak pelincir. Grafena adalah bahan 2-dimensi yang mempunyai sifat unik bagi geseran dan haus yang tidak dapat dilihat dalam bahan konvensional lain. Berdasarkan strukturnya, graphene oksida mempunyai beberapa kumpulan oksigen berfungsi. Secara am nya, kumpulan hidroksil (OH) boleh didapati di permukaan GO dan kumpulan karboksil (COOH) di bahagian tepi GO. Walaubagaimanapun, partikel tak organik akan bergumpal dengan mudah dan kebolehan untuk berselerak di dalam pelarut organik dan minyak sangat lemah. Pengumpalan GO di dalam minyak asas berlaku terutamanya dalam suhu yang tinggi. Justeru itu, beberapa pengubahsuaian kimia terhadap GO diuji untuk mengubah permukaannya bagi mendapatkan GO yang boleh berselerak di dalam minyak asas dengan sangat baik. Pengenalan unsur organik di atas permukaan GO dijangka dapat meningkatkan kebolehannya untuk berselerak dengan baik di dalam minyak. Jadi, projek ini bermula dengan sintesis GO melalui pengoksidaan serbuk grafit untuk mendapatkan GO. Kemudiannya diteruskan dengan pemfungsian GO yang akan dilakukan dengan memasukkan kumpulan berfungsi alkuna ke dalam GO dan kumpulan berfungsi azida ke dalam alkil melalui ‘kimia klik’ sebagai ejen penyelerakkan. GO yang telah diubahsuai akan dimasukkan ke dalam minyak asas dengan komposisi yang berbeza. Bahan GO yang telah diubahsuai ini akan diuji dalam aspek sifatnya di dalam minyak pelincir untuk sistem mekanikal yang bergerak.

ACKNOWLEDGEMENTS

Firstly, Alhamdulillah and thank you to Allah Almighty for giving me the ability and strength to complete this thesis, despite the many problems faced throughout the period of this study.

My sincere gratitude goes to my supervisor, Dr. Samira Bagheri for her constant guidance, valuable advice, precious understanding, and inspiration throughout the progress of this project. Without direct support and persistent involvement from her, the completion of this research and dissertation would not have been an easy task.

I am also indebted to my late supervisor, Allahyarhamah Prof Dr. Sharifah Bee Abd Hamid, for her guidance, support, and constant encouragement. Her constructive advice and suggestion have contributed to the success of this research. May her soul rest in peace - Al-Fatihah.

Much gratitude and warm thanks to Dr. Tammar Hussein Ali for his mentorship during his short time at NANOCAT. My appreciation also goes to all members of NANOCAT for their continuous assistance and guidance during this study. Most importantly, I would like to greatly acknowledge my colleagues and lab-mates, who gave me a great deal of inspiration and support throughout my entire studies.

I wish to express my special thanks to my beloved parents, Ismail bin Abd Karim and Rosita Anom binti A. Ishak for their love, prayers and unconditional support. Also to my siblings, I am very grateful for your continuous prayer and unflinching support. I love you all.

Last but not least, I wish to thank the financial support from University of Malaya Grand Challenge Grant (Grant No. GC001A-14AET) and University of Malaya

Postgraduate Research Grant (Grant No. PG058-2015B). Moreover, I would like to convey my thanks to the Ministry of Higher Education Malaysia for providing me with the MyMaster fund.

TABLE OF CONTENTS

LIST OF FIGURES

LIST OF TABLES

LIST OF SYMBOLS AND ABBREVIATIONS

GO	:	Graphene Oxide
OH	:	Hydroxyl
COOH	:	Carboxyl
FTIR	:	Fourier Transform Infrared
XRD	:	X-Ray Diffraction
TGA	:	Thermal Gravimetric Analysis
FESEM	:	Field Emission Scanning Electron Microscopy
SEM	:	Scanning Electron Microscopy
KF	:	Karl Fischer
RPVOT	:	Rotating Pressure Vessel Oxidation Test
GO_f	:	Alkyne-functionalized GO
rGO_f	:	Reduced-functionalized GO
FM	:	Friction Modifier
MWCNT	:	Multi-Walled Carbon Nanotube
RuAAC	:	Ruthenium Alkyne-Azide Cycloaddition
EDX	:	Electron Dispersive X-ray
DiPPOH	:	2,2-dipropargyl-1,3-propanediol
WSD	:	Wear Scar Diameter
CoF	:	Coefficient of Friction
VI	:	Viscosity Index
wt. %	:	Weight percentage
DiMDiPM	:	2,2-di(propynyl)malonate
0D	:	Zero-Dimensional
2D	:	Two-Dimensional

3D	:	Three-Dimensional
SAE	:	Society of Automotive Engineers
ZDDP	:	Zinc Dithiophosphate
TPa	:	Terapascal
GPa	:	Gigapascal
CCD	:	Charge-Coupled Device
NO_x	:	Nitrogen Oxide
O_2	:	Oxygen
HGO	:	Graphene Oxide by Hummers' method
HGO+	:	Graphene Oxide by Hummers' method with excess $KMnO_4$
IGO	:	Graphene Oxide by improved method
WP	:	Wear Preventative
EP	:	Extreme Pressure
C6	:	Six Carbon length
C8	:	Eight Carbon length
C10	:	Ten Carbon length
C12	:	Twelve Carbon length
ASTM	:	American Society for Testing and Materials
ppm	:	Parts-per-million
GONRs	:	Graphene Oxide Nanoribbons

LIST OF APPENDICES

CHAPTER 1: INTRODUCTION

1.1 Introduction and Overview

This chapter includes the introduction and background of graphene and its potential excellent properties as a lubricant additive, as well as the problem statement in which the study is concerned about. The objectives and scope of the study, together with the organisation of the thesis is also included in this chapter.

1.2 Research Background

Graphene is a unique (two-dimensional) 2D material with incredible electronic, thermal, optical and mechanical properties. Graphene is one of the carbon allotropes and is described as a layer of carbon atoms in planar form, with densely packed and atomically smooth surface (Novoselov *et al.*, 2012). The C-C bond length in graphene is very small - about 0.142 nm - which leads to their extreme strength properties (Hummers Jr & Offeman, 1958). Graphene is inert to chemicals and has an easy shear capability (Y. Zhu *et al.*, 2010b). Because of their high load-bearing limit, high chemical steadiness, low surface energy, strong intramolecular and weak intermolecular bonding, nanocarbon materials have gotten incredible attention from tribology scientists. Graphene has also been the focus of enthusiasm in studies, because of its excellent properties and unique structure. (L Rapoport *et al.*, 2003b). Graphene has been tested and proven to be one of the strongest materials ever measured (Lee *et al.*, 2010). It has been shown to be impermeable to liquid and gasses (Bunch *et al.*, 2008), therefore, the oxidation reaction and corrosion process that can aggravate surfaces that rub together can be slowed down.

Few reviews on graphene in tribology and mechanical applications have been reported so far (Senatore *et al.*, 2013). Graphite (Wintterlin & Bocquet, 2009) and other graphite

derivatives (Ramanathan *et al.*, 2008) together have the desirable properties mentioned earlier. The properties of graphite nanosheets in tribology as lubricant additive has been studied by Lin et. al. (Lin *et al.*, 2011). In between layers of graphite, there is weak interatomic interactions, van der Waals forces and low shear stress (Bhushan & Gupta, 1991).

The properties of graphite as lubricant additive has been investigated and found to have some improvement in reduction of friction and wear when graphite or graphite derivatives were introduced into the base oil at optimum concentration (H. Huang *et al.*, 2006). Graphene oxide films with 2D structures were successfully prepared by the improved Hummers' method, through oxidation of graphite flakes (Hakimi & Alimard, 2012).

To prepare the GO, an improved Hummers' method is used as described by Marcano (Marcano *et al.*, 2010). The improved method is done by not including the $NaNO_3$ but increasing the amount of $KMnO_4$. Improvement in efficiency of the oxidation process was shown. When compared to the Hummers' method, the GO synthesised using the improved method is more hydrophilic and highly oxidised. When both GO produced by two different methods (improved method and conventional method) were reduced using hydrazine, these two GO still have the same value in electrical conductivity (Tour & Kosynkin, 2012).

One of the differences in the improved method compared to conventional Hummers' method is that it will not produce toxic gas, and the temperature of the reaction can be controlled easily (Marcano *et al.*, 2010). Hummers' method and its modified version are the methods commonly used for the oxidation of graphite (Niyogi *et al.*, 2006). The only difference between every single layer of GO and graphene is that the edges and sides of GO were decorated with oxygen-containing functional groups (Y. Zhu *et al.*, 2010b).

However, studies show that graphene platelets are a failure as an oil additive at higher temperatures, and it could be due to damaging of the protective film formed by the graphene at higher temperatures, and the significant increase in agglomerations within the lubricant (Senatore *et al.*, 2013). Therefore, the applications thus far are quite limited. Fortunately, some of the physical and chemical approaches can be used to solve the dispersion problem. The solution to this would be the addition of a dispersant that will reduce the agglomeration and improve the dispersive ability in the lubricant.

In order to prevent agglomeration and ensure the dispersion of GO in the base oil is good with high stability, the modification and functionalization can easily be done by taking advantage of the oxygen-containing functional groups, such as -OH and -COOH on the surfaces of GO. By attaching long hydrocarbon chain compounds at the -OH or -COOH groups on the surfaces or edges of the GO, it will enhance dispersion in non-polar solvents (Lin *et al.*, 2011). On the other hand, the polarity of the GO can be enhanced through functionalization by attaching any polar group at the -OH and -COOH on the surface of the GO (W. Zhang *et al.*, 2011). To enhance the dispersion stability of the additive in any oil, the additive must have a long hydrocarbon tail that will keep it dispersing in the oil, and a polar head that will help keep the additive attached and lined up on metal surfaces (Senatore *et al.*, 2013).

By taking advantage of the oxygen-containing functional groups in GO, the functionalization of GO was carried out via click chemistry. Click chemistry is a very simple reaction that can be performed in any easily removable solvents. It can also be described as a reaction that is stereospecific and high yielding, and their resultant by-products can easily be removed without chromatography (Xiao *et al.*, 2014).

Therefore, in this study, the focus is on the functionalization of the GO using a dispersing agent to increase its stability in lubricant oil, to provide an advantage to its properties for internal combustion engines.

1.3 Problem Statement

The current issue with transportation activities is that much of the energy produced is used to overcome friction in moving mechanical systems (Kenneth Holmberg & Erdemir, 2011). Thus, the use of lube oil to reduce friction in moving mechanical systems is increasing. Graphene is suitable for use as a contact finish treatment because it exhibits unique properties where it can still reduce friction and is stable even in harsh environments such as high temperatures (Berman *et al.*, 2014). However, aggregation of particles in their composite matrix will occur due to its strong van der Waals force among its layers, and due to its large surface area. Unfortunately, the maximum improvement in its final properties can only be obtained when it is homogeneously dispersed and is stable in its dispersion matrix (Senatore *et al.*, 2013).

To get stable dispersions of graphene in its dispersion matrix, covalent functionalization of graphene oxide can be done. Because of its multiple oxygen-containing functional groups on the surface and edge of GO sheets, GO is chosen as the main precursor to carrying out the functionalization or modification of graphene. The covalent functionalization of GO will be based on the reaction between the oxygen-containing functional groups on the surfaces and edges of GO, with functional groups of other compounds (Zheng *et al.*, 2013).

1.4 Objectives

The objectives of this study are as listed below:

i. To synthesise and characterise graphene oxide, GO by using an improved Hummers' method.

ii. To functionalize graphene oxide, GO with organic moiety via click chemistry by Cu-Catalyzed Azide-Alkyne Cycloaddition (CuAAC) to have high dispersibility in oil.

iii. To demonstrate the effects of the reduced-functionalized graphene oxide, rGO_f, on the properties of lube oil.

1.5 Research Scope

This study can be divided into three stages, namely the synthesis of highly-oxidised GO, functionalization of GO and properties test of oil loaded with functionalized GO. The highly oxidised GO was synthesised via improved Hummers' method. The synthesised GO was then characterised using Fourier Transform Infrared (FTIR), Raman, X-ray Diffraction (XRD), Thermal Gravimetric Analysis (TGA), Field Emission Scanning Electron Microscope (FESEM) and Boehm titration.

Covalent functionalization of GO was carried out via click chemistry. It involved three major steps: the first is to synthesise alkyne-functionalized graphene oxide by introducing alkyne functionalities on the surface of GO. The second, to synthesise azide-functionalized alkyl. And the third, to perform the click coupling by CuAAC method between the alkyne-functionalized GO and azide-functionalized alkyl to obtain the final product: reduced functionalized GO, rGO_f. Both alkyne-functionalized GO and azide-functionalized GO were characterised using FTIR to prove the presence of expected functional groups. The rGO_f was characterised using FTIR, Raman, XRD, TGA and FESEM/EDX.

To investigate the improved properties when rGO_f was loaded into base oil, a blending process was carried out. By varying the weight percentage, wt. % of rGO_f in the base oil, its improvement in dispersibility was measured by UV-visible and a simple dispersion test. And lastly, its improvement in properties of lube oil was carried out using four-ball test, Scanning Electron Microscope (SEM), viscometer, Karl Fischer (KF) and Rotating Pressure Vessel Oxidation Test (RPVOT).

1.6 Organisation of Dissertation

This dissertation is structured into five respective chapters.

Chapter 1

Introduction and general review of the project, including problem statement, research motivation and objectives of the study.

Chapter 2

Highlights the literature review and research background of fuel consumption issues with respect to friction in moving mechanical system problems, reducing friction using lubricant, friction modifier additives, graphene as additives and functionalization of graphene oxide.

Chapter 3

Describes the materials and methodology on the synthesis of highly-oxidised graphene oxide, functionalization of graphene oxide and preparation of lube oil by blending, followed by lube oil properties test.

Chapter 4

Discusses the characterisation of synthesised GO and functionalized GO, followed by the improved properties of lube oil.

Chapter 5

Summarises overall results by answering the objectives of the study and recommendations for future research related to this study.

CHAPTER 2: LITERATURE REVIEW

2.1 Introduction

Fuel economy can be simply described as the reduction in fuel consumption. Fuel economy is one of the major factors that speeds up research in the formulation of lubricant and lubricant additives. An increase in combustion efficiency and friction reduction in the transmission and engine can lead to fuel economy (Kenneth Holmberg *et al.*, 2012). An increase in transportation activities has consumed significant portions of our energy resources. And most of the energy produced is used to overcome friction in moving mechanical systems (Kenneth Holmberg & Erdemir, 2011).

2.1.1 Friction in moving mechanical systems

Friction can result in both advantageous and disadvantageous ways. The presence of friction is required when driving and braking cars on the road. However, in the context of lubrication and tribology, friction is an unwanted phenomenon that occurs when close contact of surfaces occurs in relative motion (Berman *et al.*, 2014). Tribology is defined as the science related to lubrication, including friction and wear. The understanding of friction was developed a long time ago and has taken a long time to be understood (Meurant, 2009). Aristotle had acknowledged frictional forces, and the first person to study them scientifically was Leonardo Da Vinci in 1470 (Haycock *et al.*, 2004).

Even when a surface is carefully prepared, there is no such thing as a completely smooth surface. When compared to molecular dimensions, the surface will be seen as a surface containing large hills and valleys. The solid surfaces will slide on the peaks and the sliding contact area is very small (Buckley, 1981). Plastic deformation will take place at the exposed peaks and until the area of the sliding contact is large enough to support

the load applied (Bowden & Tabor, 2001). When sliding occurs, the friction will increase from the small contact area on the peaks. As a result, microstructural changes to the surfaces and local melting will occur, due to the rise in large surface temperatures at the rubbing contacts (Dwivedi, 2010). Adhesion will occur at the contact points and they are attached together. The shear stress of these junctions is described as the frictional force experienced, and it is proportional to the applied load (Bowden & Tabor, 2001). In Equation 2.1, the frictional force is described as the energy needed to shear the asperities and attached the place of activity for metal-to-metal friction (Bovington, 1997; Tabor, 1981).

$$\boldsymbol{F_1 = F_A + F_P} \qquad \textbf{(Equation 2.1)}$$

Where

F_A = The force required to shear the junctions = A_c*S

A_c = The contact area includes the elasticity of the surface,

S = The effective shear stress of the junction,

F_P = The force needed to shift the softer metal of the two.

To calculate the friction, F_P value can be excluded in most combinations of material, due to its significantly small value (Blau, 2001; Meyer *et al.*, 1998). Equation 2.2 described the friction coefficient, μ, as a dimensionless number.

$$\boldsymbol{\mu = \frac{F_1}{\omega} = \frac{F_A}{\omega} = \frac{S}{H}} \qquad \textbf{(Equation 2.2)}$$

Where

S = Shear strength

H = Effective surface hardness

ω = Applied load

From Equation 2.2, low friction can be generated by the material with low shear strength, S and high surface hardness, H. To have a low shear strength, the layers of the materials must be very thin. Therefore, low friction can be achieved if thin layers of materials with hard surfaces and low shear strength are used (K Holmberg *et al.*, 2000). The layers of the material must be very thin, in order not to increase the contact area, A_c (Crawford *et al.*, 1997).

2.1.2 Role of lubricants

A resistance is experienced when contact occurs between two surfaces that move in relative motion. This resistance exists in all machinery, especially moving systems, and it is called friction (Meurant, 2009). Lubricant can be placed at the interface of the two contact surfaces and lowering the friction and wear scar (McGraw-Hill, 2005).

The exact time when lubricant was consciously used is not known, but it has been used for the longest time as a friction reduction between contact surfaces. Around 1400 B.C., during a later period in Egypt, a wheel hub was discovered. Traces of both chalk and animal fats were found on the wheel hub (Feeny *et al.*, 1998). The finding suggests that some primitive grease was used on the wheel hub. The Industrial Revolution began in 1760, and large-scale machinery was developed during the era. Animal oils were used to lubricate this developed machinery that was based on iron and steel (Lawal *et al.*, 2012). During this period, distillation of coals to produce mineral oils also became available, and later, petroleum-based oils were found and have been used widely. In the 1920's, production of superior lubricants to replace animal oil began. Once internal combustion engines became common, the petroleum-based oil became very important and was developed widely (Haycock *et al.*, 2004).

Reduction of friction and wear are the primary functions of lubricant. Besides these, there are other functions that lubricants could fulfil (Mang & Dresel, 2007). Lubricant

can be a cooling, anti-corrosion, scaling, anti-oxidant and even a cleaning action. To develop a superior lubricant, it must fulfil some regulations to what an oil should not do. The oil must not be volatile, form foam, unstable to any chemical or radical attack and oxidation, produce deposits and any other destructive processes (Haycock *et al.*, 2004). Therefore, additives were developed to fulfil the requirements for the production of superior lubricants. Nowadays, all lubricants developed consists of base oil and a package of additives.

2.1.2.1 Base oil

Base oil can be classified by its origin, and its composition will be different depending on the sources (Sofer, 1984). For example, petroleum-based oil originated from crude petroleum. It is known that crude petroleum consists of a complex mixture of organic chemicals, or hydrocarbons. Therefore, petroleum-based oil is composed of organic chemicals and hydrocarbons. They also consist of small gaseous molecules, such as methane (Olah & Molnar, 2003). Most of the elements that were found in the base oil are undoubtedly desired to be produced as lubricant, but some are not. One of the undesirable components is sulphur, which will cause the oil to have low viscosity and flow easily. Some crude base oil also contains wax, which is undesirable because it will only flow when heated (Ohsol *et al.*, 1999).

The types of components such as an extensive variety of hydrocarbons and other organic particles in the oil does not define the crude, but their relative amounts (Tissot & Welte, 2013). A set of refining steps is utilised to isolate the good and bad components in the crude, and to tailor its properties, chemical reactions are carried out. Different types and grades of oil can be produced from different steps of refineries. And their viscosities and chemical properties also differ for specific desired applications (Prince, 1997).

2.1.2.2 Additives

Demand for lubricants is very high, especially for machinery with moving mechanical systems. For the moving parts in an engine, the lubricant used must be added with a package of additives to be able to function as a superior lubricant. The compatibility of one additive to other additives in the oil is very important for them to work efficiently together (Neville *et al.*, 2007). The list of different additives available and their functions are shown in Table 2.1 below:

Table 2.1: List of additives with their respective functions

Additive	Function
Detergent and dispersant	Prevents sludge deposits and suspend soot contaminant
Anti-oxidant	Reduces or prevent oxidation in the oil
Viscosity modifier	Maintains the oil's viscosity at high temperatures
Pour point depressant	Reduces the oil's viscosity at low temperatures
Anti-foam	Prevent foaming
Anti-corrosion	Reduces oxidation and prevents corrosion of metal
Anti-friction	Reduces the friction
Anti-wear	Prevents wear in the engine

(Rudnick, 2009)

Most of the additive classes – such as anti-corrosion, detergents, anti-oxidants, viscosity modifiers and depressants – emerged between 1930s and 1940s, due to the many problems that arise from the rapidly developing motor car industry (Spikes, 2004). As summarised in Table 2.1, different additives have different functions in the engine oil.

To prevent deposition of harmful carbon and sludge in the engine, the detergent and dispersant additives were used. Engine malfunction and shut-down will occur if certain

areas of the engine have deposit or sludge attached to it, which will lead to engine repair. The detergent and dispersant additives are also used to ensure proper oil flow is maintained by suppressing the deposits of carbon sludge and minimising oil thickening. The dispersants will suspend soot contaminants and at the same time, the detergents will keep deposits away and neutralise acids in engine (Colyer & Gergel, 1997).

Anti-oxidant additive is used to overcome problems arising from aging or degradation, which occurs due to exposed engine oil that undergoes oxidation reaction. The combustion chamber in the engine will generate blow-by gasses and the high temperature will result in the speeding up of the oxidation reaction. The engine oil is usually exposed to major destructive components such as free radicals, NO_x, O_2 and partially oxidised fuel (Rasberger, 1997).

Viscosity index improvers and thickeners are the other commonly used additives. Friction and wear will increase when the oils are non-viscous. At high temperatures, usually the viscous oils will thin out become non-viscous. Thus, the oils cannot keep the surfaces apart and result in high friction and wear. Therefore, it is important to use additives that will enhance the viscosity index and thickness, and these additives are mostly made out of polymers (Thong *et al.*, 2014).

When the engine is cold, especially during start-up conditions, it is very important for the engine to have the ability to flow. This is where additives that improve low-temperature characteristics are used, namely the pour depressant additives. Excessive wear will occur without the used pour point depressant (Rudnick, 2009).

Emulsions and foam may form in the engine oil. Therefore, the use of anti-foam additive is crucial, especially in high shear regime, to prevent blockage of oil channels and damages to effective lubrication by emulsions and foams. Usually, engine oil contains

corrosion inhibitors because the engine is also exposed to corrosion. General corrosion can be prevented by other types of additives, but for an electrochemical process, corrosion inhibitors are specifically needed (Crawford *et al.*, 1997). Therefore, a complex mixture of additives was added to the base oil to have a superior lubricant. The concentration of main additives added in commercial engine oils were shown in Table 2.2 (Pawlak, 2003).

Table 2.2: The weight percentage, wt. % of the additives in the engine oils

Material / Additive	**Weight percentage, wt. %**	**Material**	**Weight percentage, wt. %**
Mineral oil in SAE-40 or SAE-30 lubricants	71.5 - 96.2	Anti-oxidant Anti-wear	0.1 - 2.0
Metallic detergent	2.0 – 10.0	Friction modifier	0.1 - 3.0
Ashless detergent	1.0 – 9.0	Anti-foam agent	2.0 – 15.0
ZDDP (Anti-oxidant/anti-wear)	0.5 - 3.0	Pour point depressant	0.1 - 1.5

(Pawlak, 2003)

Different additives have different ways to be active in the base oil, either inside the oil or at the surface. The performance of the oil is significantly affected by the interaction between the additives with the base oil, and also the interaction between additives themselves (Mang & Dresel, 2007).

2.2 Reducing friction: Lubricant

2.2.1 Friction modifier additives

One of the most important additives that play a major role is the friction modifier additive. Anywhere where precise movement is required, friction modifier additives are used. Fuel saving has evolved into one of the greatest concern factors for all vehicles after

the Gulf crisis that happened in 1978. This crisis led to the need to introduce friction modifier additives in order to enhance fuel performance of the motor oil (Crawford *et al.*, 1997; Haycock *et al.*, 2004). The friction coefficient was reduced by the friction modifier additive, and this will result in better lubricity and energy efficiency (Ratoi *et al.*, 2014).

Friction modifier additives are attracted to metal surfaces. Therefore, they are significantly effective in boundary lubrication where metal-to-metal contact occurs (Jahanmir & Beltzer, 1986; Tung & McMillan, 2004). Usually, friction modifiers consist of large molecules decorated with long and straight hydrocarbon chains. Polar head groups are also one of the main requirements to be an effective friction modifier (Rudnick, 2009). Metal surfaces of the engine are covered in oxide, where the friction modifier will adsorb or chemically react. The hydrocarbon tail of the friction modifier will line up perpendicularly on the metal surfaces. The friction modifier can form either monolayer or multilayers on the surfaces. The layers in friction modifiers have only the ability to shear and not the ability to densify. The easy shear capability of the particles in friction modifiers allows for a slippery nature to the metal surfaces (Crawford *et al.*, 1997; Ratoi *et al.*, 2014).

2.2.2 Requirements for an effective friction modifier additive

There are two main requirements in order to be an effective organic friction modifier additive, the first is to have large molecules with a straight hydrocarbon tail containing ten or more C atoms, and the second is to have a polar group at one of the friction modifier ends. The polar head will help the friction modifier to attach themselves to the metal surfaces, and the hydrocarbon tail will help the friction modifier to keep dispersing in the oil and also provide a cushioning or spring-like effect to avoid contact between surfaces (Crawford *et al.*, 1997). When one of the surfaces comes into contact with another

surface, the molecules of the friction modifier can still provide a cushioning or a spring-like effect as long as the frictional contact is light.

Chemically, the required polar head of organic friction modifier additives can be one of the following groups (Crawford & Psaila, 1992):

- Carboxylic acids or its derivatives
- Amides, imides, amines or their derivatives
- Phosphoric acid or its derivatives

Organic friction modifiers can be classified by their method of process or type of friction modifier, as shown in Table 2.3. The mechanism of reduction in friction varies for each different mode of actions and category:

Table 2.3: Friction modifier types or method of process

Method of process / Type of friction modifier	**Products**
Formation of reacted layers	Saturated fatty acids, sulfur-containing fatty acids, phosphoric and thio-containing phosphoric acids
Formation of absorbed layers	Long-chain carboxylic acids, ethers, esters, amides, amines and imides
Formation of polymers	Partial complex esters, unsaturated fatty acids, methacrylates and sulfurized olefins
Mechanical types	Organic polymers

(Kenbeck & Bunemann, 2009)

2.2.3 Solid lubricant as friction modifier additives

Solid materials that are able to lower friction by avoiding mechanical interaction between metal surfaces and the load applied moving in relative motion can be considered as solid lubricants (Bowden & Tabor, 2001). Liquid additives will not be able to provide lubrication under some conditions. Therefore, the lubricant formulator provides an alternative by formulating solid materials as solid additives.

Unfortunately, the potential benefit of the friction modifier molecules will be brushed off when heavy frictional contact occurs. In conditions where Spot welds es are used, degradation and oxidation of liquid lubricant might happen, and it will result in lubrication failure. The liquid lubricant will no longer provide an advantage in lubrication (Stachowiak & Batchelor, 2013).

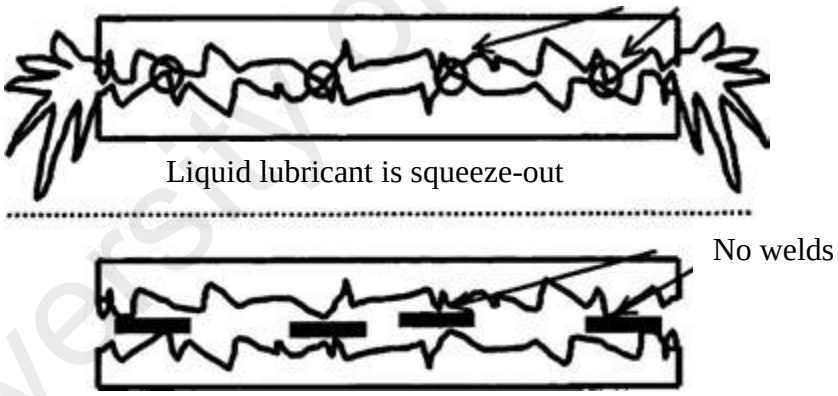

Figure 2.1: Contact under high load between mating surfaces cause a squeeze-out (Mariani, 2003)

Another example of a condition that will make liquid additives stop providing lubrication is when high loads are applied. The liquid lubricant will squeeze-out under high loads and results in lubricant starvation (Mariani, 2003). Figure 2.1 shows the comparison between liquid and solid lubricants when high loads are applied on mating surfaces.

Solid lubricant utilised either as film or powder in oil will give better lubricity in a wide range of applications. Ordinary applications that involve high temperatures incorporates oven chain lubrication and a metal deformation process (E. Braithwaite & Rowe, 1963). Solid lubricants are additionally useful for ambient-temperature applications and they are adequately utilised as a part of threading and anti-seize compounds, which gives a fixing capacity and a reduction of friction for threaded pipe assembly (Mariani, 2003). Solid lubricants are also advantageous for applications that require high contact loads and low sliding speeds. Especially in lower-viscosity base oils, the solid lubricant viably gives the required protection from wear and provides the load-bearing performance required from gear oil (Reeves *et al.*, 2013).

Solid lubricants can also assist with surfaces that come into contact which are of a harsh texture. Under these harsh or rough surfaces, the use of solid lubricants is better when compared to liquid lubricants, in order to cover the asperities on the contact surfaces (Reeves *et al.*, 2013). Lubrication to minimise wear is required for typical applications involving reciprocating motion. One of the applications that need solid lubricant is situations in which chemically active lubricant additives are unavailable for a specific surface. For this situation, a solid lubricant is able to give the required shield to the mating surfaces, that will ordinarily happen because of the response of a liquid component with the surface (Ludema, 1996).

Inorganic compounds are commonly used as solid additives. Their excellent tribological properties can be due to four mechanisms tabulated in Table 2.4 below:

Table 2.4: Mechanisms that makes inorganic compounds have excellent tribological properties

Mechanism	Description	References
Tribochemical responses	Surface protection film can be formed when the additive particles react with the surfaces in contact.	(G. Chen *et al.*, 2001) (Z. Hu *et al.*, 2000) (Zhao *et al.*, 2012)
Ball effect	Additive particles are able to roll in between the surfaces in contact and provide a pure sliding friction.	(Ouyang & Okada, 1994) (Tao *et al.*, 1996) (Tarasov *et al.*, 2002)
Mending effect	Particles can form a physical tribo-film by depositing themselves on the surface and compensates the mass loss of materials.	(G. Liu *et al.*, 2004) (L. Rapoport *et al.*, 2002)
Third body effect	Lowers the compress stress concentrations by bearing the compressive force depressively.	(L. Rapoport *et al.*, 2003a) (L. Rapoport *et al.*, 2002)

2.2.4 Requirements for an effective solid lubricant additive

To be an effective solid lubricant additive, there are five basic requirements that need to be met (Mariani, 2003).

The first requirement is yield strength. Yield strength is defined as the force required to deform the film of lubricant. High yield strength is required for forces applied perpendicular to the film of lubricant. Meanwhile, low yield strength is required for the film that is in the direction of sliding, for it to reduce the friction (Rudnick, 2009). This effect on the directional application of forces is described as an anisotropic property (Reeves *et al.*, 2013).

Secondly, the adhesion of lubricant to the substrate is also a requirement to be an effective solid lubricant additive. The film of lubricant must be maintained on the substrate for a certain necessary period for the purpose of lubrication (Rudnick, 2009). The adhesion force must be higher than the shear forces applied to the film. When any failure in adhesion to substrate occurs, a non-protective condition that results in sliding between surfaces will occur and increase friction due to poor lubrication (E. Braithwaite & Rowe, 1963).

The third requirement to be an effective solid lubricant additive is the cohesive properties. Each particle in the film of solid lubricant must be capable of forming a solid layer that can secure surfaces with high asperities and also act as a "reservoir" of lubricant for replenishment throughout the utilisation of the solid lubricant film (Kenbeck & Bunemann, 2009; Mariani, 2003).

The orientation of the particles in the lubricant is also considered to be the requirement to be an effective solid lubricant. The particles should be arranged in a way that they are parallel to the movement of the shear stress forces (Rudnick, 2009). The dimensions of

the particles must be greatest in the direction of low shear in order for them to be oriented (Reeves *et al.*, 2013).

Lastly, the lubricant must have resistance to plastic deformation. Plastic deformation might occur when the applied load is perpendicular to the direction of motion. The solid material that was used as the lubricant additive must have the ability to withstand close contact of mating surfaces in order to provide continuous lubrication (Mariani, 2003).

There are some criteria that need to be considered when selecting the solid material to be used as the optimal solid lubricant additive. Different criteria are preferred for different applications of solid lubricant (Campbell *et al.*, 1966; Kenbeck & Bunemann, 2009; Rudnick, 2009).

The first consideration is the service temperature for the application. This is the main criterion that should decide which solid lubricant can be used in its application. Generally, MoS_2 has the ability to carry higher loads when compared to graphite. However, MoS_2 will degrade at the service temperature above 400 °C, and upon its degradation, will lose the capability to provide lubrication. Therefore, for the applications with service temperature of above 400 °C, MoS_2 should be eliminated from consideration (Mang & Dresel, 2007; Rudnick, 2009).

Certain solid lubricants should be eliminated from consideration due to atmospheric restrictions since the second most important consideration is the environment. For example, the use of graphite as the solid lubricant will be eliminated from consideration in a vacuum environment (Hilton & Fleischauer, 1993). This is because, in order for graphite to provide an effective lubrication, they require water molecules to be adsorbed on its surface. In vacuum environment, graphite will not function as an effective lubricant. Contrarily, MoS_2, PTFE, and boron nitride do not require the presence of water molecules

to provide lubrication, thus they can be considered for use in a vacuum environment (Mariani, 2003).

The nature of the lubricant is the third criterion that needs to be considered. Its nature has crucial effects on its ability to be dispersed in liquids. They can exist either as a bonded solid lubricant film or as a liquid fortified with solid lubricant additives. For example, MoS_2 and graphite can be dispersed easily in liquid when compared to boron nitride and PTFE (Rudnick, 2009). This can be due to the ability of the particles to reduce the size, surface chemistry and surface energy of the solid lubricant additive. The performance of the lubricant on lubrication is influenced by the particle size. The optimisation of the particle size distribution for application should be done. For applications that involve slow speed and substrates with coarse surface roughness, better performance can be seen with solid lubricants with larger particles. However, when the application has high speeds together with constant motion and substrates with relatively fine surface roughness, better performance can be seen with finer particle size solid lubricant. Therefore, the size of particles for the solid lubricant needs to be considered for the intended use applications and also for their dispersion requirement (Mang & Dresel, 2007; Reeves *et al.*, 2013).

Cost effectiveness is the last criterion that needs to be considered and will decide which solid lubricant will be used in the applications. When two or more materials to be chosen as solid lubricant meet the requirements, their cost will dictate the choice. The most expensive solid additive is boron nitride, next is PTFE, and then MoS_2 and graphite is the cheapest solid lubricant (Mariani, 2003). The quality and formulation of the lubricant influence the cost efficiency of any solid lubricant. The efficiency of the final formulation may turn out that the most expensive solid lubricant is more cost efficient to use.

The comparison on the efficiency of solid lubricants for criteria of applications are rated and summarised in Table 2.5:

Table 2.5: Rating for solid lubricant with respective criteria

Criteria	**Graphite**	**MoS_2**	**PTFE**	**Boron Nitride**
Normal atmosphere	1	1	1	1
Vacuum atmosphere	3	1	1	1
Ambient atmosphere	1	1	1	1
Continuous service temperature to 260°C in air	1	1	1	1
Continuous service temperature to 400°C in air	1	1	1	1
Continuous service temperature to 450°C in air	2	3	N/A	1
Burnishing potential	1	1	3	2
Hydrolytic potential	1	2	1	1
Thermal potential	2	3	3	1
Thermal potential	2	3	3	1
Load-carrying lubrication	2	1	1	2
Reduction of friction	2	2	1	3
Dispersibility	1	1	3	2
Color	Black	Gray	White	White
Relative cost	1	2	2	3

Note: 1 = best, 2 = good, 3 = ok, N/A = not applicable

(Mariani, 2003)

The selection of the solid additives to be used in intended application should be considered from the criteria listed. Different solid additives can function well as an effective solid lubricant for different applications (Reeves *et al.*, 2013; Rudnick, 2009).

2.2.5 Preparation for lubricant application

For solid lubricants, the solid must be used in a way that will give an efficient interface to the contact surfaces that needs lubrication in order for them to be an effective lubricant.

Dry-powder lubrication can be applied by scattering the dry powder onto the load-bearing substrate (E. Braithwaite & Rowe, 1963; E. R. Braithwaite, 2013). However, only a few applications can efficiently use this method. The combination of natural adhesion and rubbing action of solid lubricant will result in some attachment of the lubricant to the substrate by burnishing to offer lubrication protection (Kaur *et al.*, 2001). There are some limitations when free powder is used. The film of the solid lubricant might have a short time service due to insufficient adhesion to provide continuous lubrication. It is also difficult to apply the lubricant to the intended area when dry powder is used (Mariani, 2003).

By using bonded films, this can be prevented. Strong adhesion between the solid additive and substrates that need protection can be provided by bonded films. The rate of wear that depends on the bonded film's thickness and properties of the bonding agent are also able to be controlled (Bhushan & Gupta, 1991). There are few ways of using secondary additives that provide a sturdy and long-lasting film that can be used to achieve bonded films. The choice in the type of bonding agent depends on the intended application (Rudnick, 2009). For applications that involve continual service, phenolic resins, cellulose and epoxies bonding agents are commonly used. Binders such as epoxies and phenolic resins are treatable at room temperature and elevated-temperature

correspondingly. Therefore, to choose the bonding agent, service temperature of the intended applications should be taken into consideration (Reeves *et al.*, 2013).

Alternative types of bonding agents are also used widely in order to overcome the service temperature limitations. Most typical uses included alkali silicates, phosphates, and borates which are classified as inorganic salts. The temperature restriction of organic bonding agents, can be overcome through these inorganic salts by moving the stress of temperature to the solid lubricant. However, for a coating life, bonding agents made up of inorganic salts is not provided because it is not as sturdy as an organic bonded coating. Therefore, it will limit the application that needs a constant replenishment of the lubricant (Campbell *et al.*, 1966; L. Rapoport *et al.*, 2003a).

The most commonly used method to assist the progress of application of solid lubricant is by dispersion of solid in a liquid. The liquid can be oil, water and also a solvent. Easy and precise application to the expected areas that require protection can be done by the suspension of solid lubricant in a liquid. This method can also improve the environmental cleanliness because the solid particles of the lubricant are trapped within the liquid dispersion matrix and not dispersed in the air. If the solid lubricant is used as the secondary additive, it is not an easy task to achieve proper dispersion, which is important in order to have effective lubrication (E. R. Braithwaite, 2013; Rudnick, 2009).

The shelf life of the lubricant needs to be considered when liquid suspensions are used. This is because the solid particles need to keep dispersing in the liquid carrier and eventually, sedimentation of the solid will occur in the dispersion matrix. To provide consistent lubricant performance, proper procedures of mixing the solid particles in the liquid is necessary. The time taken for the suspension to destabilise depends on their formulations, and therefore the adjustment of the lubricants' formulation is very important (Mariani, 2003).

To create a proper suspension, treatment to the surface of solid particles used as a solid lubricant can be done to make it amenable to be dispersed within the liquid matrix. The same treatment was used to prepare paint, where the surface of the colorant is chemically modified in order to have the required qualities and produce what is called as a colloidal suspension that is shown in Figure 2.2. This treatment is very important in order to have lubricant with a high degree of dispersion stability and for maximising the available particles for lubrication (Kenbeck & Bunemann, 2009).

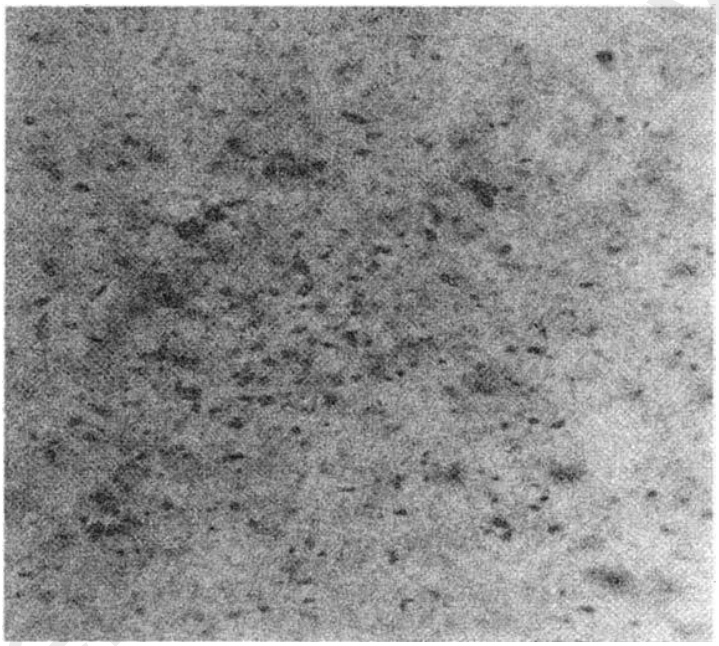

Figure 2.2: Colloidal suspension of solid additives in liquid matrix (Kenbeck & Bunemann, 2009)

Without any treatment, agglomeration of particles will occur and result in rapid sedimentation. This would give bad effects on the application of the lubricant onto the substrate by creating an ineffective film. Wetting agents such as starches and polymeric salts can be utilised to modify the surface of the solid lubricant and make them able to disperse within the liquid matrix (Mariani, 2003; Rudnick, 2009).

2.3 Solid additives: Graphene

Graphene is a fundamental building block for all graphite and its derivative materials and all its different dimensionalities (Dreyer *et al.*, 2010; Loh *et al.*, 2010). As shown in

Figure 2.3, it is able to be wrapped becoming 0D buckyballs, folded becoming 1D nanotubes or stacked into graphite. Graphene is described as a flat monolayer of the carbon atoms firmly packed into a 2D honeycomb grid (C. Zhu *et al.*, 2010a).

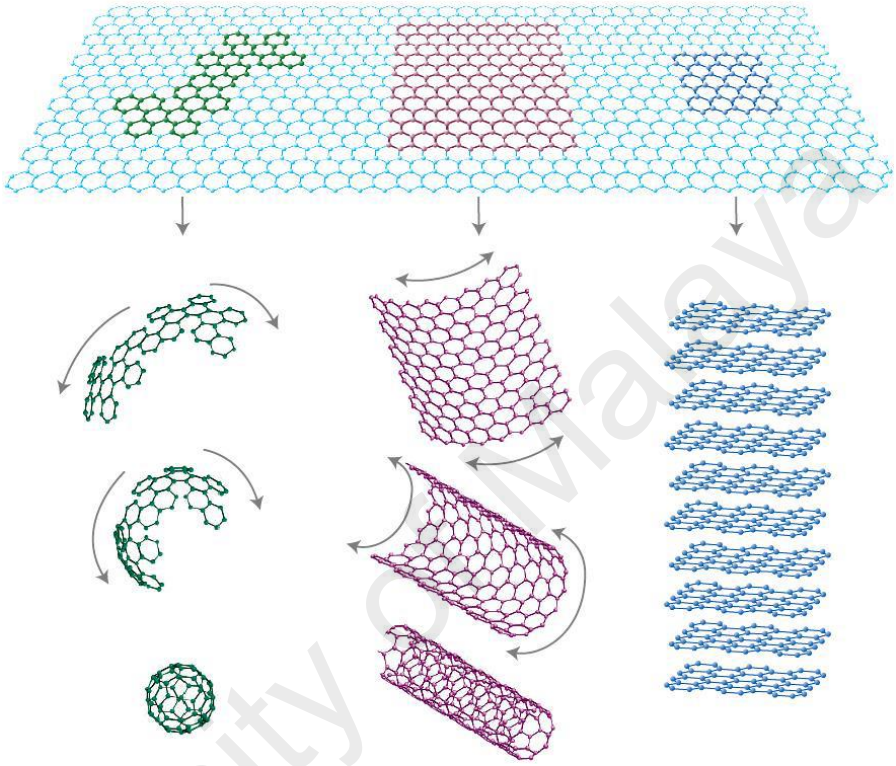

Figure 2.3: Mother of all graphitic forms (Y. Zhu *et al.*, 2010b)

Graphene had gained tremendous attention from researchers in the last few years. This is evident considering the number of rapport has increased from around 500 in 2006 to 3000 in 2010 (McAllister *et al.*, 2007). An ideal sheet of graphene consists of a 2D honeycomb structure of coal atoms in a single layer. To be considered as a graphene, the structure can have no more than ten layers (Jiang *et al.*, 2000; Kohl & Reimer, 2008).

Graphite and graphene shares many similarities and a frequent expression is that graphene is just one layer of graphite. It was confirmed that graphene has extremely high rigidity and breaking strength. The values calculated corresponds to Young's modulus of

E = 1.0 TPa and intrinsic strength of 130 GPa, proving that graphene is one of the strongest material ever determined (Ren *et al.*, 2010).

Graphene has a unique atom-thick two-dimensional structure with excellent thermal electronic, mechanical and optical properties (Novoselov *et al.*, 2012). Graphene is one of the carbon allotropes and is described as a layer of carbon atoms in planar form with densely packed and atomically smooth surface. The C-C bond length in graphene is very small, which is about 0.142 nm (Charlier *et al.*, 1991; Hummers Jr & Offeman, 1958). Graphene is inert to chemicals and has an easy shear capability (Y. Zhu *et al.*, 2010b). Due to its major favourable properties, graphene has an impressive role in tribological and mechanical applications (L Rapoport *et al.*, 2003b). Graphene has been tested and proved to be one of the strongest materials ever measured (Lee *et al.*, 2010). Graphene has also been shown to be impermeable to liquid and gasses (Bunch *et al.*, 2008), therefore, the oxidation reaction and corrosion processes that can aggravate surfaces that rub together can be slowed down.

Because of its high load-bearing limit, high chemical steadiness, low surface energy, strong intramolecular and weak intermolecular bonding, nanocarbon materials have gained incredible attention by tribology scientists. Graphene had also been the focus of enthusiasm in studies because of its excellent properties and unique structure. Few reviews on graphene in tribology and mechanical applications have been reported so far (Senatore *et al.*, 2013). Also, a few scientists have revealed that graphite (Wintterlin & Bocquet, 2009) and some of the graphite derivatives (Ramanathan *et al.*, 2008) together have the desirable properties mentioned earlier. The tribological properties of graphite nanosheets as an oil additive has been explored by Lin et.al. (Lin *et al.*, 2011). In between layers of graphite, there is weak interatomic interaction, van der Waals forces and low shear stress (Bhushan & Gupta, 1991). The properties of graphite as an additive for lube

oil has been investigated and found that to have some improvement in the reduction of friction and wear when graphite or graphite derivatives were introduced into the oil at optimum concentration (H. Huang *et al.*, 2006).

2.3.1 Synthesis of graphene

Graphene oxide, GO films with two-dimensional structure were successfully prepared using Hummers' method by oxidation of graphite flakes (Hakimi & Alimard, 2012).

A less toxic, improved method to synthesise GO is described by Marcano (Marcano *et al.*, 2010). The improved Hummers' method is done by not including the $NaNO_3$ and increasing the amount of $KMnO_4$ and conducting the reaction in a ratio of 9:1 mixture of H_2SO_4/H_3PO_4. Advantages of the improved method over the Hummers' method are that the temperature in the former can be controlled a lot easier, since it does not involve a large exotherm. Secondly, no toxic gasses are released during the process, and lastly, a greater amount of oxidised, hydrophilic carbon is recovered in the improved method. The improvement of efficiency of the oxidation process is shown. When compared to the Hummers' method, the GO synthesised using the improved method is more hydrophilic and highly oxidised. When both GO that was synthesised by two different methods (improved method and Hummers' method) were reduced using hydrazine, these two GOs will still have the same value of electrical conductivity (Tour & Kosynkin, 2012).

One of the differences in the improved method compared to the conventional Hummers' method is that it will not produce toxic gas and the temperature of the reaction can be regulated easily (Marcano *et al.*, 2010). Oxidation of graphite to get graphite oxide using the Hummers' method and its improved version are the most commonly used methods (Niyogi *et al.*, 2006). The only difference between every single layered of GO and graphene is that the edges and sides of GO are decorated with oxygen-containing functional groups(Y. Zhu *et al.*, 2010b) .Kosnykin and co-workers reported a method to

unzip GO nanoribbons (GONRs) from MWNTs, in which they used H_3PO_4 to keep the aromatic domain in place (Kosynkin *et al.*, 2009). The same logic was applied by Marcano in their synthesis procedure, which for the first time introduces H_3PO_4 into the oxidation reaction (Marcano *et al.*, 2010).

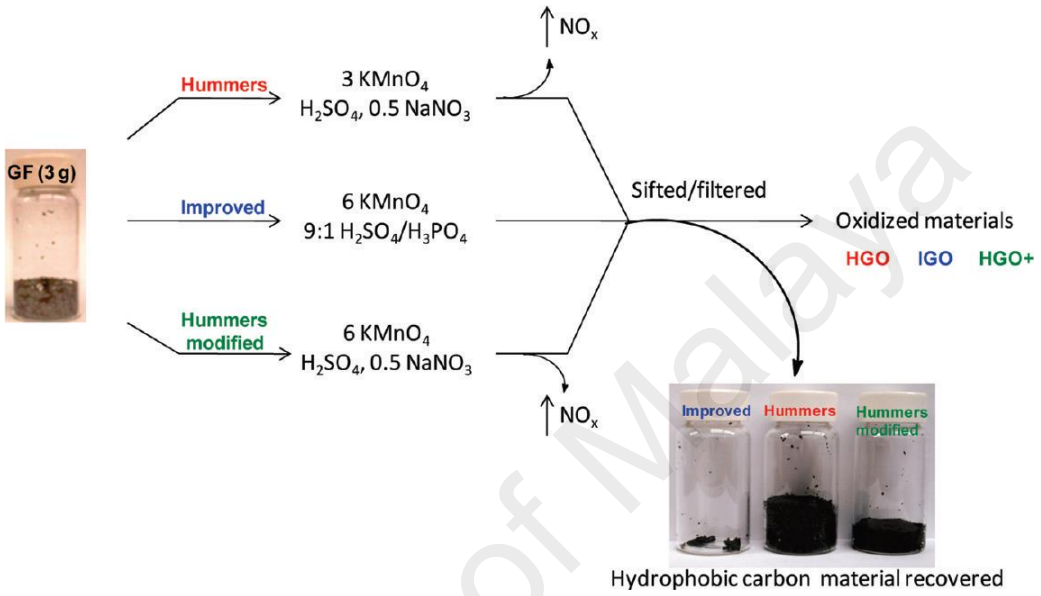

Figure 2.4: A comparative figure of GO synthesised by the improved method (IGO), Hummers' method (HGO) and Hummers' method with excess $KMnO_4$ (HGO+) (Marcano *et al.*, 2010)

Figure 2.4 shows the chemical routes of two variations of the Hummers' method in comparison to the improved method. At the bottom right, there is a drastic difference in the amount of hydrophobic carbon material recovered at the end of the three experiments, indicating a much higher efficiency of oxidation. While the actual paper by Marcano extensively characterises all three products, the XRD peaks are an example of the differences in the quality of the three GOs (Cao *et al.*, 2011; Marcano *et al.*, 2010).

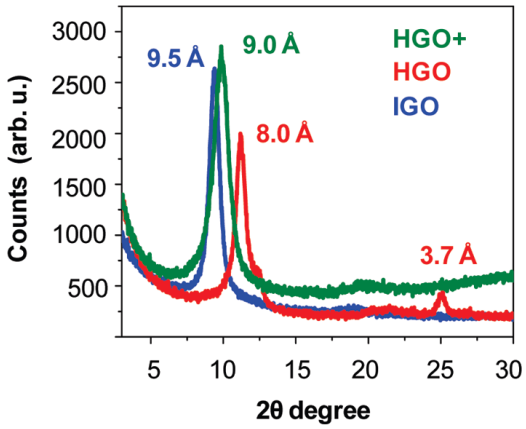

Figure 2.5: XRD spectra of HGO, HGO+ and IGO (Marcano *et al.*, 2010)

Figure 2.5 shows the interlayer spacing of each sample that was synthesised using the different methods. These interlayer spacings are 9.5 Å (IGO), 9 Å (HGO+) and 8 Å (HGO). The peak at 3.7 Å seen in the HGO spectrum represents unoxidised graphite in the sample and is not detected in the IGO and HGO+ spectrum (Marcano *et al.*, 2010).

Tour et. al explained the significance of including H_3PO_4 in the oxidation reaction of graphite to get highly-oxidised graphene oxide. In general, the methods include mixing a graphite powder in oxidant with an oxidising agent and at least one protecting agent to get graphene oxide as the product. In the presence of protecting agent, the synthesised graphene oxide is highly oxidised and their structural quality also better that the graphene oxide synthesised in the absence of protecting agent (Higginbotham *et al.*, 2010; Tour & Kosynkin, 2012).

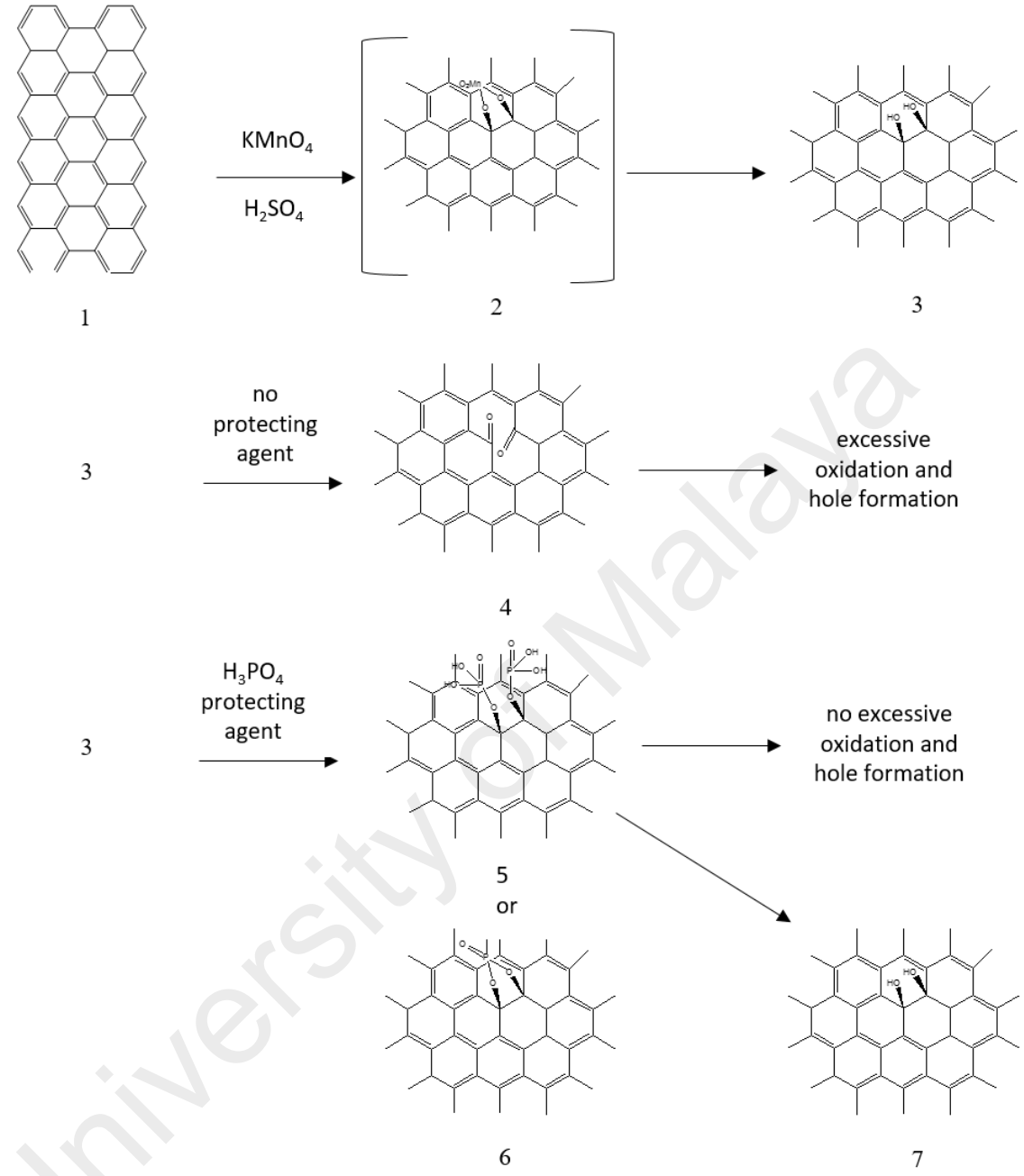

Figure 2.6: Proposed mechanism demonstrating how the inclusion of a protecting agent may provide improved chemoselectivity in the oxidation of graphite (Tour & Kosynkin, 2012)

With reference to Figure 2.6, oxidation of graphite basal plane **1** with $KMnO_4$ is demonstrated in the absence and in the presence of a protecting agent (H_3PO_4). With continued reference to Figure 2.6, oxidation of graphite basal plane **1** with $KMnO_4$ results in the formation of manganite ester **2**, which leads to vicinal diol **3**. A protonated diol may also be an intermediate. Additional edge and basal plane functionality have been

omitted from the structure of vicinal diol **3** for purpose of clarity. If left unprotected, vicinal diol **3** may be oxidised to diketone **4**, which leads to the formation of a hole in the graphene basal plane. If a protecting agent operable for protecting alcohols or diols is included in the reaction mixture, hole formation may be eliminated or minimised. With continued reference to Figure 2.6, if a protecting agent is included in the reaction mixture, the protecting agent may react with the vicinal diol in situ to prevent further oxidation and preclude hole formation. As shown in Figure 2.6, the phosphoric acid protecting agent may protect the vicinal diol via chelation in chelated vicinal diol **6** or by the individual protection of each alcohol of the vicinal diol in protected vicinal diol **5**. Regardless of the manner of protection, excessive basal plane oxidation in the graphene sheets is precluded, while the overall level of oxidation is increased relative to that of other methods for forming graphene oxide from bulk graphite. During workup of chelated vicinal diol **5**, the protecting group is released in situ to provide graphene oxide **7**. In graphene oxide **7**, additional oxidised functionality has been omitted for clarity (Higginbotham *et al.*, 2010; Marcano *et al.*, 2010; Tour & Kosynkin, 2012).

2.3.2 Limitations of graphene as additives

Studies show that the graphene platelets is a failure as oil additive at higher temperatures, and this could be due to the damaging of the protective film formed by the graphene at higher temperatures, and also due to a significant increase in agglomerations within the lubricant (Lin *et al.*, 2011). Therefore, the application thus far is considerably restricted. Nevertheless, the issue with dispersion stability can be resolved by utilising some chemical and physical methods. The solution to this would be the addition of a dispersant or modification that will reduce the agglomeration and improve the dispersive ability in the lubricant (Senatore *et al.*, 2013).

2.4 Functionalization of graphene oxide

2.4.1 Graphene oxide as precursor for functionalization

To avoid agglomeration and ensure the dispersion of GO in the base oil is excellent and stable, the modification and functionalization of GO can easily be done by taking advantage of the oxygen-containing functional groups such as -OH and -COOH on the surfaces of GO. By attaching long hydrocarbon chain compounds at the -OH or -COOH groups on the surfaces of the GO, it will enhance its dispersion in non-polar solvents (Lin *et al.*, 2011). On the other hand, the polarity of the GO can be enhanced through functionalization by attaching any polar groups at the -OH and -COOH on the surfaces of GO (W. Zhang *et al.*, 2011). To enhance the dispersion stability of the additives in any oil, the additives must have a long hydrocarbon tail that will help the additive to keep dispersing in the oil, and a polar head that will help the additive keep attached and lined up on the metal surfaces (Senatore *et al.*, 2013). Due to the multiple oxygen containing functionalities on the GO sheets, it is commonly used as the main precursor for functionalization of graphene (Park *et al.*, 2009).

2.4.2 Covalent Functionalization

To achieve a stable dispersion of graphene, both non-covalent or covalent functionalization or modification method can be used. The non-covalent method depends on the van der Waals force, electrostatic interaction or π-π stacking (Shen *et al.*, 2011; Stankovich *et al.*, 2006). This non-covalent method is easy to perform because it does not involve any alteration of the chemical structure of graphene. Besides that, this method also offers efficient measures to adjust the properties and solubility of the graphene sheets in the dispersion matrix (X. Huang *et al.*, 2012). Meanwhile, for the functionalization of graphene using the covalent method, it is based on the reaction between the functional groups of the molecules that want to be introduced and the oxygen-containing functional groups on the surfaces of GO (Z. Liu *et al.*, 2008; Salavagione *et al.*, 2009), such as

carboxyl groups (-COOH) on the edges (Park *et al.*, 2009). Between these two methods mentioned earlier, the covalent method possessed versatile probability because of the rich surface chemistry of GO. Nevertheless, it must be remembered that both the covalent or non-covalent functionalization method can enhance some properties of GO, but may diminish other properties (Veca *et al.*, 2009).

By taking advantage of the oxygen containing functional groups in GO, covalent functionalization of GO can be done. Bonds that formed between graphene and other molecules are usually stronger when covalent functionalization method is used. However, this method can cause disruption on the combination of the graphene sheets. Despite the fact that some of the graphene's natural conductivity is compromised when covalent functionalization is taken place, this method is still excellent when some other properties of graphene are desired (W. Hu *et al.*, 2014; Veca *et al.*, 2009).

2.4.3 Click Chemistry

Click chemistry is described as reactions with high yield, ample in scope, create only by-products that can be eliminated without chromatography, stereospecific, is easy to carry out and can be managed in easily removable solvents. In 2001, the "click" theory was brought in by Sharpless (Kolb *et al.*, 2001) and it is evidently one of the standout synthetic trends in both chemistry and material science research area (Hawker & Wooley, 2005; Kolb *et al.*, 2001; Lutz, 2008).

The term "click" attributes to enthusiastically preferred, specific and flexible chemical changes, that prompt a one reaction product. In other words, the click chemistry is easiness and proficiency. Click chemistry is not a new kind of chemistry, rather a term utilised for a group of reactions that can make complex molecules in an exceptionally proficient manner. This exciting idea appears to superbly justify the necessities of current scientists engaging in research fields as various as material science, biotechnology, drug

design or macromolecular chemistry (Angell & Burgess, 2007; Binder & Kluger, 2006; Bock *et al.*, 2006; Dondoni, 2007; Hansen *et al.*, 2005; Lutz, 2007; P. Wu & Fokin, 2007).

Without a doubt that over the years, complex reactions requiring either complex mechanical assembly or rigid exploratory surrounding, have been less examined than in the most recent century, and is slowly replaced by simpler devices. In this situation, the direct click reactions have turned out to be tremendously well known in academic and industrial research (Lutz, 2008).

Click chemistry is expressed as the chemistry tailored to create materials rapidly and dependably by combining small molecules as nature does. It is also described as a quick, measured, process-driven method to deal with unalterable connections of the substrates required in click reactions. Click chemistry utilises only the most dependable reactions to manufacture complex molecules from electrophiles, heteroatom linkers and olefins (Hansen *et al.*, 2005).

The benchmark of reactions to be considered as click chemistry contain a yield near 100 % and additionally a special and quickly happening irreversible, orthogonal reaction and is highly selective (Moses & Moorhouse, 2007). The conditions of the reactions ought to be mild, not sensitive to oxygen and water and utilises either mild solvents, water-based solvents or no water-based solvents. Click reactions in organic solvents have a high importance in material science. The bonds created in the product must be chemically steady under a scope of physiological conditions. Also, for click reactions that take place in polymerisation, the functionalities of the reagents must be inert under free radical polymerisation conditions or effectively secured during the polymerisation stage and functionalised thereafter (Kolb *et al.*, 2001).

Most recently, the click chemistry has been tried to functionalise GO. However, the reaction conditions and related influential factors have not been investigated. Since GO is a new type of atypical 2D macromolecules, it is vitally significant to evaluate the optimised "click" condition to modify its surface, in order to enlarge its application, especially in the areas of composites and multifunctional materials. Therefore, the azide-alkyne click chemistry have been employed by some researchers to functionalised GO with various compounds, such as polymers, amino acids, and aliphatic chains (Moses & Moorhouse, 2007).

A facile "click chemistry" approach to functionalise 2D macromolecules of GO nanosheets with poly (ethylene glycol) of different molecular weights, polystyrene, palmitic acid and various amino acids have been presented by Kou et. al (Kou *et al.*, 2010). From the results, it was reported that high degree of functionalization was achieved on the flat surfaces of GO, affording polymer-grafted 2D brushes and amino acids-immobilised nanosheets, which show improved solubility in organic solvents. The click chemistry strategy opens the door for facile functionalisation of GO with macromolecules and desired biomolecules.

One-step synthesis for chemical modification of GO have been successfully carried out by Luong et. al via thiol-ene click reaction. (Luong *et al.*, 2015). In their study, 2,2-azobis(2-methylpropionitrile) (AlBN) was used as thermal catalyst and cysteamine hydrochloride ($HS\text{-}(CH_2)_2\text{-}NH_2HCl$) was used as thiol-containing compound, which is incorporated to GO surface upon reaction with C=C bonds. The hydrochloride acts as protecting group for the amine, which is finally eliminated by adding sodium hydroxide. The modified GO contains both S- and N-containing groups (NS-GO). As the results, it was found that the NS-GO sheets form good dispersion in water, ethanol, and ethylene glycol. These graphene dispersions can be processed into functionalised graphene film.

Besides, it was demonstrated that NS-GO was proved to be an excellent host matrix for platinum nanoparticles. The developed method paves a new way for graphene modification and its functional nanocomposites.

By taking advantage of click chemistry, a general and effective methodology to covalently functionalise GO sheets with block copolymers, namely poly (styrene-*b*-ethylene-*co*-butylene-*b*-styrene) (SEBS) triblock copolymers have been proposed and studied by Cao et. al (Cao *et al.*, 2011). The covalent attachment of SEBS to GOSs, as well as the individual nature of the hybrids, was confirmed by detailed investigations. For the potential applications of the block copolymer-clicked GOSs, they were incorporated into polystyrene (PS) as reinforcing fillers. The SEBS-clicked GOSs showed excellent compatibility with a PS matrix, and as a consequence, remarkably improved mechanical properties and thermal stability of the resulting composite films were achieved. This protocol is believed to offer possibilities to fully combine the extraordinary performances of GOSs with the multifunctional properties of block copolymers, and thus be useful in a variety of technological fields.

Pan et. al have synthesised water-soluble graphene for drug delivery by grafting poly(N-isopropylacrylamide) (PNIPAm) by using click chemistry approach. For this purpose, they have synthesised alkyne derivative of GO via amide linkage and coupled a PNIPAm homopolymer (produced by ATRP) containing azide end group. This PNIPAm functionalised GO shows a lower critical solution temperature (LCST) which is lower than that of pure PNIPAm homopolymer and this lowering of LCST is attributed to the hydrophobic interaction of GO attached to PNIPAM. The PNIPAm functionalised GO can load a water insoluble anticancer drug (camptothecin, CPT) with a superior loading capacity due to π –π stacking and hydrophobic interaction between PNIPAm functionalised GO and the aromatic drug (Layek & Nandi, 2013).

An effective method of preparing graphene reinforced UV-curable materials have been presented by Yu et. al. Octamercaptopropyl polyhedral oligomeric silsesquioxane (OMP-POSS) functionalised reduced graphene oxide (FRGO) was prepared through a thiol-ene click approach and the FRGO/ polyurethane acrylate (PUA) nanocomposite was fabricated by UV irradiation technology. The results of transmission electron microscopy and X-ray photoelectron spectroscopy indicated that OMP-POSS was successfully grafted onto the surface of graphene nanosheets. Thermal and mechanical properties were investigated by thermogravimetric analysis and dynamic mechanical analysis, respectively. The initial degradation temperature, storage modulus at -65 °C and glass transition temperature of FRGO/PUA1.0 nanocomposite was remarkably improved by 12 °C, 57.8% and 10 °C, respectively, compared to those of neat PUA. Those significant enhancements are attributed to the good dispersion of the nanofiller and the strong interfacial interactions between FRGO and PUA matrix (Yu *et al.*, 2015).

Water-soluble graphene nanosheets (GNS) were fabricated by Namvari et. al via functionalization of graphene oxide (GO) with mono and disaccharides on the basal plane and edges using Cu(I)-catalyzed Huisgen 1,3-dipolar cycloaddition of azides and terminal alkynes (Click chemistry). To graft saccharides onto the plane of GO, it was reacted with sodium azide to introduce azide groups on the plane. Then, it was treated with alkyne-modified glucose, mannose, galactose, and maltose. In the next approach, 1,3-diazideoprop-2-ol was attached onto the edges of GO and it was subsequently clicked with alkyne-glucose. The products were analysed by Fourier-transform infrared spectroscopy (FTIR), field-emission scanning electron microscopy, thermogravimetric analysis (TGA), and X-ray diffraction (XRD) spectrometry. FTIR and TGA results showed both sugar-grafted GO sheets were reduced by sodium ascorbate during click-coupling reaction which is an advantage for this reaction. Besides, glycoside-grafted GNS were easily dispersed in water and stable for two weeks (Namvari & Namazi, 2014).

2.4.3.1 Huisgen 1,3-dipolar cycloaddition

There are few reactions that achieved 'click status', and from all the reactions, the Huisgen 1,3-dipolar cycloaddition of azides and alkyne to yield 1,2,3-triazoles as shown in Figure 2.7 is without a doubt considered as the primary model of the click reaction. The synthesising of alkyne and azide functionalities is easy, then combined with their kinetic stability and resistance to a broad type of functional groups and reaction conditions, make these complementary coupling accomplices especially attractive (Huisgen, 1963).

Few types of reactions have been recognised in satisfying these criteria. For instance, the investigation of the azide-alkyne cycloaddition demonstrates that it satisfies a number of the requirements (Lutz, 2007). A number of alkyne and azide functionalities as origins are accessible in the market, and a lot of them can simply be synthesised with an extensive area of functional groups, and their cycloaddition reaction specifically gives 1,2,3-triazoles.

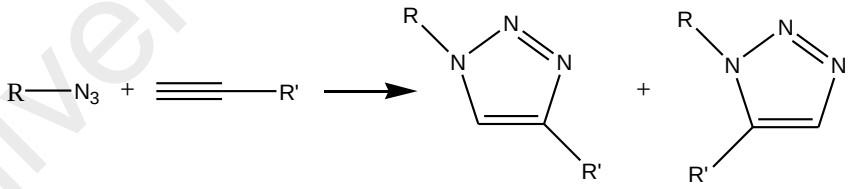

Figure 2.7: Classical thermal 1,3-dipolar cycloaddition

Unfortunately, high temperatures are required for the reactions of alkyne and azides through Huisgen-1,3-dipolar cycloaddition. Besides that, this reaction also gives a mixture of two regioisomers as the click product (Boger, 1986; Díez-González, 2011). Thus, the classic Huisgen-1,3-dipolar cycloaddition fails as a true click reaction.

2.4.3.2 Cu-Catalyzed Azide-Alkyne Cycloaddition (CuAAC)

Broad exploitation in material sciences and medicine were opened when copper (I) catalyst was discovered to be used for regioselective [3+2]-cycloaddition of alkyne and azide functionalities. Thus, the copper systems on click chemistry are reviewed with additional catalytic activities (Himo *et al.*, 2005). As one of the best click reaction, the CuAAC highlights a tremendous rate acceleration of 10^7 to 10^8 contrasted with uncatalysed 1,3-dipolar cycloaddition (Kappe & Van der Eycken, 2010).

CuAAC reactions can be done in a broad range of temperature. It is also not sensitive to aqueous conditions and a pH range from 4 to 12. Moreover, it can also bear with a broad range of functional groups (P. Wu & Fokin, 2007). Simple extraction or filtration method can be done to isolate pure products without the need for chromatography. Cu(I) salts or Cu(II) salts can be used to generate active Cu(I) catalyst by sodium ascorbate as the reducing agent as shown in Figure 2.8 (Binder & Kluger, 2006; Hansen *et al.*, 2005).

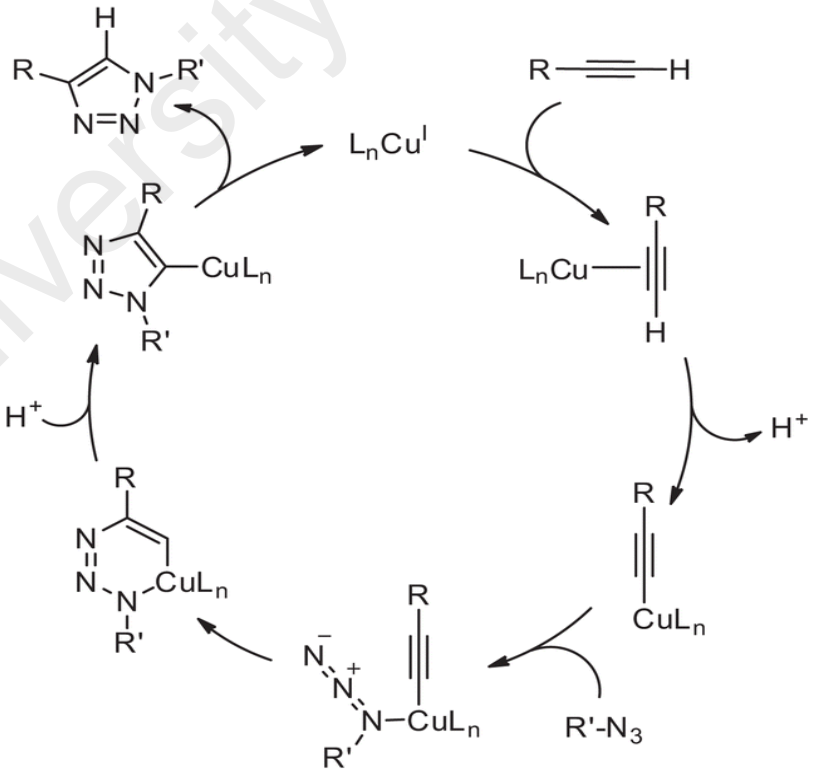

Figure 2.8: Mechanism of copper-catalyzed synthesis of 1,2,3-triazoles (Hansen *et al.*, 2005)

The formation of oxidative homocoupling products can be prevented by addition of a slight extra amount of the sodium ascorbate that acts as reducing agent. In the presence of Cu wire, active Cu(I) also can be formed by disproportionation of a Cu(II) salt (Himo *et al.*, 2005). However, only terminal alkynes work for CuAAC reactions (Ackermann & Potukuchi, 2010). A copper-catalyzed variation that takes after an alternate mechanism can be led in aqueous condition at room temperature. Moreover, the copper-catalysed reactions permit the synthesised of 1,4-disubstituted regioisomers particularly. The next developed catalysed reaction using ruthenium as catalyst results in the inverse regioselectivity with the establishment of 1,5-disubstituted triazoles (Appukkuttan *et al.*, 2004).

In 2004, Eycken et. al reported a three-component click chemistry reaction that was assisted by microwave (L. Zhang *et al.*, 2005) in order to get a series of 1,4-disubstituted-1,2,3-triazoles from alkynes, sodium azide and alkyl halides. This strategy makes them an impressive click method that is also easy to use, accessible and free from harm, by excluding the requirements to handle organic azides, since they are produced in situ (Kappe & Van der Eycken, 2010).

2.4.3.3 Ru-Catalyzed Azide-Alkyne Cycloaddition (RuAAC)

The ruthenium-catalyzed process (RuAAC) (Boren *et al.*, 2008; Majireck & Weinreb, 2006) provides access to the complementary 1,5-regioisomers of 1,2,3-triazole. Furthermore, the internal alkynes also participate in the RuAAC (not only terminal alkynes).

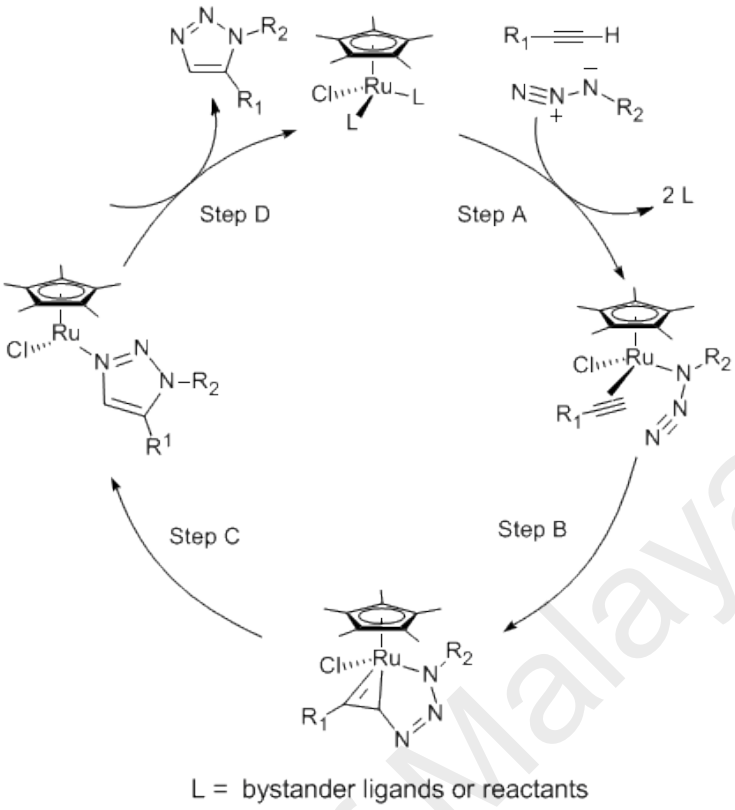

Figure 2.9: Mechanism of ruthenium-catalyzed synthesis of 1,2,3-triazoles (IJsselstijn & Cintrat, 2006)

As shown in Figure 2.9, a six-membered ruthenacycle appears as the product when the oxidative coupling between azide and alkyne is done via RuAAC approach, where the C-N bond will be produced between the most electronegative carbon of the alkyne and the terminal nitrogen of the azide. This step will then pursued by reductive elimination reaction, that will form the 1,5-regioisomeric triazole product (IJsselstijn & Cintrat, 2006).

2.5 Research gaps and novelty of dissertation

Increasing in transportation activities have been consuming much of our energy resources and significant portion of the energy produced were used to overcome friction in moving mechanical systems. Study shows that lubricant additives are one of the technology that can be used to reduce friction in any moving mechanical system. Therefore, it is expected that the demand and consumption of lubricant will be increased. Lubricant consist of base oil and package of additives. This research only focuses on friction modifier additives. The addition of additives is very important to improve the properties of the base oil. Liquid and solid additives are two types of lubricant additives that is commonly used. However, during heavy frictional contact, liquid additives will be squeezed out and cannot provide lubrication. Therefore, solid additives are chosen to be used as friction modifier additives.

Graphene is one of the solid material that offers unique friction and wear properties that cannot be seen in other conventional material. However, agglomeration and sedimentation of graphene in their dispersion matrix will occur due to their large surface area and strong van der Waals forces between them. The agglomeration can be prevented by modifying or functionalize the graphene / GO. Unfortunately, there is not much research have been carried out in details about the functionalization of graphene / GO to be used as lubricant additives. Not much research had been conducted that was intended to understand the tribological effect of the addition of surface-functionalized graphene and their compatibility with base oil. Therefore, this research intends to modify the surface of graphene / GO by functionalization method to improve their stability and dispersibility in base oil. This research also had been conducted to provide a complete route on functionalization of graphene / GO and also to understand the effects of chemically functionalized GO on the tribological properties of the lubricant.

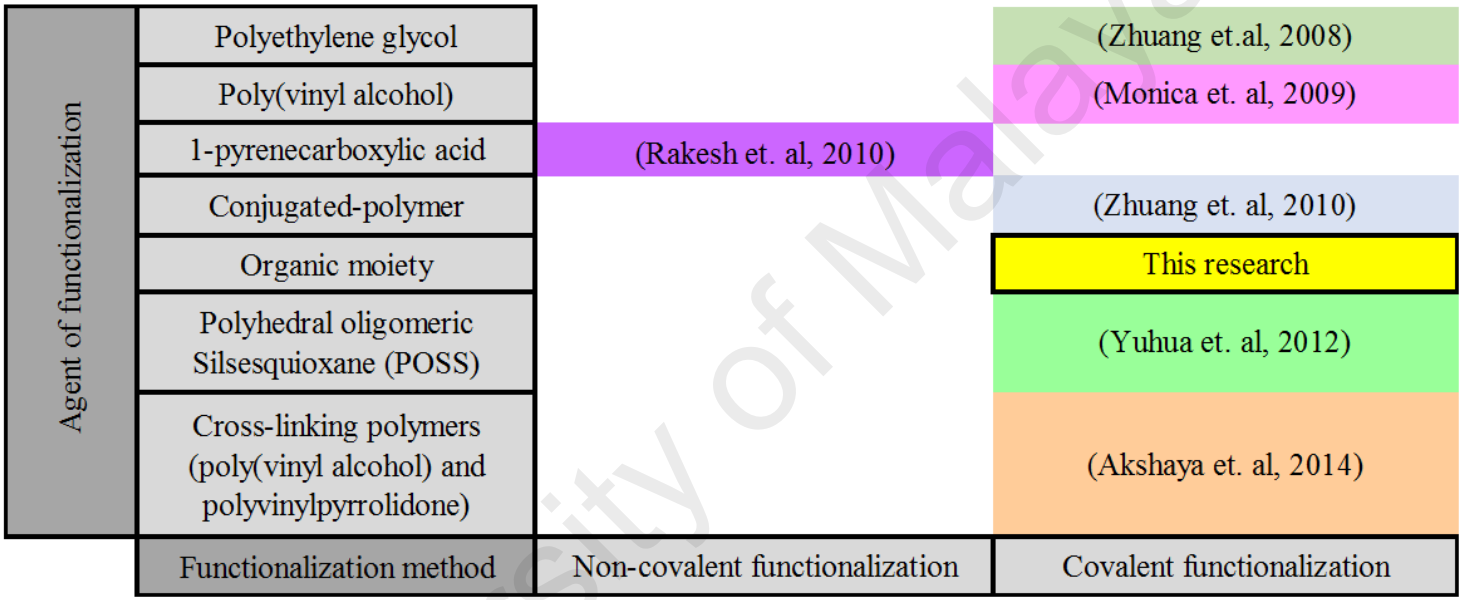

Figure 2.10: Research gaps between literature studies and current research based on method used to functionalize GO

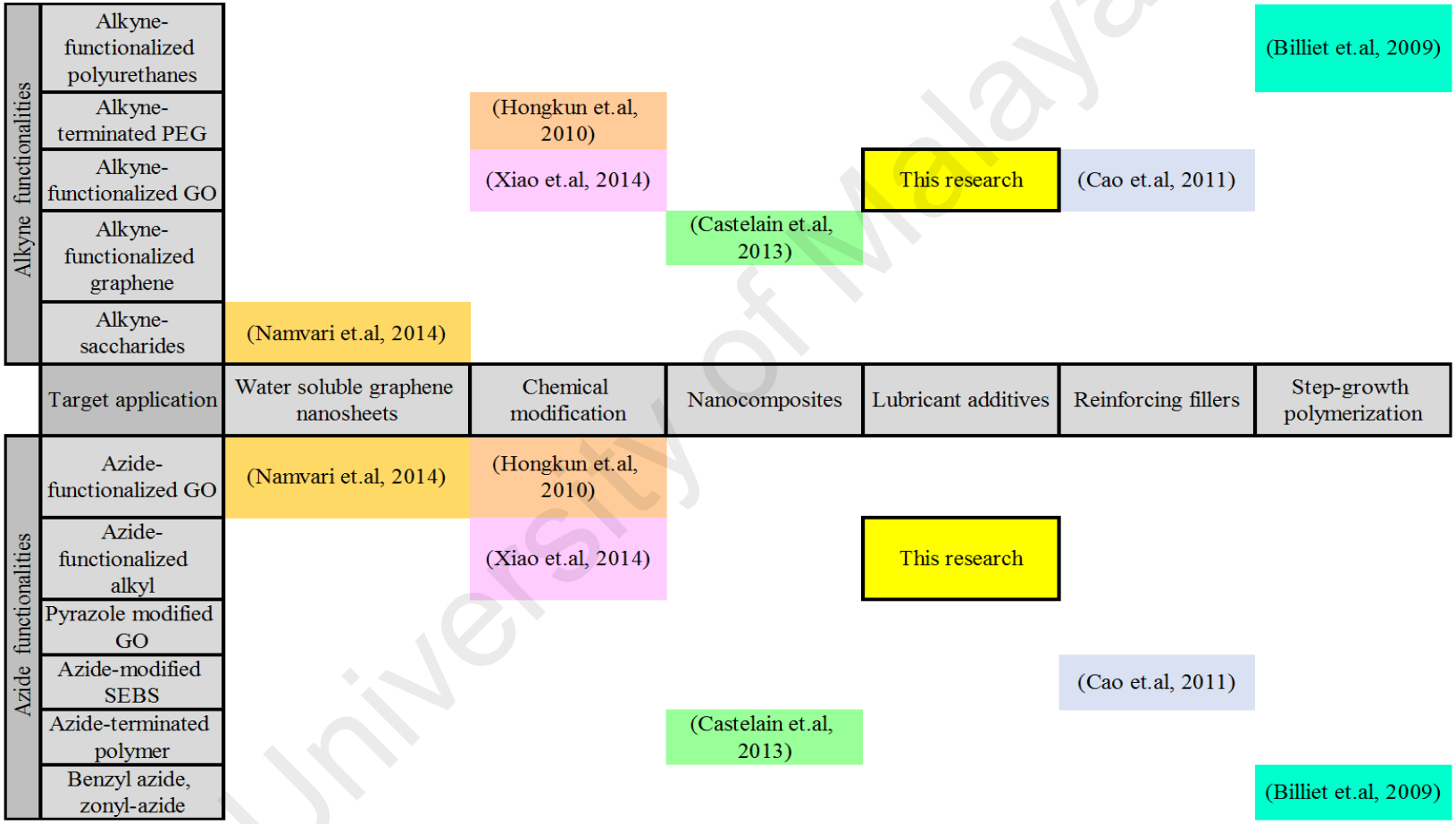

Figure 2.11: Research gaps between literature studies and current research on Click chemistry method used to functionalize GO

CHAPTER 3: MATERIALS AND METHODOLOGY

3.1 Introduction

This chapter describes five different stages of the work: from the sample preparation to the test of lube oil properties as shown in Figure 3.1. At the first stage (**Stage 1**), the highly-oxidised graphene oxide as a precursor for functionalization was synthesised via the improved Hummers' method. The second stage (**Stage 2**) is the functionalization of graphene oxide which includes the preparation of alkyne-functionalized graphene oxide, preparation of azide-functionalized alkyl and click coupling between alkyne-functionalized graphene oxide and azide-functionalized alkyl by CuAAC via click chemistry. The next stage (**Stage 3**), involves all prepared samples of graphene oxide and functionalized graphene oxide being analysed using the Fourier Transform Infrared Analysis (FTIR), X-ray Diffraction (XRD), Raman, Field Emission Scanning Electron Microscopy (FESEM), Electron Dispersive X-ray (EDX) and Thermal Gravimetric Analysis (TGA) to understand their structural and morphological properties. Boehm titration is carried out to determine the negative surface charge of highly-oxidised graphene oxide. The functionalized graphene oxide is introduced into base oil (**Stage 4**) for blending purpose with different concentration of additive in the base oil. The dispersibility of the solid additives in the base oil is measured by their absorbance using UV-visible. In the last stage (**Stage 5**), the improved properties of the lube oil with different concentrations of additive in base oil was observed by measuring their friction coefficient, wear scar diameter, wear rate, viscosity, viscosity index, density, water content and oxidation stability.

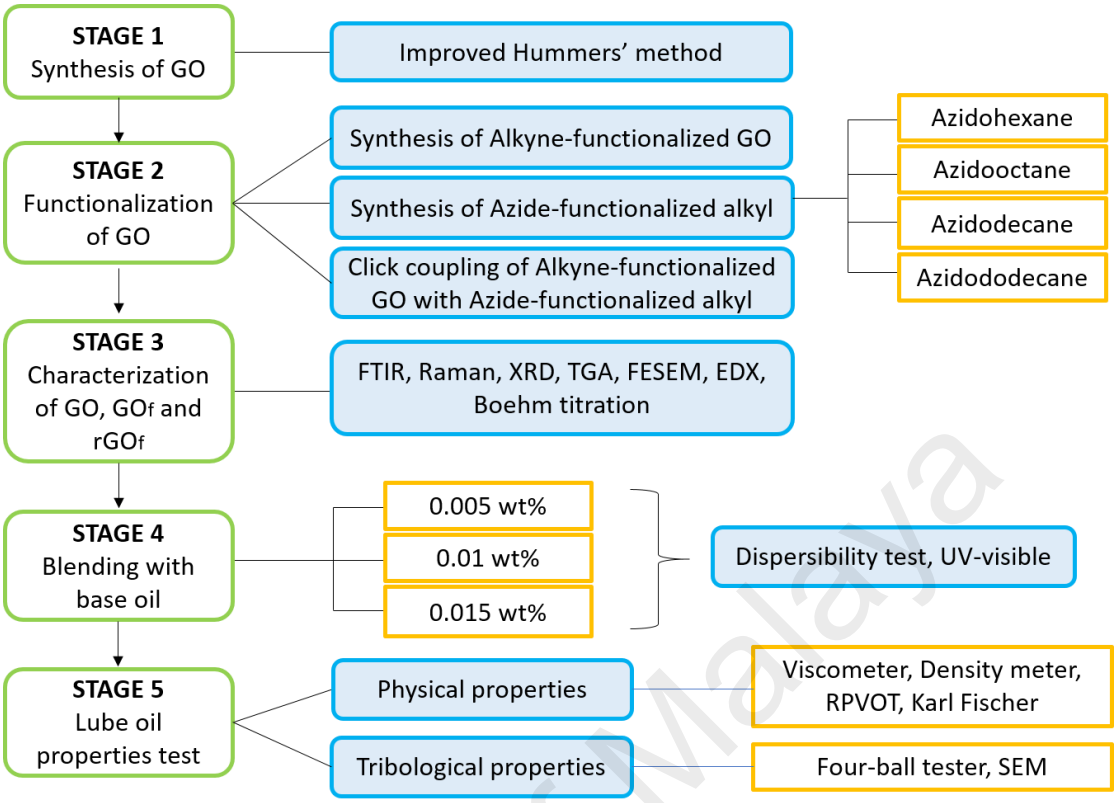

Figure 3.1 : The stage of experiments in this study

3.2 Materials

Graphite powder, sulphuric acid (H_2SO_4, 98 %), potassium permanganate ($KMnO_4$, 99.99 %), phosphoric acid (H_3PO_4, 85 %), sodium hydride (NaH), dimethyl malonate, lithium aluminium hydride ($LiAlH_4$), magnesium sulphate ($MgSO_4$), chloroform, thionyl chloride ($SOCl_2$) and hydrogen peroxide (H_2O_2, 30 %) were purchased from Merck. Hydrochloric acid (HCl, 37 %), 1-bromohexane ($CH_3(CH_2)_5Br$), 1-bromooctane ($CH_3(CH_2)_7Br$), 1-bromodecane ($CH_3(CH_2)_9Br$), 1-bromododecane ($CH_3(CH_2)_{11}Br$), propargyl bromide ($CHCCH_2Br$) and sodium azide (NaN_3) were purchased from Sigma-Aldrich. Tetrahydrofuran (THF), dichloromethane (DCM), diethyl ether, dimethyl formamide (DMF), dimethyl sulphoxide (DMSO), and trimethylamine (Et_3N) were purchased from Friendemann Schmidt. Dichloromethane (DCM), sodium ascorbate and copper sulphate pentahydrate ($CuSO_4.5H_2O$) were purchased from Fischer Scientific.

Group II 500 N petroleum-based oil used was obtained from Caltex Korea. The properties of the group II base oil that was used in the blending were shown in Table 3.1.

Table 3.1: The properties of Group II base oil

Base oil: Petroleum-based Group II		
Density	ASTM D 4052-96	0.8649 g/cm^3
Viscosity at 40 °C	ASTM D 445-06	92.9 cSt
Viscosity at 100 °C	ASTM D 445-06	10.32 cSt
Water by KF	ASTM D 6304-07	48.32 ppm
TAN	ASTM D 664-04	0.06 mg KOH/g
Surface Tension	ASTMD 1331-11	31.678 mN/m

3.3 Experimental methods

3.3.1 Stage 1: Synthesis of highly-oxidised graphene oxide, GO

Graphene oxide was synthesised using the improved Hummers' method (Tour & Kosynkin, 2012). The detailed procedure is as follows: 120 mL of H_2SO_4 and 13 mL of H_3PO_4 was stirred in an ice bath to keep the mixture cold. After 10 min, graphite powder is added to the mixture. After mixing the suspension for 10 min, $KMnO_4$ was slowly added to make sure the temperature of the mixture does not exceed 40 °C. Next, the mixture was heated to about 35 °C and was kept stirring at this temperature for 3 days. As the reaction progresses, the reaction suspension became brownish in colour. At the ends of 3 days period, cold deionised water was slowly poured into the mixture to prevent effervescence, that will cause an increase in temperature. The suspension was maintained at room temperature for 15 min. The suspension was then added with 7 mL of 30 % H_2O_2 and left to cool at room temperature. The suspension was subsequently washed with 1M HCl, followed by water. Finally, the suspension was subjected to mild sonication to

exfoliate graphite oxide into graphene oxide. Finally, the product was dried at 75 °C (J. Chen *et al.*, 2013a; Shahriary & Athawale, 2014).

3.3.2 Stage 2: Functionalization of graphene oxide

Functionalization of graphene oxide involves three major steps. The first step is to synthesis alkyne-functionalized graphene oxide, GO_f. The second step is the synthesis of azide-functionalized alkyl, N_3R and the last step is the click coupling between GO_f and N_3R by CuAAC method via click chemistry. The overview on functionalization of GO is shown in Figure 3.2.

3.3.2.1 Preparation of alkyne-functionalized graphene oxide, GO_f

In an ice bath, 12 mL of dimethyl malonate was added to a 4.22 g of sodium hydride suspension (60 % wt in mineral oil) in dry THF. Then the reaction mixture was left stirring for 10 mins. 24 mL of propargyl bromide (80 % wt in toluene) was added dropwise. The mixture was left stirred overnight and lastly extracted using water and followed by dichloromethane. The combined organic phase was concentrated using a rotary evaporator, leaving dimethyl 2,2-di(propynyl)malonate, DiMDiPM as the product.

5.0 g of DiMDiPM was then stirred in anhydrous THF. 1.10 g of lithium aluminium hydride was added to the stirred solution and the mixture left stirred for overnight. Water and 10 % NaOH solution was added carefully to stop the reaction (Gaylord, 1957). The mixture was then left stirred for 30 min until the solids become white. The mixture was filtered and the filtrate was dried using $MgSO_4$. Concentrate the product using a rotary evaporator to have the 2,2-dipropargyl-1,3-propanediol, DiPPOH.

1.0 g of graphene oxide was stirred in chloroform. In an ice bath, 1.24 mL of thionyl chloride and 3.18 mL of trimethylamine was added dropwise into the mixture (Freeman & Smith, 1958; Truce *et al.*, 1952). The mixture was then stirred for 2 hours and further

concentrated using a rotary evaporator to produce chlorinated GO. In anhydrous THF, NaH was added followed by the chlorinated GO and DiPPOH prepared. The mixture was stirred overnight then concentrated using a rotary evaporator to produce alkyne-functionalized graphene oxide.

3.3.2.2 Preparation of azide-functionalized alkyl, N_3R

5.0 g of 1-bromohexane and anhydrous sodium azide added into DMF and the reaction mixture was stirred at 80 °C under reflux for overnight (D. Liu & Bielawski, 2016). The mixture was then extracted using water and diethyl ether. The combined organic phases were added with $MgSO_4$ to remove water. The mixture was filtered and the filtrate was concentrated by rotary evaporator to give 1-azidohexane as the product. The 1-bromohexane was replaced by 1-bromooctane, 1-bromodecane and 1-bromododecane with same procedure to give the product of 1-azidooctane, 1-azidodecane, and 1-azidododecane respectively.

3.3.2.3 Click coupling by CuAAC method

The prepared alkyne-functionalized graphene oxide and four different azide-functionalized alkyls followed by sodium ascorbate were added to the mixture of water and DMSO (20:10) and sonicated for 1 hour. $CuSO_4.5H_2O$ was added and then sonicated for 2 hours. The mixture was stirred overnight and then wash with water and ethanol (Cao *et al.*, 2011; Kou *et al.*, 2010; Namvari & Namazi, 2014). The product dried overnight and give reduced-functionalized graphene oxide, rGO_f as the final product.

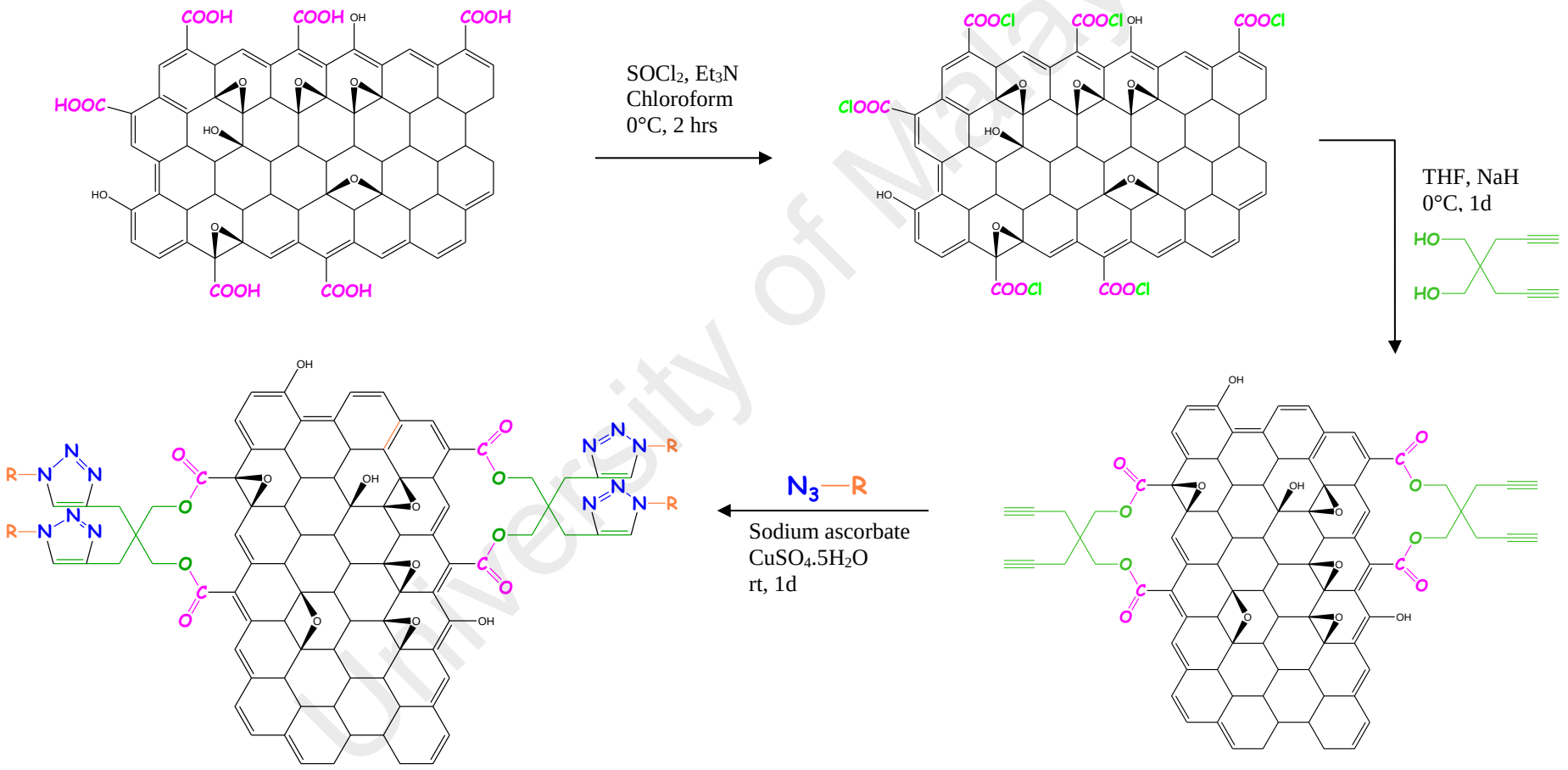

Figure 3.2: Functionalization of graphene oxide by CuAAC via click chemistry

3.3.3 Stage 3: Characterisation of the GO, GO_f, and rGO_f

The structural, elemental and morphological characteristics of the synthesised GO, GO_f and rGO_f were analysed using FTIR, XRD, Raman, FESEM/EDX, TGA and Boehm Titration.

3.3.3.1 Fourier Transform Infrared (FTIR) Spectroscopy

The FTIR spectrum determines the molecular absorption and transmission which is useful in analysing the samples of GO, GO_f, and rGO_f functional groups. The sample holder was cleansed using acetone before the samples were placed on it. 0.3 mg of sample was mixed with 4 mg of KBr and moulded to form a pellet. The pellet was placed in the FTIR sample holder and bombarded with IR radiation. Some of the IR radiation was absorbed by the sample, while others passed through via transmission. The resolution of the FTIR was set to 4 cm^{-1}, with 16 scans in the wavelength range in between 400 cm^{-1} to 4000 cm^{-1}. The FTIR spectrum was collected, with its peaks labelled. The FTIR spectrum was obtained using Perkin-Elmer 100 spectrophotometer.

3.3.3.2 Raman Spectroscopy

Raman spectroscopy gives information on rotational, vibrational and other low frequency transitions that occurs in molecules. This technique is based on the inelastic scattering of monochromatic light that is commonly obtained from a laser source. The Raman spectra were obtained using Renishaw InVia Raman spectroscopy, equipped with a charge-coupled device (CCD) detector. For the analysis, 514 nm excitation wavelength was used. For each analysis, the sample was placed inside the spectrometer after it had been pressed into a self-supporting wafer. Scattered rays that result from the interaction between monochromatic light and sample were measured using the CCD detector. The measured data was subsequently saved and evaluated on a computer.

For graphitic materials, the crystallite size, L_a of the materials can be calculated using the intensity ratio of D and G bands (I_D/I_G) according to the following equation (Marcano *et al.*, 2010):

$$\mathbf{L_a\ (nm) = 2.4 \times 10^{-10} \times \lambda^4 \times (I_D/I_G)^{-1}} \qquad \textbf{(Equation 3.1)}$$

Where,

λ = laser excitation wavelength

from this equation, the density of defects can be accessed indirectly, in terms of crystallite size (Marcano *et al.*, 2010).

3.3.3.3 X-ray Diffraction (XRD) Analysis

XRD analysis depends on the dual wave of X-rays. It is a non-destructive technique that is utilised to get data about the structure of crystalline materials. Diffraction patterns that obtained from XRD can help in characterising and identifying compounds. The XRD is based on the constructive interference of a crystalline sample and monochromatic X-rays.

The XRD analysis was carried out using PANalytical diffractometer operating at 40 kV. For each analysis, the samples were finely ground and packed tightly in a sample holder. Prior to placing the sample holder (with the sample in it) in the diffractometer for analysis, the sample surface was smoothened with a glass slide. The data was recorded in the 2θ ranges of 5 - 50° with a scan rate of 10°.

3.3.3.4 Thermal Gravimetric Analysis (TGA)

The measurement of the changes in weight that occurs to samples when they are held at constant temperature, cooled or heated is possible using TGA technique. Selected

characteristics of materials that exhibit either mass gain or mass loss as the results of decomposition, loss of volatiles or oxidation were decided by TGA. This method relies on a high level of accuracy in three measurements, which are temperature, mass change and also temperature change. Despite the furnace programming, the sample is set in a little, electrically warmed furnace furnished with a thermocouple to screen the exact measurements of the temperature. In order to prevent any undesired reactions or oxidation reaction from occurring, the sample chamber is purged with inert gas (Gabbott, 2008). The TGA results were obtained by utilising the TGA (Mettler Toledo) thermal analyser. The samples were inspected by putting it into a 100 µL open alumina crucible. The experiment was set at a heating rate of 10 °C/min under inert gas and the temperature in the range of 50 °C to 800 °C.

3.3.3.5 Field Emission Scanning Electron Microscopy (FESEM)

The FESEM is an analytical equipment that provides topographical and elemental information at high magnifications. The sample is scanned with a focused beam of electrons and the FESEM produces the images. Various signals containing information about the topography and composition of the samples were produced when the atoms in the sample interact with the electron beam. The electron beam is scanned in a scan pattern. To produce an image, the detected signal will combine with the position of the beam. Scanning images can be observed either in a low or high vacuum (Bonard *et al.*, 2002).

The FESEM images were taken on an FEI Quanta 200 electron microscope operating at 5 kV. At first, the samples were made conductive by dispersing on a carbon tape. The samples were then mounted on a sample holder and loaded into the FESEM chamber. The vacuum was created in the chamber by evacuating air prior to scanning. Scanning was done under high vacuum.

3.3.3.6 Electron Dispersive X-ray (EDX) Analysis

To identify the elemental composition of the sample or at any area of interest on the sample, the EDX analysis technique is used. The system of EDX analysis works together with the feature of the SEM. When EDX analysis was carried out, the sample is bombarded with an electron beam inside the SEM. Colliding between the electrons from the electron beam and the electrons from the sample's atom will occur and some of the electrons are knocked out of the process. The higher-energy electron from an outer shell will occupy the position that was emptied out by the ejected electrons from the inner shell. In order to do so, the transferring electron from the outer shell must surrender some of its energy by transmitting an X-ray. The amount of energy present in the X-rays produced will be measured and the atom's identity can be established from which the X-ray emitted (Goldstein *et al.*, 2012).

The EDX spectrum was obtained using the Quanta FEG 450 EDX-OXFORD. At first, the samples were made conductive by dispersing on a carbon tape. The samples were then mounted on a sample holder and loaded into the FESEM chamber. Scanning was done under high vacuum.

3.3.3.7 Boehm Titration

Boehm titration is used to measure the number of surface oxygen groups either in an acidic or basic form that is present on carbon surfaces. It is based on the acid-base titration method. Boehm titration is considered as a simple method that only utilises Na_2CO_3, NaOH, HCl, and $NaHCO_3$. By assuming that the Na_2CO_3, NaOH, and $NaHCO_3$ can neutralise the acid sites in the samples, the number of acid sites can be determined by titration method. The amount of base required to neutralise the acid in titration is calculated and reported as a number of acid sites (Boehm, 2002).

The carbon sample was added into 0.1 N of NaOH and then left stirred for 24 hours. Next, the mixture was filtered and the filtrate was mixed with HCl (0.1 N). Lastly, the mixture was titrated with NaOH (0.1 N) and the volume of NaOH used to neutralise the sample was reported as the negative surface charge was expressed in mmol/g.

3.3.4 Stage 4: Blending with base oil

Three different wt. % of rGO_f in base oil were prepared and shown in the Table 3.2 below.

Table 3.2: Lube oil prepared with different wt.% of rGO_f

Base oil			
wt. % of rGO_f_C6	**wt. % of rGO_f_C8**	**wt. % of rGO_f_C10**	**wt. % of rGO_f_C12**
0.005	0.005	0.005	0.005
0.01	0.01	0.01	0.01
0.015	0.015	0.015	0.015

3.3.4.1 UV-Visible (UV-Vis) Analysis

To measure the light that is scattered and absorbed by a sample, UV-Vis spectroscopy technique is used. This spectroscopy method can also be used to monitor the stability of particles in solutions. The intensity of absorbance peak will decrease if the particles in the solution are destabilised. The sample will be placed in between a photodetector and light source directly after been prepared, and then the intensity of a beam of light before and after passing through the sample can be measured. To quantify the wavelength dependent extinction spectrum of the sample, the measured intensity will be compared at each wavelength. Usually, the data obtained is plotted as extinction as a function of

wavelength. Blank is used as background correction for each spectrum (Q. Chen *et al.*, 2013b).

Beer-Lambert law stated that the absorbance is directly proportional to the concentration of the sample and that their concentration represent the dispersion stability of particles in liquid (Alexander & Michael, 2004).

$$A = \varepsilon Lc \qquad \textbf{(Equation 3.2)}$$

Where

A = absorbance

ε = absorptivity

L = width of colorimetric ware

c = concentration

The data on absorbance of the samples were acquired from the optical spectra, recorded using UV-Vis Spectrophotometer Model UV-2600 Shimadzu with wavelengths between 200 – 500 nm.

3.3.5 Stage 5: Lube oil properties test

3.3.5.1 Four-ball Tester

Four-ball tester is the standard test used to measure a lubricant's extreme properties in metal to metal contact situation. The test can perform both Wear Preventative (WP) and Extreme Pressure (EP) analysis for measuring the wear and friction characteristic. In the case of WP or EP lubricants, the ability to resist scuffing is the primary concern. The four-ball tester is a good laboratory tool for developing oil with good engine wear and friction control (Y. Wu *et al.*, 2007).

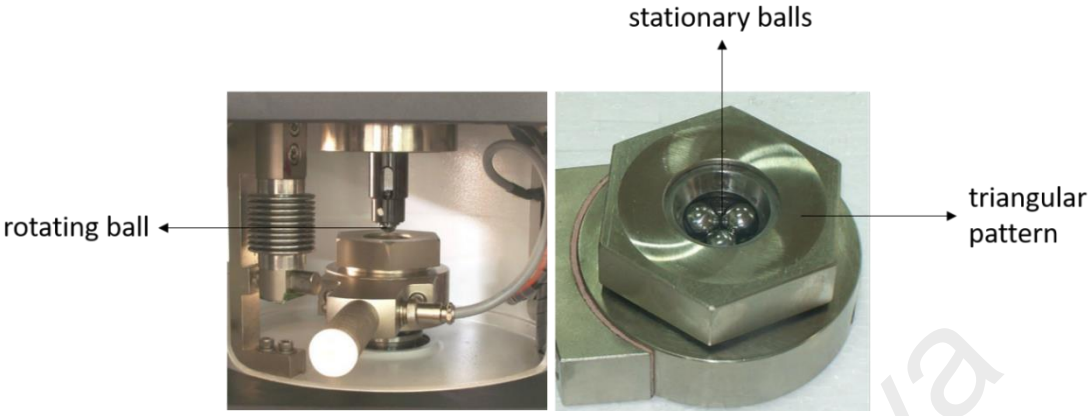

Figure 3.3 : The four-ball test setup

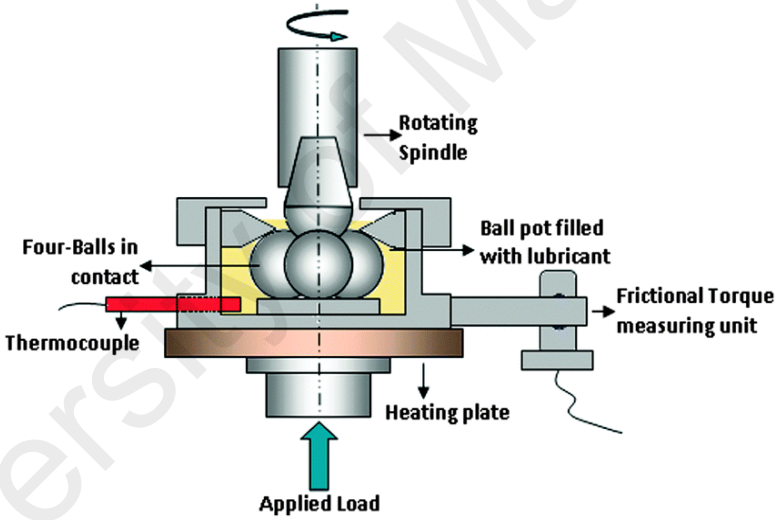

Figure 3.4: Schematic diagram of four-ball test (Khatri *et al.*, 2016)

When a steel ball is rotating against another three stationary steel balls that were secured and placed in a triangular pattern as shown in Figure 3.3 in a bath of lubricant under applied load, the point contact interface can be obtained. The schematic of the four-ball test is shown in Figure 3.4. The torque is transferred between the rotating and the stationary balls. The digital timer can be used to control the duration of the test. The rotating speed and load applied can vary depending on the test parameter required. Four-ball tester from Ducom Instrument was carried out at steady state for 1 hour to get the friction coefficient.

3.3.5.2 Desktop Scanning Electron Microscope (SEM)

Loads were applied during a four-ball test, producing wear scar on each ball. The images of the worn surface of each ball will be captured using SEM, and then their wear scar diameter (WSD) was able to be measured without any difficulty. The SEM images of the wear scar on the steel ball were obtained with Phenom ProX desktop SEM that operates at 15 kV. The sample wear scar diameter (WSD) can be physically examined. The average wear scar diameter (WSD) on each steel ball was measured and reported for comparison.

3.3.5.3 Viscometer

Viscosity can be described as the internal friction of a fluid. Viscosity determines the load carrying ability of the oil and how easily it circulates. There are two ways to define and measure the viscosity of lubricating oil, which are dynamic and kinematic viscosity. Viscosity index (VI) is a dimensionless number which represents how the viscosity of a hydraulic fluid changes with variation of temperature. Although oil viscosity changes with temperature, it is not so important in machines that run at constant load, speed, and temperature. But when conditions are not constant, high VI fluids are recommended to help maintain the near-optimum viscosity over a wider range of temperature (Stachowiak & Batchelor, 2013).

The viscosity, viscosity index (VI) and density were measured using SVM^{TM} 3001 Stabinger Viscometer^{TM} from Anton Paar. A single measuring cycle on a small sample volume can give the results of kinematic and dynamic viscosity at both 40 °C and 100 °C, viscosity index (VI) and also density.

3.3.5.4 Rotating Pressure Vessel Oxidation Test (RPVOT)

The RPVOT was utilised to determine the oxidation stability of an oil. RPVOT measures the actual resistance to oil oxidation whereas other tests detect oxidation that is already present in the oil (Barrett & Williams, 2012).

A pressure vessel containing an oil sample, water, and copper catalyst was first pressurised with pure oxygen. The pressurised vessel is then rotating at 150 °C with 60 rpm. The conditions where oxygen, copper, water and high temperature are present which can be considered as extreme conditions that can speed up the oxidation of the oil's sample. A longer time required for this process represents higher resistance towards oxidation of the oil. Results are reported in minutes. The RPVOT was carried out using RPVOT by NORMALAB.

3.3.5.5 Karl Fischer (KF)

The KF method is one of the few techniques that will measure water content and not be affected by other volatiles. Both free and bound water can be determined. The method works over a wide range from 5 ppm up to 100 % and supplies reproducible and accurate results. Volumetric and coulometric titration are two of the methods used to perform Karl Fischer titration test. Both solvent and reagent are combined together in the titration cell for the coulometric titration method. The reagent will be released through the induction of an electrical current once a sample is introduced and dissolved in the titration cell. The amount of current needed to consume the water is considered as the moisture. This coulometric method has an advantage in its ability to measure small amounts of moisture accurately. For samples having less than 200 micrograms of moisture, this method is commonly used (Scholz, 2012).

The KF Titration was carried out using 831 Karl Fischer Coulometer by Metrohm. Samples are placed in sealed vials which are placed in a temperature controlled oven. The

vial is pierced with a needle through which the water vapour travels to a titration vessel. Only water is evaporated while the oil sample remains in the vial to eliminate interferences and contamination. Results are reported as either percent water or parts-per-million (ppm). These units are easily converted by recognising that 1 % = 10,000 ppm.

CHAPTER 4: RESULTS AND DISCUSSION

4.1 Characterisation of highly-oxidised graphene oxide, GO

GO which are highly oxidised was required for functionalization purpose. The GO synthesised was characterised using FTIR, XRD, Raman, FESEM, TGA and Boehm Titration.

4.1.1 Fourier Transform Infrared (FTIR) Spectroscopy

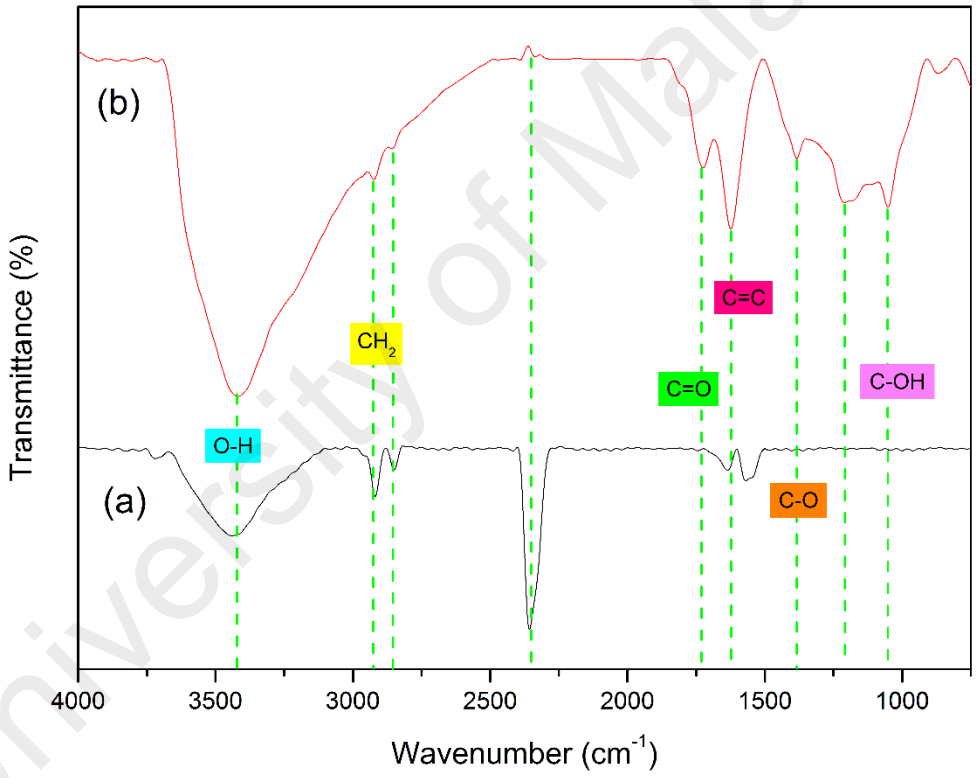

Figure 4.1: FTIR spectra of (a) graphite and (b) synthesised GO

FTIR was used to study the different oxygen-containing functional groups formed in the synthesised GO. Figure 4.1 shows the FTIR spectra of graphite and synthesised GO. The FTIR spectrum of GO shows a broad peak at wavenumber of 3418 cm^{-1} signifying the stretching of -OH groups of water molecules adsorbed on GO. Both graphite and GO has the absorption peaks at 2930 cm^{-1} and 2850 cm^{-1} indicates the symmetric and anti-symmetric stretching vibrations of CH_2. Besides that, the existence of absorption peak at

1624 cm^{-1} for both graphite and GO spectrum attribute to the stretching of C=C vibration (J. Chen *et al.*, 2013a).

When compared with the FTIR spectrum of graphite, the existence of oxygen-containing functional groups in GO can be proved by the FTIR spectrum of GO. For the GO, the absorption peak at 1725 cm^{-1} indicating the stretching vibration of C=O of carbonyl and carboxylic acid can be observed in the medium frequency area. Lastly, the absorption peaks at 1110 cm^{-1} and 1385 cm^{-1} were indicated to the stretching vibration of C-OH of alcohol and C-O of carboxylic acid correspondingly. The existence of these oxygen-containing functional groups proved that the graphite had been oxidised and oxygen-containing groups are introduced into the graphite to have graphene oxide (Tour & Kosynkin, 2012).

4.1.2 Raman Spectroscopy

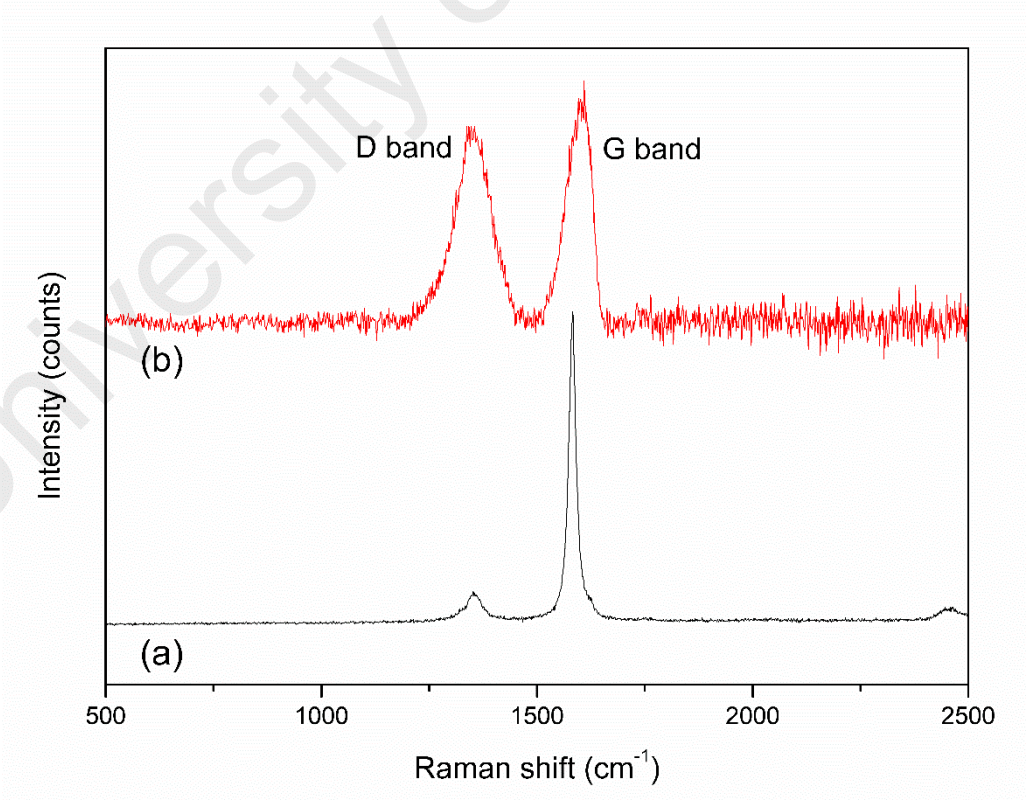

Figure 4.2: Raman spectra of (a) graphite and (b) synthesised GO

Raman was carried out for all the samples for the analysis of structural clarification of carbon materials. The main characteristics of graphitic carbon-based materials in the Raman spectra are the G and D peaks. G band results from the bond stretching of sp^2 carbon pairs in chain and rings, while the D band indicates the presence of defects in the material. Raman spectrum of GO and graphite at an excitation wavelength of 514 nm is shown in Figure 4.2. Raman spectra for graphite reported in the literature (J. Chen *et al.*, 2013a; Tour & Kosynkin, 2012) was a sharp peak of G band and a very weak peak of D band. Meanwhile, a large band width of D peak at 1350 cm^{-1} with an intensity as broad as the G peak at 1580 cm^{-1} can be seen in Raman spectra for synthesised GO. It proved that, GO has a high degree of disorder when compared to graphite. The disorder is indicated by the presence of D band which proved the presence of defects in the graphite materials. Having D and G peaks confirms a lattice distortion in the graphene oxide (Shahriary & Athawale, 2014; Tour & Kosynkin, 2012).

4.1.3 X-ray Diffraction (XRD) Analysis

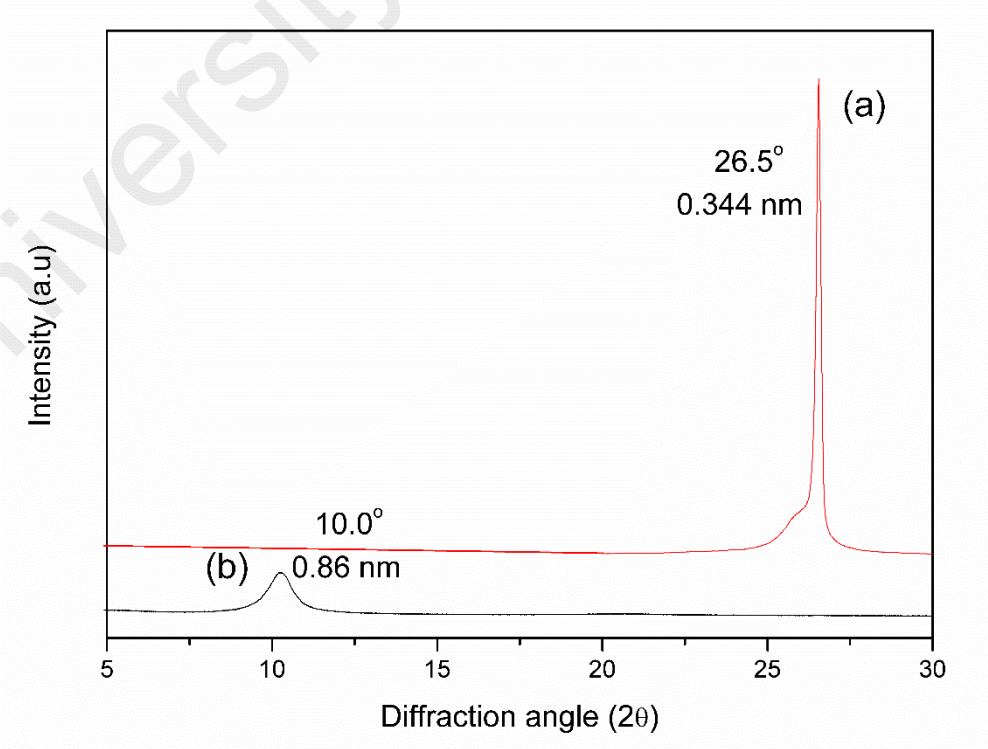

Figure 4.3: XRD patterns of (a) graphite and (b) synthesised GO

XRD is a very important characterisation method to compare graphite with GO. It provides the information about the interlayer spacing and corresponding diffraction angle. Figure 4.3 shows the pattern of graphite and GO, in which graphite exhibits an intense peak at 2θ = 26.5° and GO at 2θ = 10.0°, which is in good agreement with the literature (Kashyap *et al.*, 2014; Song *et al.*, 2014). It precisely demonstrates that the oxidation of graphite affects its crystal structure and the interlayer spacing which has enlarged from 0.344 nm to 0.860 nm (Spyrou & Rudolf, 2014).

4.1.4 Thermal Gravimetric Analysis (TGA)

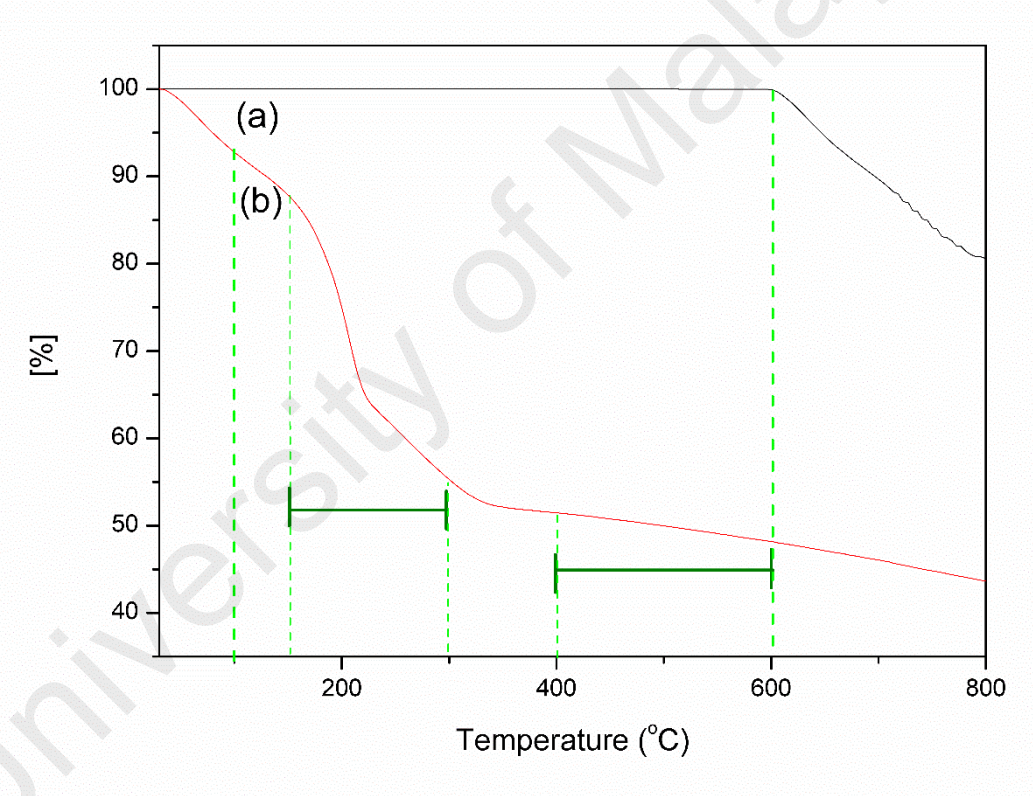

Figure 4.4: TGA diagram of (a) graphite and (b) synthesised GO

The thermal stability of synthesised GO was measured using TGA and the results are shown in Figure 4.4. From literature, it reports that graphite does not show any mass loss between room temperature to 600 °C and minor mass loss at higher than 600 °C to 800 °C. For synthesised GO, minor mass loss occurred at the temperature of 100 °C, primarily due to the loss of H_2O molecules which can be observed. As indicated in the TGA diagram, synthesised GO showed a major mass loss between 150-300 °C, indicates the

decomposition of the most labile oxygen-containing functional groups in the GO. Slower mass loss can be observed in between the temperature range of 400-600 °C, as the results of decomposition of more stable oxygen-containing functionalities. Finally, a loss of mass occurred for both graphite and synthesised GO at higher than 600 °C to 800 °C was mainly due to the combustion of the carbon skeleton (Song *et al.,* 2014; Tour & Kosynkin, 2012).

4.1.5 Field Emission Scanning Electron Microscopy (FESEM)

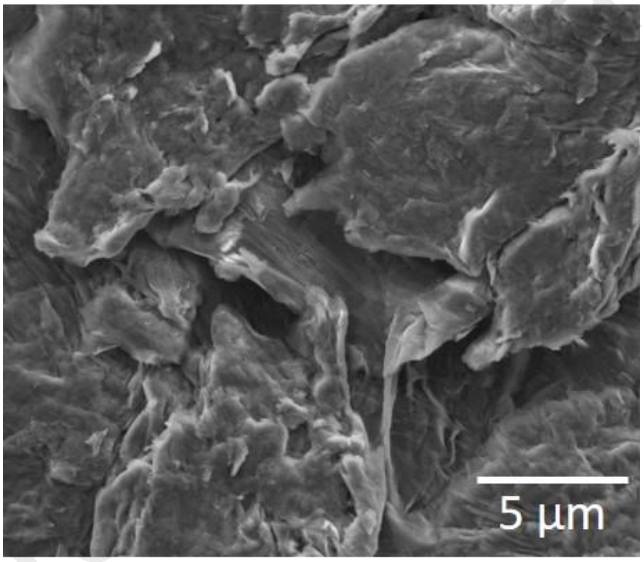

Figure 4.5: FESEM image of synthesised GO

The morphology of synthesised GO is shown in Figure 4.5. From literature, it was reported that graphite consists of flakes with flat and smooth surfaces. After oxidation and exfoliation, the FESEM image of GO shows an agglomeration of the exfoliated sheets with some wrinkles and folding on the surfaces and edges (Dreyer *et al.*, 2010; Song *et al.*, 2014).

4.1.6 Boehm Titration

Boehm titration was used to calculate the amount of acidic oxygen groups present on samples (Boehm, 2002; Z. Wang *et al.*, 2009). The number of acid sites are calculated from the amount of NaOH required in titration (Shaaban *et al.*, 2014) and expressed in mmol/g as reported in Table 4.1.

Table 4.1: The total surface negative charge for graphite and synthesised GO

Sample	**Total negative surface charge, C_s (mmol/g)**
Graphite	0.2
Graphene oxide	11.4

By compare the value of the total surface negative charge for both graphite and synthesised GO, it can be summarised that the synthesised GO had been highly oxidised by introducing acidic oxygen groups on the surface of GO.

4.2 Characterisation of alkyne-functionalized graphene oxide, GO_f

To introduce alkyne functionalities on GO, two major steps were involved. First, synthesis of 2,2-dipropargyl-1,3-propanediol, DiPPOH that will provide the alkyne functionalities. Second, to attach the DiPPOH onto the graphene oxide.

4.2.1 Synthesis of 2,2-dipropargyl-1,3-propanediol, DiPPOH

4.2.1.1 Fourier Transform Infrared (FTIR) Spectroscopy

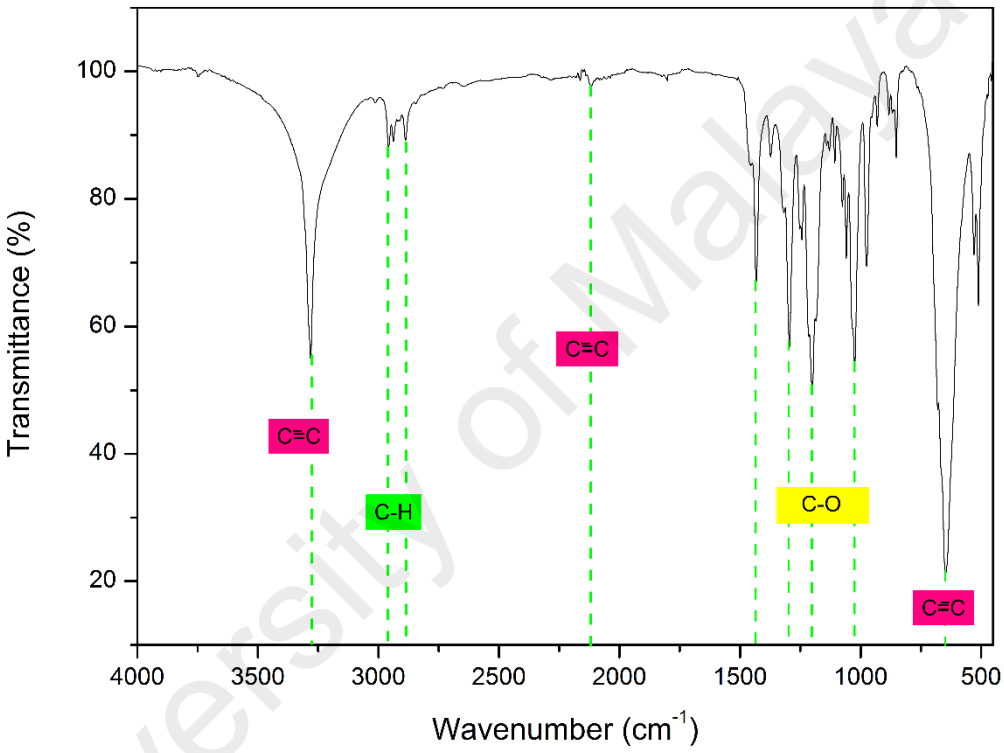

Figure 4.6: The FTIR spectrum of synthesised DiPPOH

Figure 4.6 shows the spectrum for the synthesised alkyne functionalities, DiPPOH. Few peaks can be observed that can prove the success of DiPPOH synthesised. The absorption peaks at 3282 cm^{-1}, 2117 cm^{-1} and 646 cm^{-1} corresponding to the presence of C≡C terminal stretching, C≡C stretching and C≡C bending respectively (H.-X. Wang *et al.*, 2011). Absorption peaks indicating the C-H stretching of alkanes can be seen at 2958 cm^{-1} and 2888 cm^{-1}. At around 1024 cm^{-1} to 1295 cm^{-1}, numbers of absorption peaks were observed, indicating the presence of C-O stretching of alcohol. The functional groups observed in spectrum of DiPPOH proved that the synthesis of DiPPOH was a success.

4.2.2 Synthesis of alkyne-functionalized graphene oxide, GO_f

4.2.2.1 Fourier Transform Infrared (FTIR) Spectroscopy

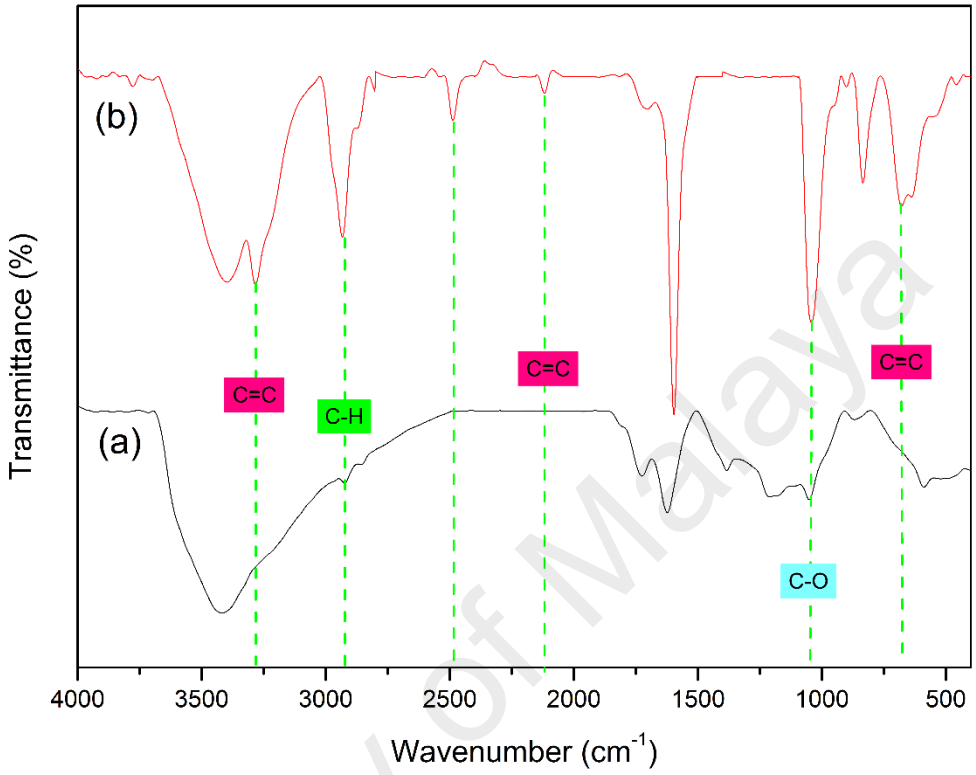

Figure 4.7: The FTIR spectra of (a) GO and (b) GO_f

Figure 4.7 shows the comparison of GO and GO_f spectrum. Figure 4.7 (b) showed the FTIR spectrum of GO_f. Few new peaks in GO_f spectrum can be observed that can prove the success of alkyne-functionalized GO when compared with GO in Figure 4.7 (a). The absorption peaks at 3282 cm^{-1}, 2112 cm^{-1} and 676 cm^{-1} corresponding to the presence of C≡C terminal stretching, C≡C stretching and C≡C bending respectively. The intensity of C-H stretching at 2930 cm^{-1} increased in GO_f, thus proving that the GO have been attached by the organic moiety synthesised, DiPPOH (Namvari & Namazi, 2014).

The intensities of the vibration peak of O-H groups at 3418 cm^{-1} reducing proved that the O-H groups had been replaced by other functionalities. This may be due to the covalent functionalization that covalently attached the alkyne-functionalized molecule at

the –OH groups on the surface of GO thus reducing their –OH group's intensity. Lastly, the intensities of C-O stretching for ester was increased at 1041 cm^{-1} proving that, the covalent attachment of the alkyne functionalities was a success.

4.2.2.2 Field Emission Scanning Electron Microscopy / Electron Dispersive X-ray Spectroscopy (FESEM/EDX)

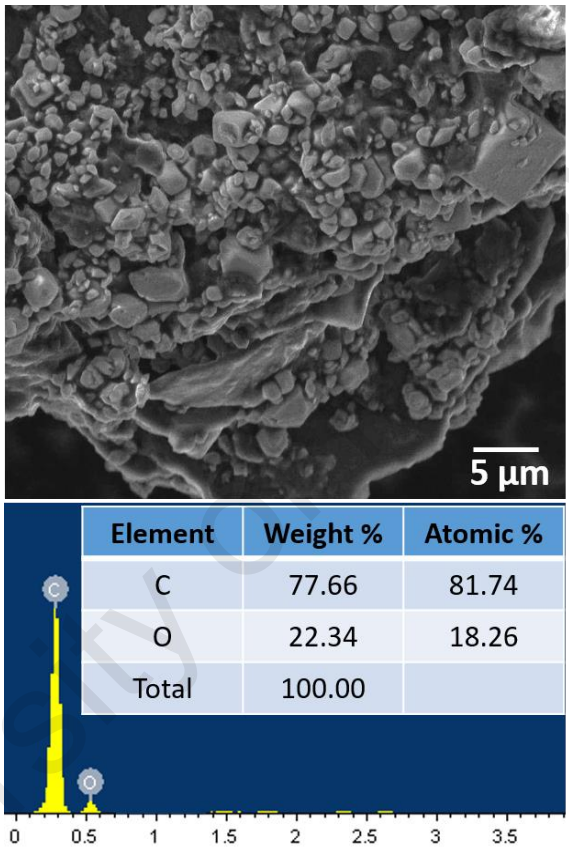

Figure 4.8: The FESEM/EDX image of GO_f

To investigate the change in morphology of GO when covalently attached by alkyne functionalities, DiPPOH, FESEM images were taken and EDX analysis was carried out. The results were shown in Figure 4.8. The objects observed on the sheets in FESEM image of GO_f are the alkyne functionalities decorated on the GO.

In literature, the reported weight percentage of C element in GO is approximately about 68% (Dreyer *et al.*, 2010). Thus, when compared to GO, GO_f have higher weight percentage of C, as the results of DiPPOH attachment. This could be possible explanation to prove the successful of alkyne functionalities attachment on GO.

4.3 Characterisation of azide-functionalized alkyl, N_3R

4.3.1 Fourier Transform Infrared (FTIR) Spectroscopy

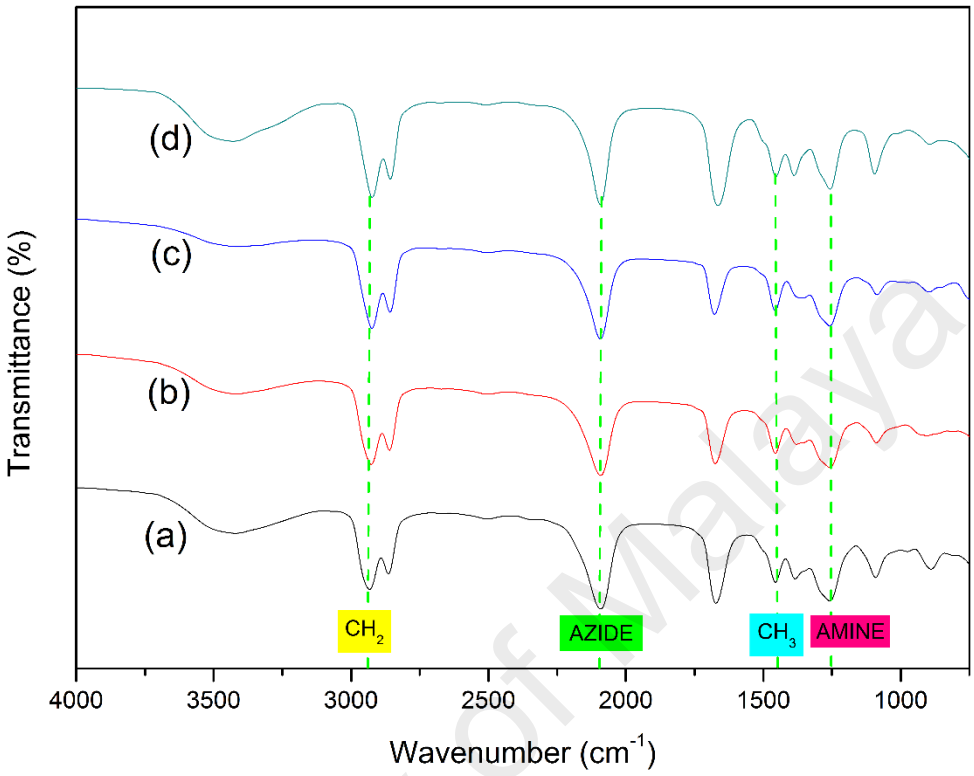

Figure 4.9: The FTIR spectra of synthesised azide-functionalized alkyl

Four main functionalities group can be observed in all four FTIR spectra of azide-functionalized alkyl; (a) azidohexane, (b) azidooctane, (c) azidodecane, (d) azidododecane, shown in Figure 4.9. In all four different azide-functionalized alkyls, similar peaks can be observed. The peak at 2900 cm^{-1} indicated the alkane stretching. The peak at 2100 cm^{-1} are the major peaks that indicated the success of the azidation reaction, which is related to the azide stretching. Peaks at 1455 cm^{-1} and 1257 cm^{-1} represents the presence of methyl group alkane bending and aliphatic amine stretching respectively (D. Liu & Bielawski, 2016).

4.4 Characterisation of reduced-functionalized graphene oxide, rGO_f

By using click chemistry via CuAAC method, four different reduced-functionalized GO, rGO_f as tabulated in Table 4.2 were synthesised by varying the azide-functionalized alkyl that were clicked to the alkyne-functionalized GO.

Table 4.2: The synthesied reduced-functionalized GO, rGO_f

Alkyne-functionalized GO (GO_f) + Azide-functionalized alkyl (N_3R)	**rGO_f**
GO_f + azidohexane (N_3C6)	rGO_f_C6
GO_f + azidooctane (N_3C8)	rGO_f_C8
GO_f + azidodecane (N_3C10)	rGO_f_C10
GO_f + azidododecane (N_3C12)	rGO_f_C12

4.4.1 Fourier Transform Infrared (FTIR) Spectroscopy

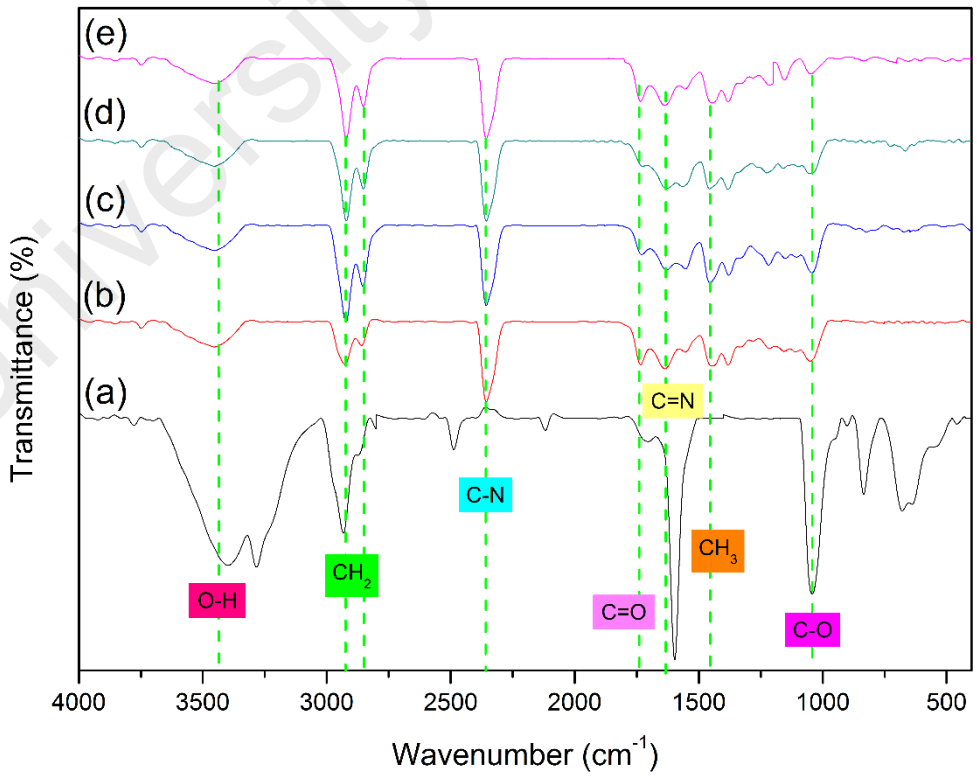

Figure 4.10: The FTIR spectra of (a) GO_f, (b) rGO_f_C6, (c) rGO_f_C8, (d) rGO_f_C10 and (e) rGO_f_C12

Figure 4.10 showed the FTIR spectrum of (a) GO_f and four different rGO_f. All the four final products, rGO_f; (b) rGO_f_C6, (c) rGO_f_C8, (d) rGO_f_C10, (e) rGO_f_C12 have almost similar peaks. The peaks at 1725 cm^{-1} and 1624 cm^{-1} were indicated to the stretching of C=O and the stretching of aromatic C=C respectively. The presence of peaks at 1051 cm^{-1} and 3418 cm^{-1} related to the stretching of C-O groups and O-H groups respectively. When compared to the FTIR spectra of GO_f as shown in Figure 4.10 (a), one crucial peak observed at 2358 cm^{-1} related to the stretching of C-N indicated the success of azide-alkyne coupling reaction on the GO sheets can be observed on all the four different spectra of rGO_f as shown in Figure 4.10 (b-e). Besides that, the disappearance of alkyne stretching peaks at 3282 cm^{-1}, 2112 cm^{-1} and 676 cm^{-1} along with the presence of a peak at 1635 cm^{-1} which corresponds to the presence of C=N stretching are the evidence of ring closure between the azide and alkyne functionalities that results in the formation of triazole ring (Dondoni, 2007; Namvari & Namazi, 2014).

The intensities of the peaks indicating the presence of oxygen-containing functionalities showed a dramatic reduction from GO_f to rGO_f. The intensities of the peak indicated to O-H of carboxylic acid groups at 3418 cm^{-1} was reduced in broadness due to esterification. This may be due to the covalent functionalization that covalently attached the alkyne-functionalized molecule at the –OH groups on the surface of GO, thus reducing their –OH group's intensity. However, the peak at 1725 cm^{-1} indicated the stretching of C=O remains the same from GO_f to rGO_f. These observations proved that C=O stretch of esters remains throughout the functionalization process. The functionalization of GO introduces new absorption peaks, apparently arising from the azidoalkyl into the products. For example, the doublet at 2918 cm^{-1} and 2850 cm^{-1} is indicated to the stretching of asymmetric C-H of alkanes in azidoalkyl. Absorption peak

on all four different rGO_f at 1451 cm^{-1} related to the presence of C-H bend of alkane, proving that it has been successfully attached on GO.

4.4.2 Raman Spectroscopy

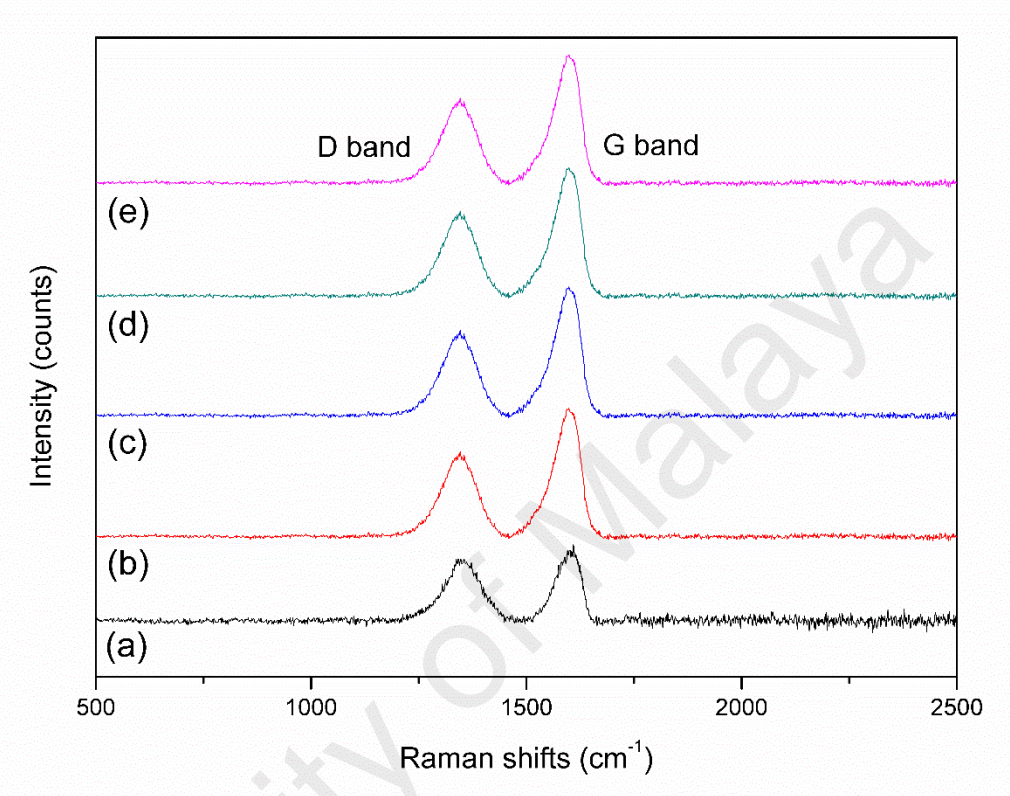

Figure 4.11: The Raman spectra of (a) GO, (b) rGO_f_C6, (c) rGO_f_C8, (d) rGO_f_C10 and (e) rGO_f_C12

Generally, defects will surely be introduced in both graphene oxide and covalently functionalized graphene oxide materials. Thus, information from Raman spectroscopy was used to study these defects in all synthesised products, GO, and rGO_f. Raman spectra for the GO and rGO_f is shown in Figure 4.11. In both GO and all the four different rGO_f, two prominent peaks can be seen clearly, indicating the existence of D and G bands at ~1353 cm^{-1} and ~1600 cm^{-1}, respectively. The qualities of the carbon allotropes or graphitic material can be evaluated by calculating the intensity ratio of the D and G bands (I_D/I_G) (J. Chen *et al.*, 2013a). The ratio of I_D/I_G decreases gradually from GO (1.3172) to rGO_f (0.9176). It can be due to attachment of the non-carbon material onto the surface of GO.

Based on the calculations using the following equation, La (nm) = 2.4 x 10^{-10} x λ^4 x $(I_D/I_G)^{-1}$, the crystallite sizes of GO and rGO_f are 12.718 nm and 18.256 nm respectively. This indicated that, upon functionalization, the decrease in carbon qualities and increase in crystallite sizes will occur, demonstrating that covalent bonding occurred on the surface of GO.

4.4.3 X-ray Diffraction (XRD) Analysis

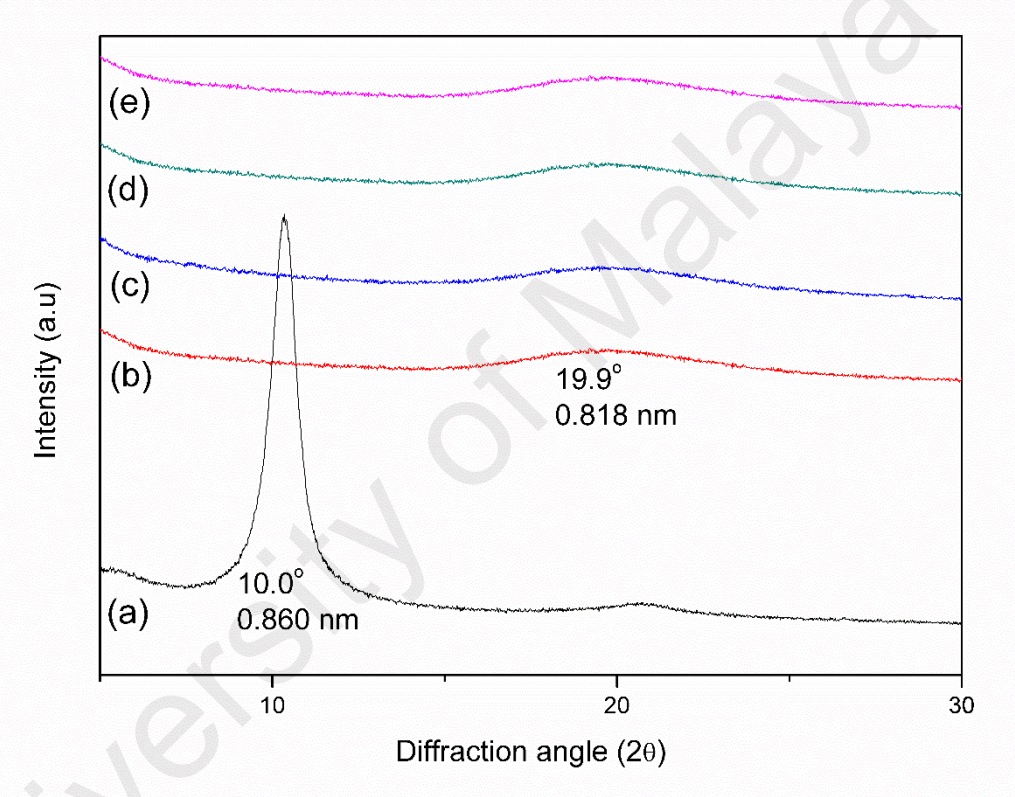

Figure 4.12: The XRD patterns of (a) GO, (b) rGO_f_C6, (c) rGO_f_C8, (d) rGO_f_C10 and (e) rGO_f_C12

The changes in the structure of the samples can be further studied by performing the XRD measurement. The XRD patterns for GO and rGO_f is shown in Figure 4.12. For GO, a broad peak at 2θ = 10.0° can be observed, referring to a d-spacing of 0.860 nm. The peak of GO was not observed in all the four different final products, rGO_f. rGO_f shows a new diffraction peak at 2θ = 19.9°, referring to a d-spacing of 0.818 nm. Reduction in the d-spacing after functionalization, indicated that upon functionalization, organic moiety was introduced into the interlayer spacing of GO.

4.4.4 Thermal Gravimetric Analysis (TGA)

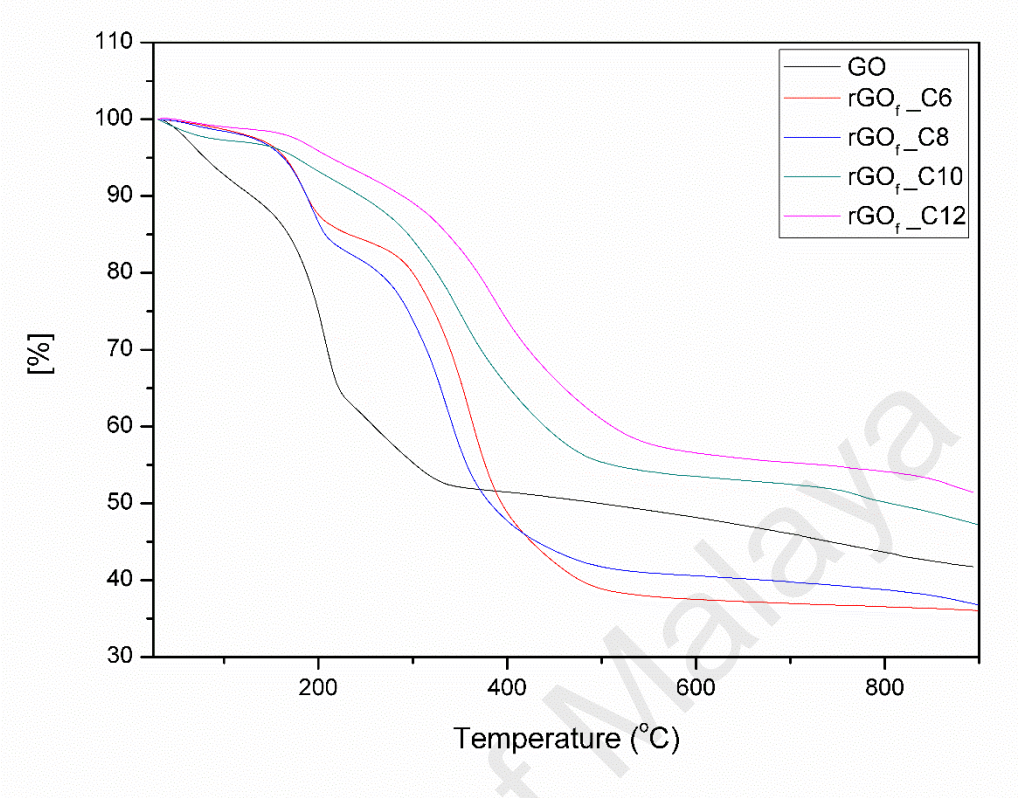

Figure 4.13: The TGA diagram of GO and four different rGO_f

TGA diagram of GO and four different rGO_f are shown in Figure 4.13. Firstly, the loss occurred at the temperature below 125 °C, primarily due to the loss of water molecules. Mass loss below 125 °C indicated that the content of adsorbed water for rGO_f was lower when compared to GO. It shows that rGO_f has lower water content than GO. This can prove that the hydroxyl groups in the rGO_f have been reduced by covalent functionalization of the organic moiety on the surface of GO (Namvari & Namazi, 2014; Tour & Kosynkin, 2012).

Secondly, the unstable oxygen-containing functional groups will be thermally decomposed at a temperature of 225 °C (Marcano *et al.*, 2010; Tour & Kosynkin, 2012). Weight loss of rGO_f at 225 °C was very low compared to weight loss of GO. It proved that upon functionalization of GO, the oxygen-containing functional groups were also reduced during the click-coupling reaction.

4.4.5 Field Emission Scanning Electron Microscopy / Electron Dispersive X-ray Spectroscopy (FESEM/EDX)

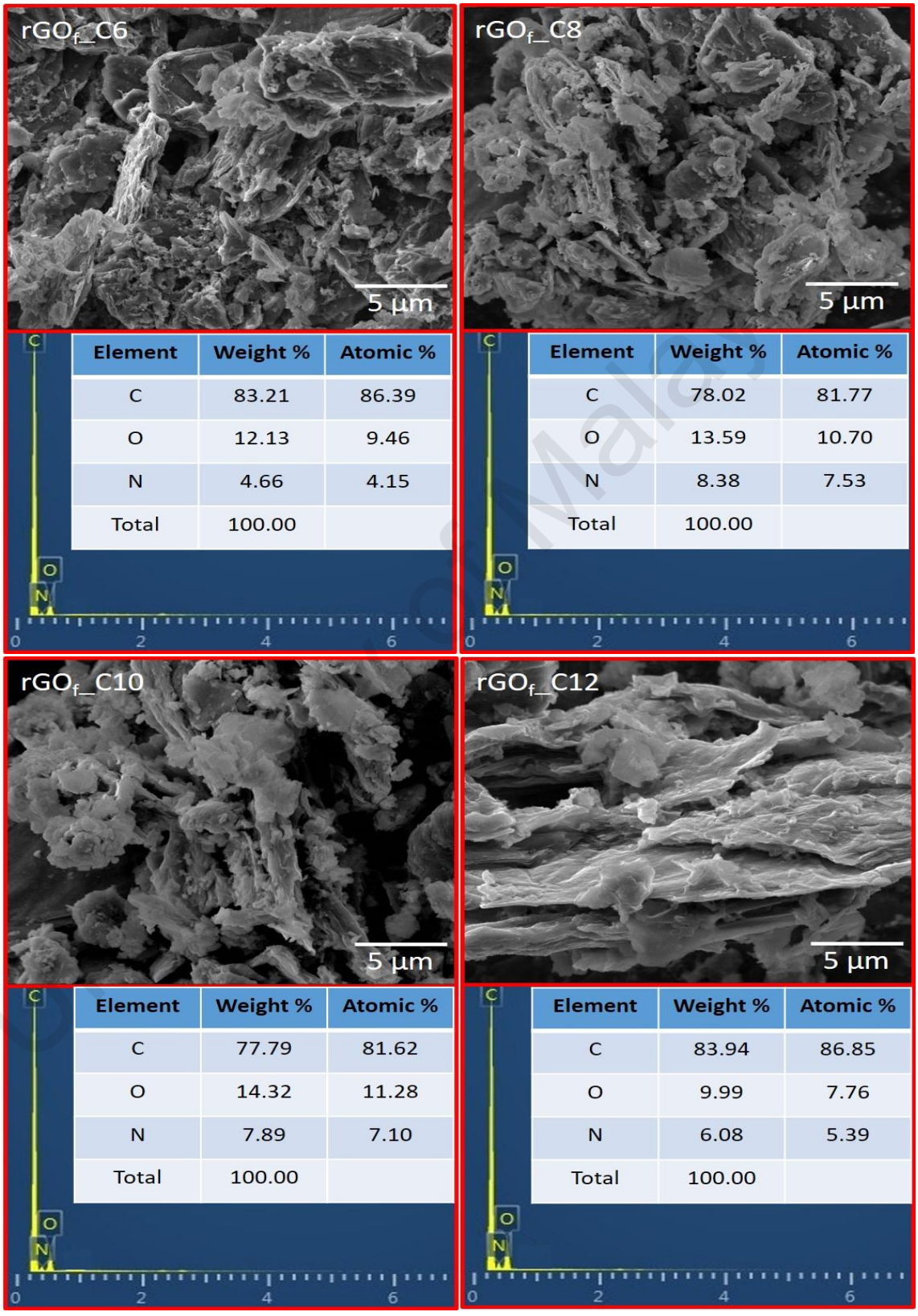

Element	Weight %	Atomic %
C	83.21	86.39
O	12.13	9.46
N	4.66	4.15
Total	100.00	

Element	Weight %	Atomic %
C	78.02	81.77
O	13.59	10.70
N	8.38	7.53
Total	100.00	

Element	Weight %	Atomic %
C	77.79	81.62
O	14.32	11.28
N	7.89	7.10
Total	100.00	

Element	Weight %	Atomic %
C	83.94	86.85
O	9.99	7.76
N	6.08	5.39
Total	100.00	

Figure 4.14: The FESEM images including EDX spectra of four different rGO$_f$

To study the morphology of the rGO_f, FESEM was carried out, and the images are shown in Figure 4.14. All the four different rGO_f have almost similar SEM images. When compared to the FESEM image of GO_f which was shown in previous discussion (Figure 4.8), fluffy aggregates can be clearly observed on rGO_f due to the presence of organic moiety on their surfaces (Namvari & Namazi, 2014). The FESEM image of rGO_f shows that functionalization was successfully done by decorating organic molecules on the GO.

The EDX analysis proved the appearance of element nitrogen, N in the rGO_f. It proved that the rGO_f has been decorated with a triazole ring that results from the reaction between alkyne and azide functionalities. From the results of EDX analysis, it can be observed that the weight percentage of C elements were increased for all the four different rGO_f, together with decreased in the weight percentage of O elements when compared to GO_f. The increased in C elements weight percentage for all the four rGO_f can be due to the attachment of the azidoalkyl on the alkyne group of GO_f during click coupling. Besides that, there is no trace of the Cu element in the rGO_f, proving that there are no residues of Cu that was used as the catalyst in the click coupling reaction left.

4.5 Dispersion of rGO_f in base oil

4.5.1 Dispersibility test

Simplest qualitative test was carried out to determine whether the reduced functionalized GO, rGO_f has better dispersibility in oil than GO. The dispersibility of GO and four different rGO_f in oil was observed.

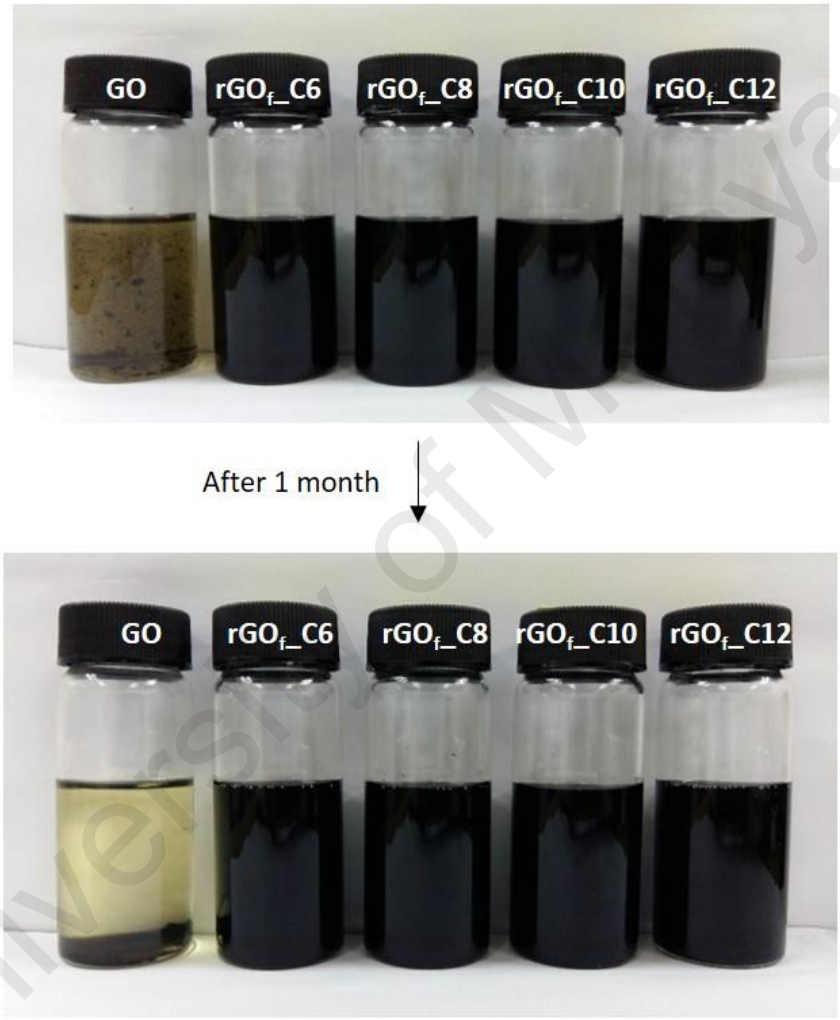

Figure 4.15: The GO and four different rGO_f dispersed in base oil (a), after 1 month (b)

Upon preparation of the dispersibility test, GO and all four different rGO_f separately dispersed in base oil subjected to the same sonication time. After sonication, it can be seen that GO cannot be uniformly dispersed in base oil, but for the rGO_f, it can easily disperse in the base oil. After one month of observation, it can be observed that the GO in base oil sedimented to the bottom and while the rGO_f is still uniformly dispersed in

base oil. Comparisons between GO and the four different rGO_f before and after 1 month are shown in Figure 4.15. It proved that upon functionalization, the dispersibility of the rGO_f in the base oil improved.

4.5.2 UV-Visible (UV-Vis) Analysis

Beer-Lambert Law stated that the absorbance is directly proportional to the dispersion stability of particles in a liquid. Therefore, UV-visible spectroscopy analysis is used to compare the absorbance of GO and rGO_f in base oil in order to determine their stability in the base oil (Q. Chen *et al.*, 2013b).

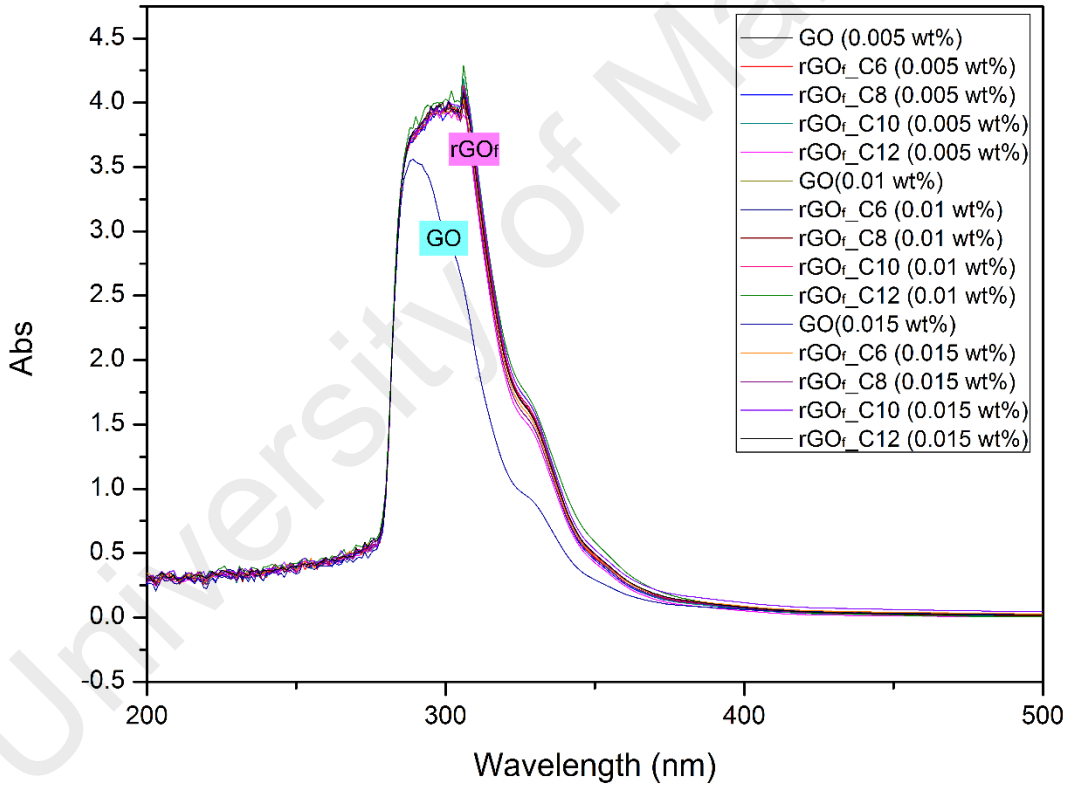

Figure 4.16: The absorbance of dispersion in the range of 200 to 500 nm

Figure 4.16 shows the absorbance of prepared sample with different wt. % in the wavelength range between 200 to 500 nm. In the wavelength range of 250 to approximately 350 nm, one-to-one relationship between wavelength and absorbance can be observed. To evaluate the stability of the dispersion, any wavelength between 250 to

350 nm can be utilised as the characteristic absorption wavelength. In this study, the fixed selected detection wavelength is at 300 nm.

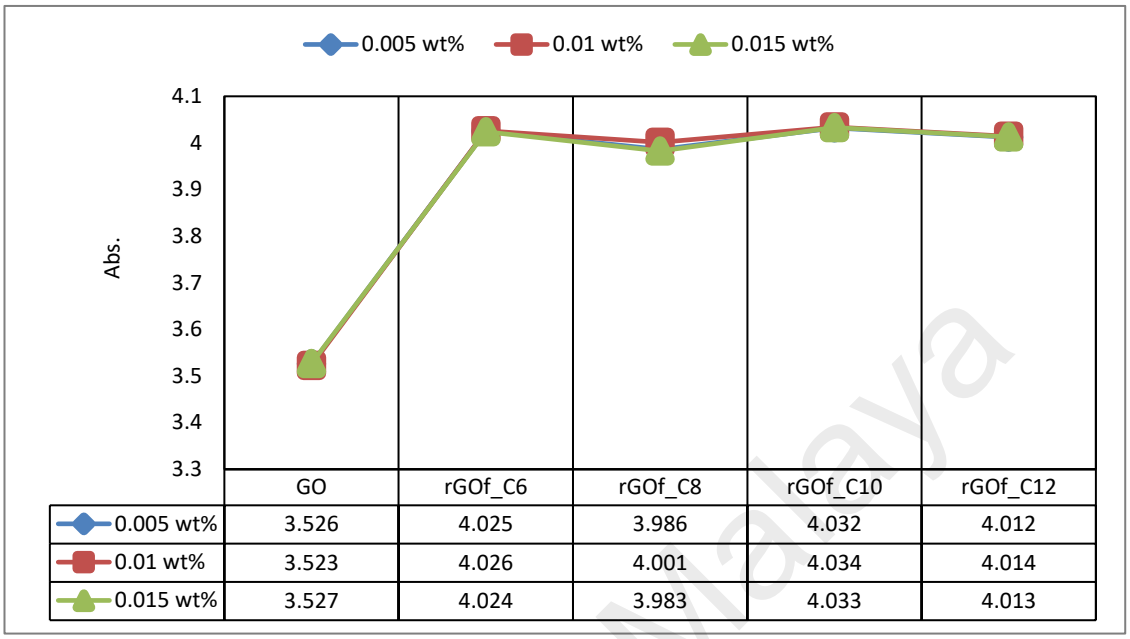

	GO	rGOf_C6	rGOf_C8	rGOf_C10	rGOf_C12
0.005 wt%	3.526	4.025	3.986	4.032	4.012
0.01 wt%	3.523	4.026	4.001	4.034	4.014
0.015 wt%	3.527	4.024	3.983	4.033	4.013

Figure 4.17: Absorbance of GO and rGO_f at different wt. % in the base oil

The absorbance of different samples at 300 nm is shown in Figure 4.17. From Figure 4.17, the rGO_f_C10 with 0.01 wt. % in base oil have the maximum absorbance value. When comparing the absorbance between all rGO_f with GO, it can be seen clearly that the absorbance of GO was much lower, indicating that its dispersion stability in base oil is not good.

4.6 Results for lube oil properties test

For lube oil properties test, three different wt. % of four different rGO_f namely rGO_f_C6, rGO_f_C8, rGO_f_C10, and rGO_f_C12 in base oil were prepared.

4.6.1 Viscosity analysis

Table 4.3 shows the kinematic viscosity base oil prior to additives addition and after addition of additives at test temperatures of 40 and 100 °C. From the results obtained, there is no significant difference in kinematic viscosity before and after addition of additives. The viscosity slightly increases when the base oil was added with synthesised

rGO_f. The kinematic viscosity of base oil at 40 and 100 °C are 98.902 and 11.679 mm^2/s respectively. However, for rGO_f_C6 at 0.015 wt.% and rGO_f_C8 at both 0.01 and 0.015 wt. %, there are no difference in viscosity when compared to the viscosity of only base oil.

Table 4.3: Kinematic viscosity at 40 and 100 °C and Viscosity Index (VI) of base oil with and without the addition of synthesised additives at different concentration

Sample	Concentration in base oil (wt. %)	Viscosity (mm^2/s)		Viscosity Index (VI)
		At 40°C	At 100°C	
Base oil	0	98.9	11.7	106
Base oil + rGO_f_C6	0.005	99.0	11.7	106
	0.01	99.2	11.7	107
	0.015	98.9	11.7	107
Base oil + rGO_f_C8	0.005	98.7	11.7	106
	0.01	98.9	11.7	107
	0.015	98.9	11.7	107
Base oil + rGO_f_C10	0.005	99.0	11.7	106
	0.01	99.9	11.8	107
	0.015	98.7	11.7	107
Base oil + rGO_f_C12	0.005	99.1	11.7	106
	0.01	99.4	11.7	107
	0.015	98.7	11.7	107

Generally, the viscosity of oil increases with molecular weight, and decreases with unsaturation level. Besides that, the viscosity of oil also affected by the dispersion of additives particles in the oil. Higher viscosity of oil can be attributed to the fact that the

additives particles in oil broke up any agglomerates particles and dispersed the particles well (Su *et al.*, 2016) and vice versa. This can be possible explanation base oil with rGO_f_C6 at 0.015 wt.% and rGO_f_C8 at both 0.01 and 0.015 wt. % have same viscosity with base oil without any additives.

Meanwhile, for the base oil with the other rGO_f at different concentrations, a slight increase of viscosity was observed and shown in Table 4.3. It is known that the chain lengths, saturation and unsaturation of chain influence the viscosity. It is well known that the oil containing additive with greater chain length has greater viscosity since the force of van der Waals grows with the particle size (Barrett & Williams, 2012; Gros & Feuge, 1952).

In general, the viscosity of lubricating oils is extremely sensitive to the operating temperature. When the temperature increases, the viscosity of oils decreases very quickly. The VI of the base oil before and after the addition of four different synthesised rGO_f at different concentrations are reported in Table 4.3. The VI of oil is a number that signifies the result of temperature changes on its viscosity. A low VI indicates a relatively large change in viscosity and a high VI indicates a relatively little change in viscosity over a wide range of temperatures. In simple words, the oil turns out to be extremely thin at high temperatures and extremely thick at low temperatures (Stachowiak & Batchelor, 2013).

Slight changes in the VI can be observed between base oil with and without the addition of rGO_f. However, there is no difference between the VI of base oil with base oil added with only 0.005 wt. % rGO_f. Increased in the value of VI were observed for all the four different rGO_f at concentration of 0.01 wt. % and 0.015 wt. %. From the results, it shows that the VI increases as the concentration of additive load increases. The VI was slightly higher when rGO_f was added in the base oil. The viscosity of liquids having high

VI changes very little with temperature. This is highly desired in the application as lubricants.

4.6.2 Density analysis

In general, the density of lubricant, mainly hydrocarbons, differs in the range of 0.860 g/cm^3 to 0.980 g/cm^3. Table 4.4 compares the density at 15 °C between base oil with and without the addition of rGO_f.

Table 4.4: Density of base oil with and without the addition of synthesised additive at 15 °C

Sample	Concentration in base oil (wt. %)	Density at 15 °C (g/cm^3)
Base oil	0	0.868
rGO_f_C6	0.005	0.869
	0.01	0.871
	0.015	0.871
rGO_f_C8	0.005	0.869
	0.01	0.871
	0.015	0.871
rGO_f_C10	0.005	0.870
	0.01	0.872
	0.015	0.872
rGO_f_C12	0.005	0.870
	0.01	0.871
	0.015	0.871

From the results obtained, it shows that the density of base oil with the addition of rGO_f was slightly increased. It can be due to the increased in the number of hydrocarbons in the base oil with rGO_f (Gros & Feuge, 1952). Density is also one of the nature of the entire system for lube oil which will significantly influences both the interaction between additive particles and those between the additive particles and the base oil (Spalla & Kékicheff, 1997). Therefore, similar to viscosity, density of oil also affected by the dispersion and concentration of additive particles in the oil (Z. J. Zhang *et al*., 2014). This can be possible explanation for the results which shows a slight increase in the density with increase in concentration of rGO_f in the base oil.

4.6.3 Oxidation stability by Rotating Pressure Vessel Oxidation Test, RPVOT

RPVOT was carried out to compare the oxidation stability of base oil with and without the addition of the synthesised additives. Since oxidation is a critical mode of lube oil degradation, it is therefore very important to make sure the synthesised FM does not lead to increase in oxygen concentration that will, in turn, lead to low oxidation stability.

Table 4.5: The oxidation stability of base oil with and without the addition of 0.01 wt. % rGO_f

Sample	Oxidation stability (mins)
Base oil	176
Base oil + 0.01 wt. % rGO_f_C6	178
Base oil + 0.01 wt. % rGO_f_C8	177
Base oil + 0.01 wt. % rGO_f_C10	179
Base oil + 0.01 wt. % rGO_f_C12	178

The RPVOT results shown in Table 4.5 demonstrates that there are no critical changes to the oxidation stability of base oil with and without the addition of synthesised rGO_f.

Thus, it is convinced that the rGO_f added in the base oil will not lead to an increase in the oxidation reaction.

4.6.4 Water content analysis by Karl Fischer, KF

Water truly harms the properties of lubrication oil and enhances corrosion (Scholz, 2012). Water will increase the rate of wear and friction and if left unchecked, water will result in premature machine failure. The KF titration method by ASTM D6304 was carried out to further quantify the amount of water when synthesised additives were added in the base oil. Results are reported as either percent by mass or parts-per-million (ppm). These units are easily converted by recognizing that 1 % = 10,000 ppm (Scholz, 2012).

Table 4.6: Water content of four different rGO_f in base oil

Sample		Parts-per-million (ppm)	Percent by mass (%)
rGO_f_C6	0.005 wt. %	42.9	0.004
	0.01 wt. %	43.1	0.004
	0.015 wt. %	43.1	0.004
rGO_f_C8	0.005 wt. %	43.0	0.004
	0.01 wt. %	43.1	0.004
	0.015 wt. %	43.2	0.004
rGO_f_C10	0.005 wt. %	43.3	0.004
	0.01 wt. %	42.8	0.004
	0.015 wt. %	42.9	0.004
rGO_f_C12	0.005 wt. %	43.5	0.004
	0.01 wt. %	44.5	0.004
	0.015 wt. %	44.1	0.004

In most of the systems, the water content should not be higher than 500 ppm. Low levels of water (0.5 %) are typically the result of condensation. No significant difference of water content can be observed between all four different rGO_f at different wt. % in base oil as reported in Taable 4.6. After conversion from parts-per-million (ppm) to percent by mass (%), all the different wt. % of rGO_f have approximately the same value of water content, which is about 0.004 %.

4.6.5 Coefficient of Friction (CoF) analysis

The CoF data were collected after a four-ball friction test. The variation of CoF with different concentrations of the synthesised additives in the base oil was measured by applying 400 N load. Figure 4.21 presents the CoF as a function of time for base oil with and without the addition of rGOf at different concentrations.

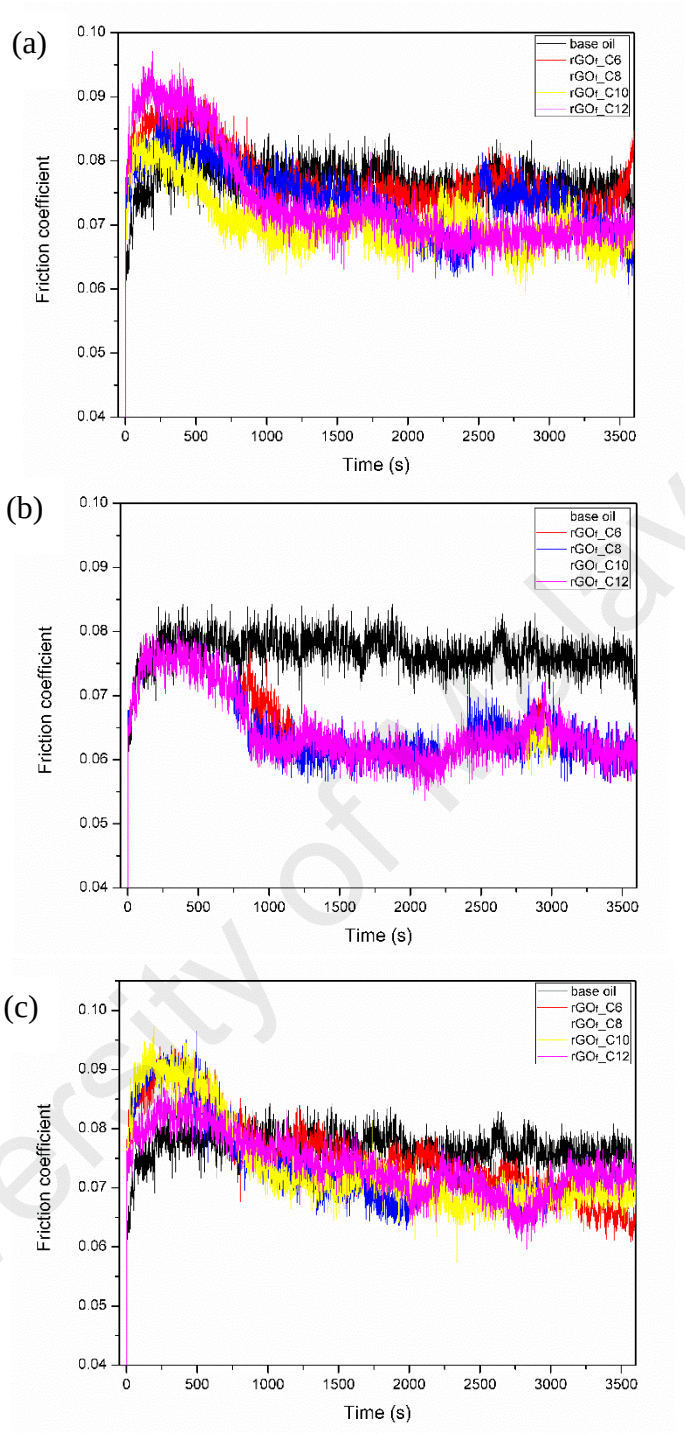

Figure 4.18: CoF of four different rGO_f at the concentration of (a) 0.005 wt. % (b) 0.01 wt. % and (c) 0.015 wt. % in the base oil

Figure 4.21 presents the CoF as a function of time for base oil with and without the addition of rGO_f at different concentrations. The results of CoF for base oil with and without all the four different rGO_f at different wt. % are summarised in Figure 4.22.

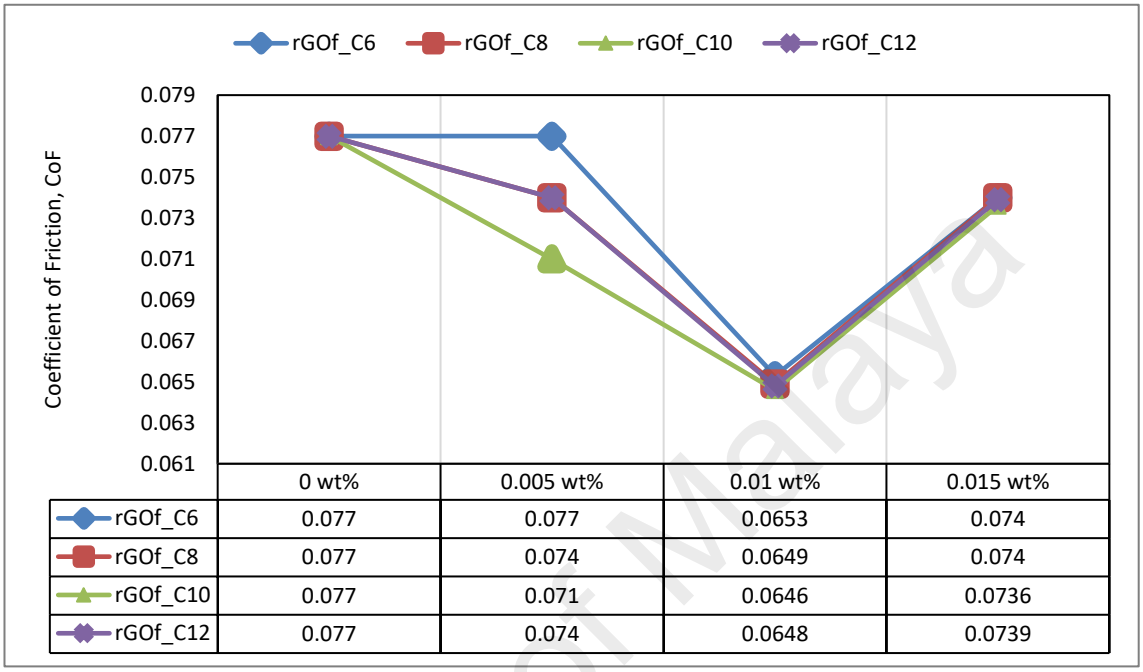

	0 wt%	0.005 wt%	0.01 wt%	0.015 wt%
rGOf_C6	0.077	0.077	0.0653	0.074
rGOf_C8	0.077	0.074	0.0649	0.074
rGOf_C10	0.077	0.071	0.0646	0.0736
rGOf_C12	0.077	0.074	0.0648	0.0739

Figure 4.19: Coefficient of friction of base oil at different wt. % of additives addition

Figure 4.22 shows the CoF of four different rGO_f as a function of additive concentration in the base oil. The experiments were repeated three times with fixed load to check its stability of the CoF value. From the results presented in Appendix A-1, which shows the variation of mean and standard variation value, it can be noted that the lubricant yielded consistent CoF value over multiple runs with the maximum deviation of 7.662 x 10^{-3}.

It can be seen clearly that all the four different rGO_f synthesised have almost the same trend on reduction in friction depending on their concentration in base oil. It is also clear that all these synthesised rGO_f causes a reduction in the CoF of the additive-added lubricant when compared to base oil without any rGO_f. The longer the chain length of the alkyl group attached to the rGO_f results in a lower CoF value (Havet *et al.*, 2001).

However, the CoF starts to increase when longer chain length of the alkyl group with 12 carbon number (C12) was attached to rGO_f.

From the results of CoF shown in Figure 4.22, it clearly proves that the concentration of rGO_f added in the base oil also causes a different reduction in CoF. It can be seen that the best concentration of rGO_f in base oil is when they are added with 0.01wt. % where it can be observed that they show the highest reduction in friction. Three different concentrations of rGO_f in base oil were prepared, and all the three differently prepared concentrations showed a reduction in CoF after the four-ball test with 400 N applied force. The highest reduction of CoF can be seen when 0.01wt. % of rGO_f were added into the base oil. It can be due to the optimum concentration of rGO_f added which is able to embed into the worn surfaces and the pan furrows on the metal surface were filled with additives. The boundary film becomes thicker and smoother, thus reducing friction between contacting metal surfaces.

At slightly lower and higher concentration of rGO_f in base oil which is 0.005 wt. % and 0.015 wt. % respectively, the reduction in CoF is very low. At concentration of 0.005 wt. %, very small reduction in CoF can be due to not enough additives to cover the metal surfaces from direct metal to metal contact that results in friction.

4.6.6 Wear rate analysis

Mass loss measurement is a convenient method for wear measurement, especially when the worn surface is irregular and unsymmetrical in shape. The difference in weight before and after the test represents the weight loss caused by wear. Wear rates are calculated and the results reflect wear mass loss under unit applied normal force (Stachowiak & Batchelor, 2013).

$$wear\ rate = \frac{mass\ loss\ (g)}{applied\ force\ (N)}$$ (**Equation 4.1)**

Table 4.7: The difference in wear rate with different wt. % of rGO_f in base oil

Sample	Wt. % in base oil	Weight before test (g)	Weight after test (g)	Mass loss (g)	Wear rate (g/N) x 10^{-4}
Base oil	0.00	8.4	8.3531	0.0469	1.196
rGO_f_C6	0.005	8.4	8.3562	0.0438	1.117
	0.01	8.4	8.3603	0.0397	1.012
	0.015	8.4	8.3559	0.0441	1.124
rGO_f_C8	0.005	8.4	8.3577	0.0423	1.078
	0.01	8.4	8.3604	0.0396	1.010
	0.015	8.4	8.3562	0.0438	1.117
rGO_f_C10	0.005	8.4	8.3595	0.0405	1.032
	0.01	8.4	8.3609	0.0391	0.997
	0.015	8.4	8.3587	0.0413	1.053
rGO_f_C12	0.005	8.4	8.3584	0.0416	1.061
	0.01	8.4	8.3606	0.0394	1.004
	0.015	8.4	8.3561	0.0439	1.119

Comparison of wear rate between all prepared samples is tabulated in Table 4.7. From Figure 4.23, it can be clearly observed that the lowest wear rate was achieved when 0.01 wt. % of rGO_f_C10 was introduced into the base oil.

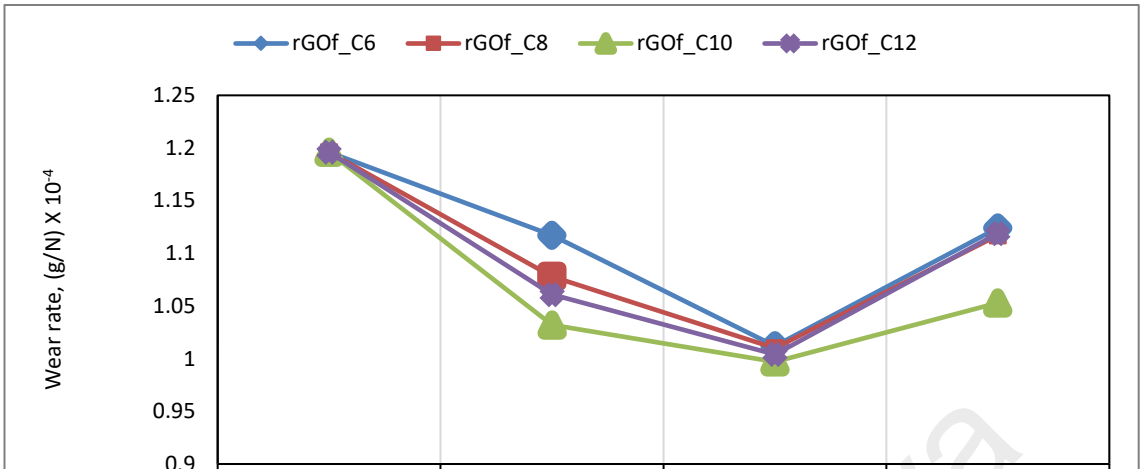

	0 wt%	0.005 wt%	0.01 wt%	0.015 wt%
rGOf_C6	1.196	1.117	1.012	1.124
rGOf_C8	1.196	1.078	1.01	1.117
rGOf_C10	1.196	1.032	0.997	1.053
rGOf_C12	1.196	1.061	1.004	1.119

Figure 4.20: Wear rate of base oil at different wt. % of additives addition

By comparing the wear rate behaviour of four different rGO_f at three different weight percentages in base oil for each product, it can be seen that at a concentration of 0.01 wt. % in base oil, all the four different rGO_f showed lower wear rate when compared to other concentrations. It proved that the wear process that takes place are slower and will result in smaller wear on metal surfaces.

4.6.7 Wear Scar Diameter (WSD) analysis

In relation with average CoF obtained previously, the addition of rGO_f in base oil also has a direct impact on their wear scar diameter (WSD). From the SEM metallographs of wear surfaces on the steel balls used in four-ball test, the average wear scar diameter (WSD) were measured. Wear scar diameter (WSD) of the steel ball was set as the benchmark to calculate the reduction in WSD after the addition of four different rGO_f at three different wt. %.

SEM metallographs of wear surface for rGO_f_C6 at different wt. % are shown in Figure 4.24 together with their average WSD.

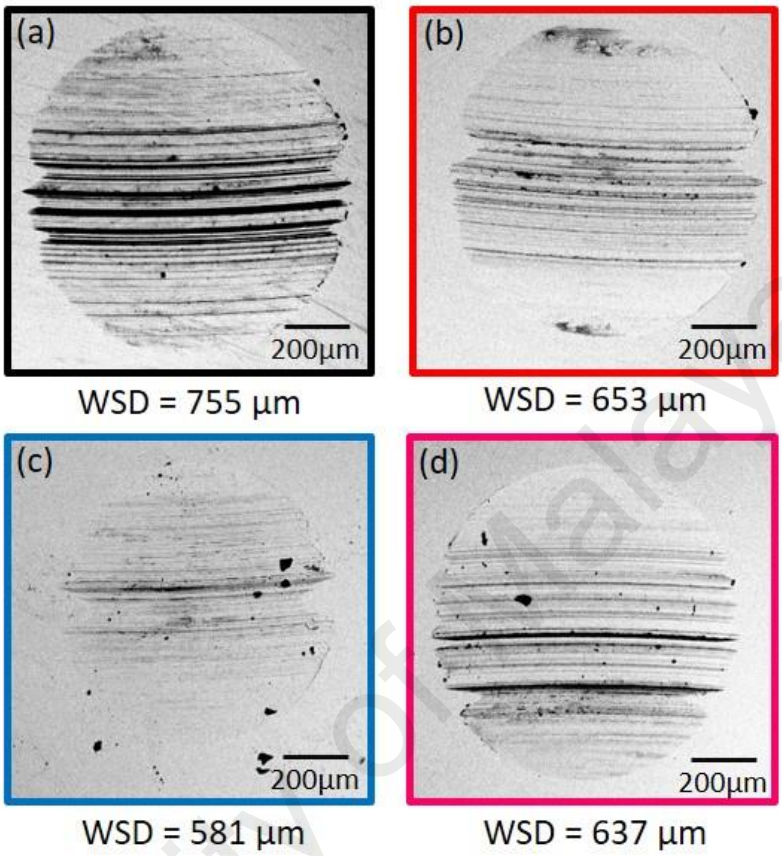

Figure 4.21: SEM metallographs of wear surfaces with rGO_f_C6 at different wt% in base oil (a) base oil (b) 0.005 wt. % (c) 0.01 wt. % (d) 0.015 wt. %

When compared to the WSD of base oil, all the three different wt. % of rGO_f_C6 showed significantly smaller WSD. The smallest WSD can be observed with the use of 0.01 wt. % that gave the highest reduction of WSD, which is about 23 %. For WSD with 0.005 wt. % and 0.015 wt. %, their reductions of WSD were 14 % and 16 % respectively.

Figure 4.25 shows the SEM metallographs of wear surface for rGO_f_C8 at different wt. % together with their average WSD.

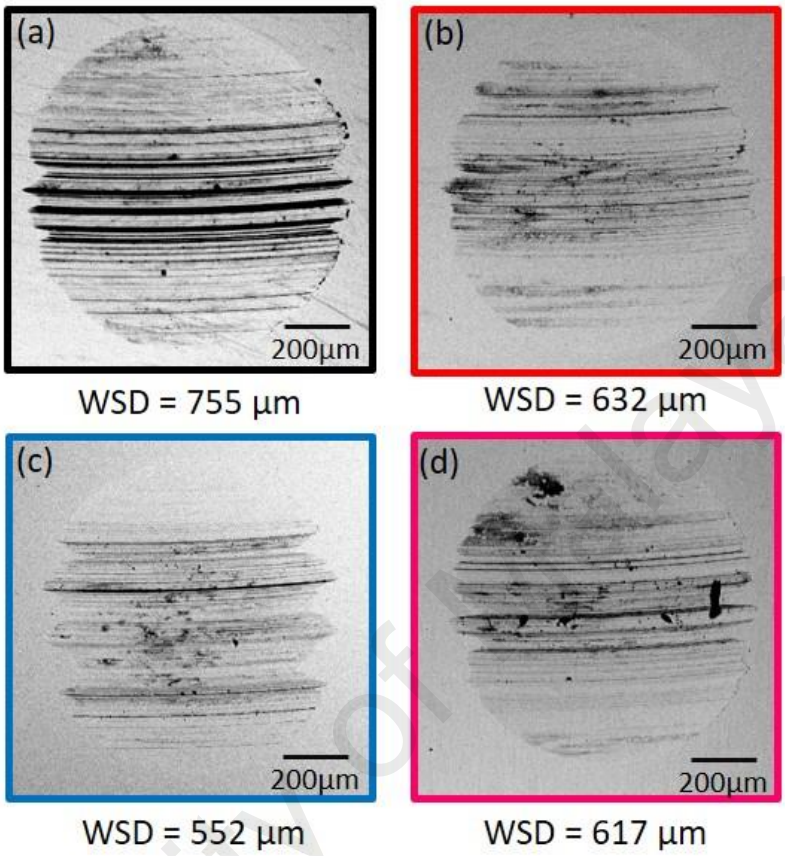

Figure 4.22: SEM metallographs of wear surfaces with rGO_f_C8 at different wt. % in base oil (a) base oil (b) 0.005 wt. % (c) 0.01 wt. % (d) 0.015 wt. %

When compared to the WSD of base oil, all the three different wt. % of rGO_f_C8 showed significantly smaller WSD. The smallest WSD can be observed with the use of 0.01 wt. % that gave the highest reduction of WSD, which is about 27 %. For WSD with 0.005 wt. % and 0.015 wt. %, their reductions of WSD were 16 % and 18 % respectively.

SEM metallographs of wear surface for rGO_f_C10 at different wt. % were shown in Figure 4.26, together with their average WSD.

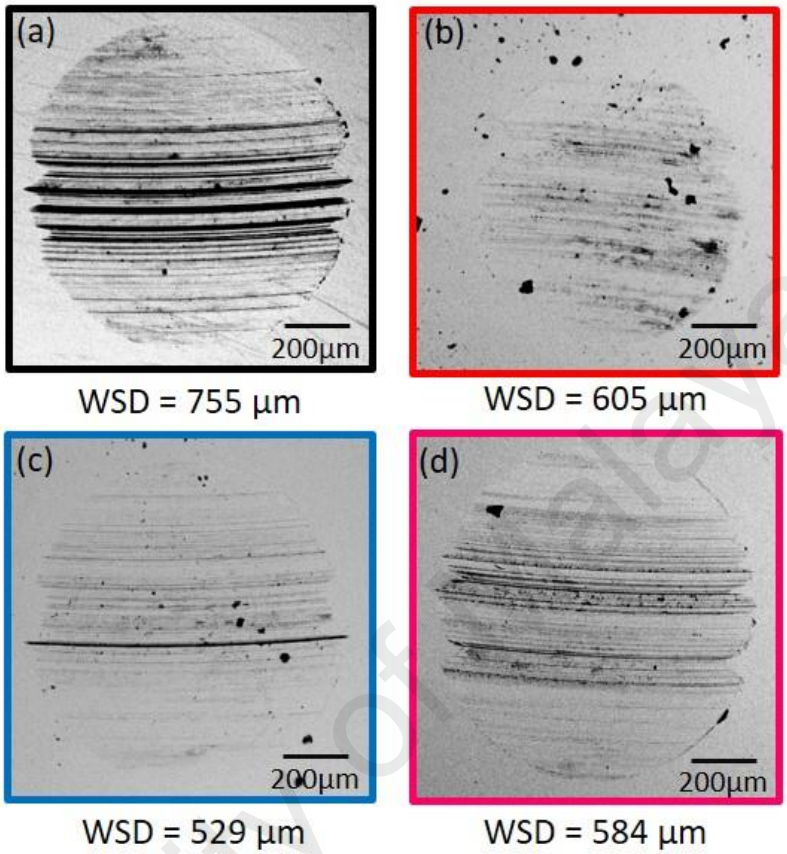

Figure 4.23: SEM metallographs of wear surfaces with rGO_f_C10 at different wt. % in base oil (a) base oil (b) 0.005 wt. % (c) 0.01 wt. % (d) 0.015 wt. %

When compared to the WSD of base oil, all the three different wt. % of rGO_f_C10 showed significantly smaller WSD. The smallest WSD can be observed with the use of 0.01 wt. % that gave the highest reduction of WSD, which is about 30 %. For WSD with 0.005 wt. % and 0.015 wt. %, their reductions of WSD were 20 % and 23 % respectively.

Figure 4.27 shows the SEM metallographs of wear surface for rGO_f_C12 at different wt. %, together with their average WSD.

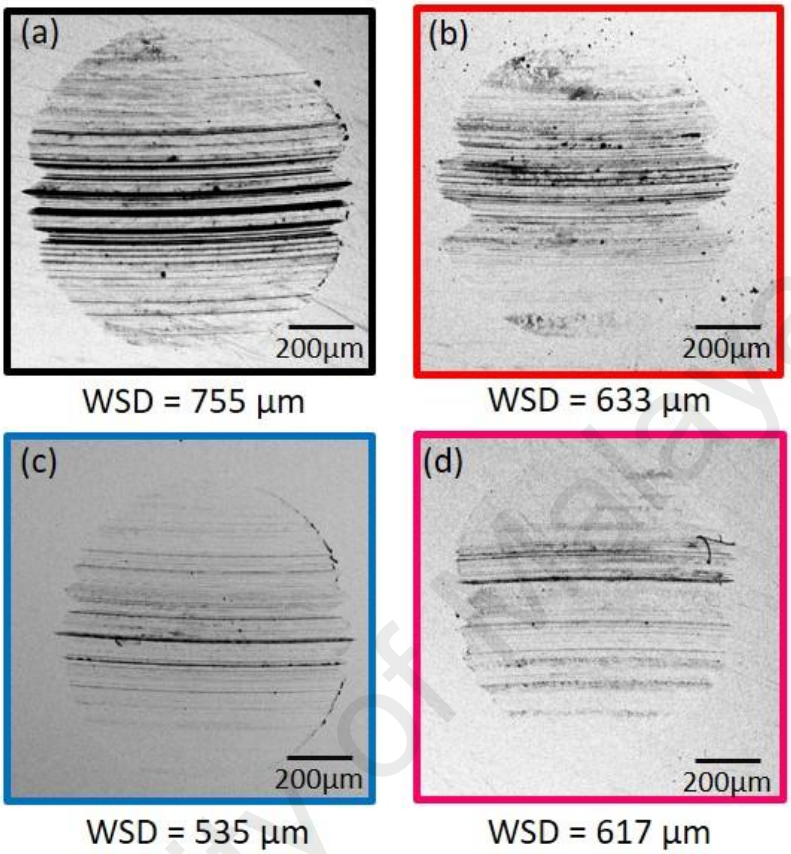

Figure 4.24: SEM metallographs of wear surfaces with rGO_f_C12 at different wt. % in base oil (a) base oil (b) 0.005 wt. % (c) 0.01 wt. % (d) 0.015 wt. %

When compared to the WSD of base oil, all the three different wt. % of rGO_f_C12 showed significantly smaller WSD. The smallest WSD can be observed with the used of 0.01 wt. % that gave the highest reduction of WSD, which is about 29 %. For WSD with 0.005 wt. % and 0.015 wt. %, their reductions of WSD were 16 % and 18 % respectively.

The trend in reduction of WSD for all the prepared samples can be clearly observed in Figure 4.28. Significant reduction of WSD for all the prepared samples can be observed when compared to the WSD of base oil without any addition of rGO_f.

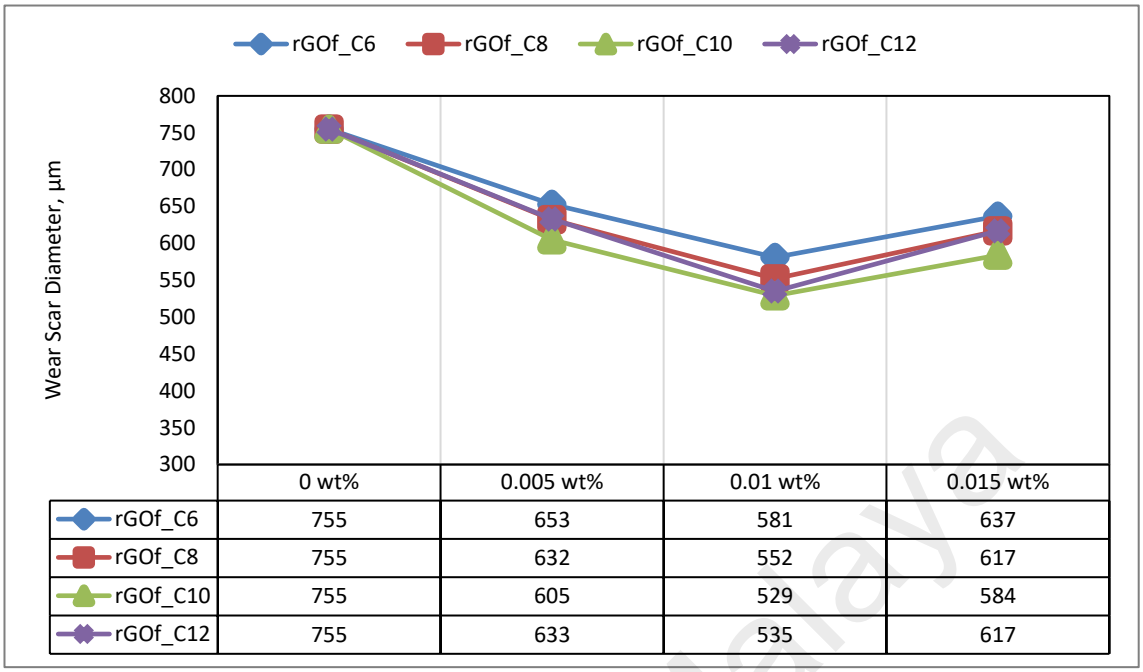

	0 wt%	0.005 wt%	0.01 wt%	0.015 wt%
rGOf_C6	755	653	581	637
rGOf_C8	755	632	552	617
rGOf_C10	755	605	529	584
rGOf_C12	755	633	535	617

Figure 4.25: Wear scar diameter (WSD) on steel ball after four-ball test for base oil at different wt. % of additives addition

From all the four different rGO_f, the highest reduction in WSD can be observed with the use of rGO_f_C10 at every different wt. %. The highest reduction of WSD was obtained with the use of 0.01 wt. % of rGOf_C10, which is about 30 %. The trend is the same with the trend in reduction of CoF reported previously.

Previous studies (Berman *et al.*, 2013a, 2013b) demonstrated the friction and wear properties of an unmodified graphene oxide. Using a fixed load (1 N), the results confirm that 0.1 to 3.0 wt. % of unmodified GO may also be used to lubricate by providing the CoF below 0.2. However, the wear rate stays at higher levels which results in large WSD (Berman *et al.*, 2014). When compared to the unmodified GO, the rGO_f which has been synthesised in this study have significantly better CoF and WSD reduction even with higher load applied (400 N).

Tribological test on GO nanosheets also have been carried out by Senatore et al. and the results are surprisingly excellent with the highest reduction in CoF and WSD are 16% and 30% respectively (Senatore *et al.*, 2013). It was reported that the highest reduction in

both CoF and WSD can be achieved with 0.1 wt. % of GO in oil, which claimed to be lower than the usual concentrations used with inorganic nanoadditives. The same excellent percentage of reduction can be achieved when much lower concentration (0.01 wt. %) of rGO_f was used as discussed in previous discussion. Senatore et al. also stated that the improvement in dispersion of GO in oil must be addressed in future works. Luckily, with the used of rGO_f which has been synthesised in this study, their dispersion in oil has been greatly improved as reported in the previous section.

CHAPTER 5: CONCLUSION AND RECOMMENDATIONS

5.1 Conclusion

The following conclusions were drawn based on the research objectives stated at the beginning.

1. Graphene oxide had been successfully synthesised using the improved Hummers method and confirmed by characterisation using FTIR, Raman, XRD, TGA and FESEM. From the FTIR result, the presence of oxygen-containing functional groups can be confirmed and it was similar as reported in the literature. The presence of defects in synthesised GO as the result of oxidation and exfoliation was confirmed by Raman. The interlayer spacing of graphite to graphene oxide was enlarged because of the presence of oxygen-containing functional groups, proved by XRD. From TGA, major mass loss of GO was observed in the range of 100-600 °C, indicating the decomposition of oxygen-containing functional groups. The morphology analysis by FESEM showed agglomeration of the exfoliated sheets with some wrinkles and folding on the surfaces, proving that oxidation and exfoliation of graphite to graphene oxide had taken place. Boehm titration test confirmed that the synthesised GO has high negative surface charge, indicating the high amount of COOH groups in GO.

2. An efficient covalent functionalization method to functionalize GO have been presented to improve the dispersion of GO in oil, that will lead to a highly oil-dispersed GO sheets. To functionalize GO involves three major steps. First is to synthesize alkyne-functionalized GO, GO_f. The GO_f was successfully synthesised and had been confirmed using FTIR. From the results obtained, the FTIR spectra proved

the presence of alkyne groups attached on GO. The second step is to synthesise four different azide-functionalized alkyls and the presence of azide groups was confirmed by FTIR. Lastly, the click coupling between GO_f and azide-functionalized alkyl gave rGO_f as the final product. The success in functionalization of GO to get rGO_f have been confirmed with characterisation using FTIR, Raman, XRD, FESEM/EDX and also TGA. The FTIR confirmed the presence of triazole ring as the result of ring closure between alkyne and azide groups. The decrease in carbon qualities and increase in crystallite sizes after functionalization was observed using Raman. It proved that covalent bonding occurred on the surface of GO. Supported by XRD, it showed that the interlayer spacing of rGO_f was reduced due to the presence of organic moiety that was introduced on the GO. The morphology analysis of rGO_f by FESEM showed fluffy aggregates of organic moiety on their surfaces and EDX analysis confirmed the presence of element N proved that the rGO_f had been decorated with a triazole ring.

Four different reduced-functionalized graphene oxide, rGO_f synthesised successfully improved their dispersibility in base oil when compared with GO in the base oil. Simple dispersibility test was carried out for one month and proved that the dispersibility of all the four rGO_f was improved. From the result of UV-visible, the synthesised rGO_f have better absorption when compared to GO, indicating that it has better dispersibility in the base oil.

3. The tribology tests confirmed a good reduction in friction and wear can be accomplished with base oil formulated with functionalized graphene oxide. Their good friction properties also tribute to good anti-wear properties. Different rGO_f with

variations in their alkyl chain gives different values of CoF and WSD. The highest reduction in both CoF and WSD can be seen with the use of C10 attached on rGO_f. The CoF and WSD were also influenced by the concentration of synthesised additives added into the base oil. The highest reduction in CoF and WSD may be achieved when 0.01 wt. % of rGO_f were used. The recorded reduction of CoF and WSD were 16 % and 30 % respectively. The outcomes apparently confirmed that graphene sheets in oil create protective films with ease to avoid the rubbing surfaces from coming into direct contact and, by that, completely enhances the tribology behaviour of the oil.

5.2 Recommendations for future work

Though this study has provided good lubrication properties of functionalized graphene oxide as FM additives, there is still a need for further study on these achievements. This includes:

1. The synthesised rGO_f shows significant improvement in friction and wear properties at mild conditions with constant temperature, pressure, and load. Further studies on the effectiveness of rGO_f when extreme conditions are applied as friction and wear improver can be done in future works by varying the conditions (temperature, pressure, time, load) for lubrication test.
2. To investigate the applicability and compatibility of the synthesised additives, rGO_f with other additives, for example anti-oxidant and anti-corrosion additives in the base oil.

REFERENCES

Ackermann, L., & Potukuchi, H. K. (2010). Regioselective syntheses of fully-substituted 1, 2, 3-triazoles: the CuAAC/C–H bond functionalization nexus. *Organic & biomolecular chemistry, 8*(20), 4503-4513.

Alexander, P., & Michael, G. (2004). Water-graphite interaction and behavior of water near the graphite surface. *J Phys Chem B, 108*. doi:10.1021/jp0356968

Angell, Y. L., & Burgess, K. (2007). Peptidomimetics via copper-catalyzed azide–alkyne cycloadditions. *Chemical Society Reviews, 36*(10), 1674-1689.

Appukkuttan, P., Dehaen, W., Fokin, V. V., & Van der Eycken, E. (2004). A microwave-assisted click chemistry synthesis of 1, 4-disubstituted 1, 2, 3-triazoles via a copper (I)-catalyzed three-component reaction. *Organic letters, 6*(23), 4223-4225.

Barrett, M., & Williams, K. (2012). Oil Analysis. *Materials Evaluation, 70*(1), 32-40.

Berman, D., Erdemir, A., & Sumant, A. V. (2013a). Few layer graphene to reduce wear and friction on sliding steel surfaces. *Carbon, 54*, 454-459.

Berman, D., Erdemir, A., & Sumant, A. V. (2013b). Reduced wear and friction enabled by graphene layers on sliding steel surfaces in dry nitrogen. *Carbon, 59*, 167-175.

Berman, D., Erdemir, A., & Sumant, A. V. (2014). Graphene: a new emerging lubricant. *Materials Today, 17*(1), 31-42.

Bhushan, B., & Gupta, B. K. (1991). Handbook of tribology: materials, coatings, and surface treatments.

Binder, W. H., & Kluger, C. (2006). Azide/alkyne-"click" reactions: applications in material science and organic synthesis. *Current Organic Chemistry, 10*(14), 1791-1815.

Blau, P. J. (2001). The significance and use of the friction coefficient. *Tribology International, 34*(9), 585-591.

Bock, V. D., Hiemstra, H., & Van Maarseveen, J. H. (2006). CuI-Catalyzed Alkyne–Azide "Click" Cycloadditions from a Mechanistic and Synthetic Perspective. *European Journal of Organic Chemistry, 2006*(1), 51-68.

Boehm, H. P. (2002). Surface oxides on carbon and their analysis: a critical assessment. *Carbon, 40*(2), 145-149. doi:http://dx.doi.org/10.1016/S0008-6223(01)00165-8

Boger, D. L. (1986). Diels-Alder reactions of heterocyclic aza dienes. Scope and applications. *Chemical Reviews, 86*(5), 781-793.

Bonard, J.-M., Dean, K. A., Coll, B. F., & Klinke, C. (2002). Field emission of individual carbon nanotubes in the scanning electron microscope. *Physical review letters, 89*(19), 197602.

Boren, B. C., Narayan, S., Rasmussen, L. K., Zhang, L., Zhao, H., Lin, Z., . . . Fokin, V. V. (2008). Ruthenium-catalyzed azide− alkyne cycloaddition: scope and mechanism. *Journal of the American Chemical Society, 130*(28), 8923-8930.

Bovington, C. (1997). Friction, wear and the role of additives in their control *Chemistry and Technology of Lubricants* (pp. 320-348): Springer.

Bowden, F. P., & Tabor, D. (2001). *The friction and lubrication of solids* (Vol. 1): Oxford university press.

Braithwaite, E., & Rowe, G. (1963). Principles and applications of lubrication with solids. *Industrial Lubrication and Tribology, 15*(3), 92-111.

Braithwaite, E. R. (2013). *Solid lubricants and surfaces*: Elsevier.

Buckley, D. H. (1981). *Surface effects in adhesion, friction, wear, and lubrication* (Vol. 5): Elsevier.

Bunch, J. S., Verbridge, S. S., Alden, J. S., Van Der Zande, A. M., Parpia, J. M., Craighead, H. G., & McEuen, P. L. (2008). Impermeable atomic membranes from graphene sheets. *Nano letters, 8*(8), 2458-2462.

Campbell, M., Loser, J. B., & Sneegas, E. (1966). *Solid Lubricants*. Retrieved from

Cao, Y., Lai, Z., Feng, J., & Wu, P. (2011). Graphene oxide sheets covalently functionalized with block copolymers via click chemistry as reinforcing fillers. *Journal of Materials Chemistry, 21*(25), 9271-9278.

Charlier, J.-C., Michenaud, J.-P., Gonze, X., & Vigneron, J.-P. (1991). Tight-binding model for the electronic properties of simple hexagonal graphite. *Physical Review B, 44*(24), 13237.

Chen, G., Hu, Z., Nai, R., Wang, L., Peng, Y., & Dong, J. (2001). Preparation and tribology of ultrafine and amorphous strontium borate. *Proceedings of the Institution of Mechanical Engineers, Part L: Journal of Materials Design and Applications, 215*(3), 133-140.

Chen, J., Yao, B., Li, C., & Shi, G. (2013a). An improved Hummers method for eco-friendly synthesis of graphene oxide. *Carbon, 64*, 225-229.

Chen, Q., Wang, X., Wang, Z., Liu, Y., & You, T. (2013b). Preparation of water-soluble nanographite and its application in water-based cutting fluid. *Nanoscale research letters, 8*(1), 1-8. doi:10.1186/1556-276x-8-52

Colyer, C., & Gergel, W. (1997). Detergents and dispersants *Chemistry and technology of lubricants* (pp. 75-97): Springer.

Crawford, J., & Psaila, A. (1992). In RM Mortier and ST Orszulik, eds. *Chemistry and Technology of Lubricants, Miscellaneous Additives and Vegetable Oils*, 181-187.

Crawford, J., Psaila, A., & Orszulik, S. (1997). Miscellaneous additives and vegetable oils *Chemistry and Technology of Lubricants* (pp. 181-202): Springer.

Díez-González, S. (2011). Well-defined copper (I) complexes for Click azide–alkyne cycloaddition reactions: one Click beyond. *Catalysis Science & Technology, 1*(2), 166-178.

Dondoni, A. (2007). Triazole: the keystone in glycosylated molecular architectures constructed by a click reaction. *Chemistry–An Asian Journal, 2*(6), 700-708.

Dreyer, D. R., Park, S., Bielawski, C. W., & Ruoff, R. S. (2010). The chemistry of graphene oxide. *Chemical Society Reviews, 39*(1), 228-240.

Dwivedi, D. (2010). Adhesive wear behaviour of cast aluminium–silicon alloys: overview. *Materials & Design, 31*(5), 2517-2531.

Feeny, B., Guran, A., Hinrichs, N., & Popp, K. (1998). A historical review on dry friction and stick-slip phenomena. *Applied Mechanics Reviews, 51*(5), 321-341.

Freeman, J., & Smith, M. (1958). The preparation of anhydrous inorganic chlorides by dehydration with thionyl chloride. *Journal of Inorganic and Nuclear Chemistry, 7*(3), 224-227.

Gabbott, P. (2008). *Principles and applications of thermal analysis*: John Wiley & Sons.

Gaylord, N. G. (1957). Reduction with complex metal hydrides. *J. Chem. Educ, 34*(8), 367.

Goldstein, J., Newbury, D. E., Echlin, P., Joy, D. C., Romig Jr, A. D., Lyman, C. E., . . . Lifshin, E. (2012). *Scanning electron microscopy and X-ray microanalysis: a text for biologists, materials scientists, and geologists*: Springer Science & Business Media.

Gros, A. T., & Feuge, R. O. (1952). Surface and interfacial tensions, viscosities, and other physical properties of some n-aliphatic acids and their methyl and ethyl esters. *Journal of the American Oil Chemists Society, 29*(8), 313-317. doi:10.1007/bf02639809

Hakimi, M., & Alimard, P. (2012). Graphene: synthesis and applications in biotechnology-a review.

Hansen, T. V., Wu, P., Sharpless, W. D., & Lindberg, J. G. (2005). Just click it: undergraduate procedures for the copper (I)-catalyzed formation of 1, 2, 3-triazoles from azides and terminal acetylenes. *J. Chem. Educ, 82*(12), 1833.

Havet, L., Blouet, J., Valloire, F. R., Brasseur, E., & Slomka, D. (2001). Tribological characteristics of some environmentally friendly lubricants. *Wear, 248*(1), 140-146.

Hawker, C. J., & Wooley, K. L. (2005). The convergence of synthetic organic and polymer chemistries. *Science, 309*(5738), 1200-1205.

Haycock, R. F., Caines, A. J., & Hillier, J. E. (2004). *Automotive lubricants reference book* (Vol. 354): John Wiley & Sons.

Higginbotham, A. L., Kosynkin, D. V., Sinitskii, A., Sun, Z., & Tour, J. M. (2010). Lower-defect graphene oxide nanoribbons from multiwalled carbon nanotubes. *ACS nano, 4*(4), 2059-2069.

Hilton, M. R., & Fleischauer, P. D. (1993). *Lubricants for high-vacuum applications*. Retrieved from

Himo, F., Lovell, T., Hilgraf, R., Rostovtsev, V. V., Noodleman, L., Sharpless, K. B., & Fokin, V. V. (2005). Copper (I)-catalyzed synthesis of azoles. DFT study predicts unprecedented reactivity and intermediates. *Journal of the American Chemical Society, 127*(1), 210-216.

Holmberg, K., Andersson, P., & Erdemir, A. (2012). Global energy consumption due to friction in passenger cars. *Tribology International, 47*, 221-234.

Holmberg, K., & Erdemir, A. (2011). Global Impact of Friction on Energy Consumption, Economy and Environment.

Holmberg, K., Ronkainen, H., & Matthews, A. (2000). Tribology of thin coatings. *Ceramics International, 26*(7), 787-795.

Hu, W., Song, L., Wang, L., Hu, Y., & Zhang, P. (2014). Covalent functionalization of graphene oxide with flame retardant and its effect on thermal stability and flame retardancy of epoxy composites. *Fire Safety Science, 11*, 895-904.

Hu, Z., Dong, J., Chen, G., & He, J. (2000). Preparation and tribological properties of nanoparticle lanthanum borate. *Wear, 243*(1), 43-47.

Huang, H., Tu, J., Gan, L., & Li, C. (2006). An investigation on tribological properties of graphite nanosheets as oil additive. *Wear, 261*(2), 140-144.

Huang, X., Qi, X., Boey, F., & Zhang, H. (2012). Graphene-based composites. *Chemical Society Reviews, 41*(2), 666-686.

Huisgen, R. (1963). 1, 3-dipolar cycloadditions. Past and future. *Angewandte Chemie International Edition in English, 2*(10), 565-598.

Hummers Jr, W. S., & Offeman, R. E. (1958). Preparation of graphitic oxide. *Journal of the American Chemical Society, 80*(6), 1339-1339.

IJsselstijn, M., & Cintrat, J.-C. (2006). Click chemistry with ynamides. *Tetrahedron, 62*(16), 3837-3842.

Jahanmir, S., & Beltzer, M. (1986). An adsorption model for friction in boundary lubrication. *ASLE transactions, 29*(3), 423-430.

Jiang, W., Nadeau, G., Zaghib, K., & Kinoshita, K. (2000). Thermal analysis of the oxidation of natural graphite—effect of particle size. *Thermochimica Acta, 351*(1), 85-93.

Kappe, C. O., & Van der Eycken, E. (2010). Click chemistry under non-classical reaction conditions. *Chemical Society Reviews, 39*(4), 1280-1290.

Kashyap, S., Mishra, S., & Behera, S. K. (2014). Aqueous Colloidal Stability of Graphene Oxide and Chemically Converted Graphene. *Journal of Nanoparticles, 2014*, 6. doi:10.1155/2014/640281

Kaur, R. G., Higgs III, C., & Heshmat, H. (2001). Pin-on-disc tests of pelletized molybdenum disulfide. *Tribology Transactions, 44*(1), 79-87.

Kenbeck, D., & Bunemann, T. F. (2009). Organic friction modifiers *Lubricant Additives: Chemistry and Applications, Second Edition* (pp. 195-210): CRC Press.

Khatri, P. K., Joshi, C., Thakre, G. D., & Jain, S. L. (2016). Halogen-free ammonium-organoborate ionic liquids as lubricating additives: the effect of alkyl chain lengths on the tribological performance. *New Journal of Chemistry, 40*(6), 5294-5299. doi:10.1039/C5NJ02225H

Kohl, H., & Reimer, L. (2008). *Transmission Electron Microscopy: Physics of Image Formation*: Springer-Verlag New York.

Kolb, H. C., Finn, M., & Sharpless, K. B. (2001). Click chemistry: diverse chemical function from a few good reactions. *Angewandte Chemie International Edition, 40*(11), 2004-2021.

Kosynkin, D. V., Higginbotham, A. L., Sinitskii, A., Lomeda, J. R., Dimiev, A., Price, B. K., & Tour, J. M. (2009). Longitudinal unzipping of carbon nanotubes to form graphene nanoribbons. *Nature, 458*(7240), 872-876.

Kou, L., He, H., & Gao, C. (2010). Click chemistry approach to functionalize two-dimensional macromolecules of graphene oxide nanosheets. *Nano-Micro Letters, 2*(3), 177-183.

Lawal, S., Choudhury, I., & Nukman, Y. (2012). Application of vegetable oil-based metalworking fluids in machining ferrous metals—a review. *International Journal of Machine Tools and Manufacture, 52*(1), 1-12.

Layek, R. K., & Nandi, A. K. (2013). A review on synthesis and properties of polymer functionalized graphene. *Polymer, 54*(19), 5087-5103.

Lee, C., Li, Q., Kalb, W., Liu, X.-Z., Berger, H., Carpick, R. W., & Hone, J. (2010). Frictional characteristics of atomically thin sheets. *Science, 328*(5974), 76-80.

Lin, J., Wang, L., & Chen, G. (2011). Modification of graphene platelets and their tribological properties as a lubricant additive. *Tribology Letters, 41*(1), 209-215.

Liu, D., & Bielawski, C. W. (2016). Direct azidation of isotactic polypropylene and synthesis of ‘grafted to’ derivatives thereof using azide–alkyne cycloaddition chemistry. *Polymer International*, n/a-n/a. doi:10.1002/pi.5180

Liu, G., Li, X., Qin, B., Xing, D., Guo, Y., & Fan, R. (2004). Investigation of the mending effect and mechanism of copper nano-particles on a tribologically stressed surface. *Tribology Letters, 17*(4), 961-966.

Liu, Z., Robinson, J. T., Sun, X., & Dai, H. (2008). PEGylated nanographene oxide for delivery of water-insoluble cancer drugs. *Journal of the American Chemical Society, 130*(33), 10876-10877.

Loh, K. P., Bao, Q., Ang, P. K., & Yang, J. (2010). The chemistry of graphene. *Journal of Materials Chemistry, 20*(12), 2277-2289.

Ludema, K. C. (1996). *Friction, wear, lubrication: a textbook in tribology*: CRC press.

Luong, N. D., Sinh, L. H., Johansson, L. S., Campell, J., & Seppälä, J. (2015). Functional Graphene by Thiol-ene Click Chemistry. *Chemistry–A European Journal, 21*(8), 3183-3186.

Lutz, J. F. (2007). 1, 3-Dipolar cycloadditions of azides and alkynes: a universal ligation tool in polymer and materials science. *Angewandte Chemie International Edition, 46*(7), 1018-1025.

Lutz, J. F. (2008). Copper-Free Azide–Alkyne Cycloadditions: New Insights and Perspectives. *Angewandte Chemie International Edition, 47*(12), 2182-2184.

Majireck, M. M., & Weinreb, S. M. (2006). A study of the scope and regioselectivity of the ruthenium-catalyzed [3+ 2]-cycloaddition of azides with internal alkynes. *The Journal of organic chemistry, 71*(22), 8680-8683.

Mang, T., & Dresel, W. (2007). *Lubricants and lubrication*: John Wiley & Sons.

Marcano, D. C., Kosynkin, D. V., Berlin, J. M., Sinitskii, A., Sun, Z., Slesarev, A., . . . Tour, J. M. (2010). Improved synthesis of graphene oxide. *ACS nano, 4*(8), 4806-4814.

Mariani, G. (2003). *Selection and application of solid lubricants as friction modifiers*: CRC Press, Taylor & Francis Group.

McAllister, M. J., Li, J.-L., Adamson, D. H., Schniepp, H. C., Abdala, A. A., Liu, J., . . . Prud'homme, R. K. (2007). Single sheet functionalized graphene by oxidation and thermal expansion of graphite. *Chemistry of Materials, 19*(18), 4396-4404.

McGraw-Hill. (2005). *McGraw-Hill concise encyclopedia of physics*: McGraw-Hill Companies.

Meurant, G. (2009). *Tribology: a systems approach to the science and technology of friction, lubrication, and wear* (Vol. 1): Elsevier.

Meyer, E., Gyalog, T., Overney, R. M., & Dransfeld, K. (1998). *Nanoscience: friction and rheology on the nanometer scale*: World Scientific.

Moses, J. E., & Moorhouse, A. D. (2007). The growing applications of click chemistry. *Chemical Society Reviews, 36*(8), 1249-1262.

Namvari, M., & Namazi, H. (2014). Sweet graphene I: toward hydrophilic graphene nanosheets via click grafting alkyne-saccharides onto azide-functionalized

graphene oxide. *Carbohydrate Research, 396*, 1-8. doi:http://dx.doi.org/10.1016/j.carres.2014.06.012

Neville, A., Morina, A., Haque, T., & Voong, M. (2007). Compatibility between tribological surfaces and lubricant additives—how friction and wear reduction can be controlled by surface/lube synergies. *Tribology International, 40*(10), 1680-1695.

Niyogi, S., Bekyarova, E., Itkis, M. E., McWilliams, J. L., Hamon, M. A., & Haddon, R. C. (2006). Solution properties of graphite and graphene. *Journal of the American Chemical Society, 128*(24), 7720-7721.

Novoselov, K. S., Fal, V., Colombo, L., Gellert, P., Schwab, M., & Kim, K. (2012). A roadmap for graphene. *Nature, 490*(7419), 192-200.

Ohsol, E. O., Pinkerton, J. W., Gillespie, T. E., & Laity, T. H. (1999). Process for upgrading heavy crude oil production: Google Patents.

Olah, G. A., & Molnar, A. (2003). *Hydrocarbon chemistry*: John Wiley & Sons.

Ouyang, Q., & Okada, K. (1994). Nano-ball bearing effect of ultra-fine particles of cluster diamond. *Applied Surface Science, 78*(3), 309-313.

Park, S., An, J., Jung, I., Piner, R. D., An, S. J., Li, X., . . . Ruoff, R. S. (2009). Colloidal suspensions of highly reduced graphene oxide in a wide variety of organic solvents. *Nano letters, 9*(4), 1593-1597.

Pawlak, Z. (2003). *Tribochemistry of lubricating oils* (Vol. 45): Elsevier.

Prince, R. (1997). Base oils from petroleum *Chemistry and Technology of Lubricants* (pp. 1-33): Springer.

Ramanathan, T., Abdala, A., Stankovich, S., Dikin, D., Herrera-Alonso, M., Piner, R., . . . Ruoff, R. (2008). Functionalized graphene sheets for polymer nanocomposites. *Nature nanotechnology, 3*(6), 327-331.

Rapoport, L., Leshchinsky, V., Lvovsky, M., Lapsker, I., & Volovik, Y. (2003a). Superior tribological properties of powder materials with solid lubricant nanoparticles. *Wear, 255*. doi:10.1016/s0043-1648(03)00285-0

Rapoport, L., Leshchinsky, V., Lvovsky, M., Nepomneyashchy, O., Volovik, Y., & Tenne, R. (2002). Mechanism of friction of fullerene. *Industrial Lubrication and Tribology, 54*. doi:10.1108/00368790210431727

Rapoport, L., Leshchinsky, V., Volovik, Y., Lvovsky, M., Nepomnyashchy, O., Feldman, Y., . . . Tenne, R. (2003b). Modification of contact surfaces by fullerene-like solid lubricant nanoparticles. *Surface and Coatings Technology, 163*, 405-412.

Rasberger, M. (1997). Oxidative degradation and stabilisation of mineral oil based lubricants *Chemistry and technology of lubricants* (pp. 98-143): Springer.

Ratoi, M., Niste, V. B., Alghawel, H., Suen, Y. F., & Nelson, K. (2014). The impact of organic friction modifiers on engine oil tribofilms. *RSC Advances, 4*(9), 4278-4285.

Reeves, C. J., Menezes, P. L., Lovell, M. R., & Jen, T.-C. (2013). Tribology of solid lubricants *Tribology for Scientists and Engineers* (pp. 447-494): Springer.

Ren, P.-G., Yan, D.-X., Ji, X., Chen, T., & Li, Z.-M. (2010). Temperature dependence of graphene oxide reduced by hydrazine hydrate. *Nanotechnology, 22*(5), 055705.

Rudnick, L. R. (2009). *Lubricant additives: chemistry and applications*: CRC press.

Salavagione, H. J., Gomez, M. A., & Martínez, G. (2009). Polymeric modification of graphene through esterification of graphite oxide and poly (vinyl alcohol). *Macromolecules, 42*(17), 6331-6334.

Scholz, E. (2012). *Karl Fischer titration: determination of water*: Springer Science & Business Media.

Senatore, A., D'Agostino, V., Petrone, V., Ciambelli, P., & Sarno, M. (2013). Graphene oxide nanosheets as effective friction modifier for oil lubricant: materials, methods, and tribological results. *ISRN Tribology, 2013*.

Shaaban, A., Se, S.-M., Dimin, M. F., Juoi, J. M., Mohd Husin, M. H., & Mitan, N. M. M. (2014). Influence of heating temperature and holding time on biochars derived from rubber wood sawdust via slow pyrolysis. *Journal of Analytical and Applied Pyrolysis, 107*, 31-39. doi:http://dx.doi.org/10.1016/j.jaap.2014.01.021

Shahriary, L., & Athawale, A. A. (2014). Graphene oxide synthesized by using modified hummers approach. *IJREEE, 2*(1), 58-63.

Shen, B., Zhai, W., Chen, C., Lu, D., Wang, J., & Zheng, W. (2011). Melt blending in situ enhances the interaction between polystyrene and graphene through π–π stacking. *ACS applied materials & interfaces, 3*(8), 3103-3109.

Sofer, Z. (1984). Stable carbon isotope compositions of crude oils: application to source depositional environments and petroleum alteration. *AAPG Bulletin, 68*(1), 31-49.

Song, J., Wang, X., & Chang, C.-T. (2014). Preparation and characterization of graphene oxide. *Journal of Nanomaterials, 2014*.

Spalla, O., & Kékicheff, P. (1997). Adhesion between oxide nanoparticles: Influence of surface complexation. *Journal of colloid and interface science, 192*(1), 43-65.

Spikes, H. (2004). The history and mechanisms of ZDDP. *Tribology Letters, 17*(3), 469-489.

Spyrou, K., & Rudolf, P. (2014). An introduction to graphene. *Functionalization of graphene*, 1-20.

Stachowiak, G., & Batchelor, A. W. (2013). *Engineering tribology*: Butterworth-Heinemann.

Stankovich, S., Piner, R. D., Chen, X., Wu, N., Nguyen, S. T., & Ruoff, R. S. (2006). Stable aqueous dispersions of graphitic nanoplatelets via the reduction of exfoliated graphite oxide in the presence of poly (sodium 4-styrenesulfonate). *Journal of Materials Chemistry, 16*(2), 155-158.

Su, Y., Gong, L., & Chen, D. (2016). Dispersion stability and thermophysical properties of environmentally friendly graphite oil–based nanofluids used in machining. *Advances in Mechanical Engineering, 8*(1), 1687814015627978.

Tabor, D. (1981). Friction—the present state of our understanding. *Journal of lubrication technology, 103*(2), 169-179.

Tao, X., Jiazheng, Z., & Kang, X. (1996). The ball-bearing effect of diamond nanoparticles as an oil additive. *Journal of Physics D: Applied Physics, 29*(11), 2932.

Tarasov, S., Kolubaev, A., Belyaev, S., Lerner, M., & Tepper, F. (2002). Study of friction reduction by nanocopper additives to motor oil. *Wear, 252*(1), 63-69.

Thong, D., Hutchinson, P. A., Wincierz, C., & Schimmel, T. (2014). Viscosity modifiers *Encyclopedia of Lubricants and Lubrication* (pp. 2292-2316): Springer.

Tissot, B. P., & Welte, D. H. (2013). *Petroleum formation and occurrence*: Springer Science & Business Media.

Tour, J. M., & Kosynkin, D. V. (2012). Highly oxidized graphene oxide and methods for production thereof: Google Patents.

Truce, W. E., Birum, G., & McBee, E. (1952). Chlorination of Dimethyl Sulfide and Some of Its Derivatives with Sulfuryl Chloride and Thionyl Chloride1. *Journal of the American Chemical Society, 74*(14), 3594-3599.

Tung, S. C., & McMillan, M. L. (2004). Automotive tribology overview of current advances and challenges for the future. *Tribology International, 37*(7), 517-536.

Veca, L. M., Lu, F., Meziani, M. J., Cao, L., Zhang, P., Qi, G., . . . Sun, Y.-P. (2009). Polymer functionalization and solubilization of carbon nanosheets. *Chemical Communications*(18), 2565-2567.

Wang, H.-X., Zhou, K.-G., Xie, Y.-L., Zeng, J., Chai, N.-N., Li, J., & Zhang, H.-L. (2011). Photoactive graphene sheets prepared by "click" chemistry. *Chemical Communications, 47*(20), 5747-5749.

Wang, Z., Shirley, M. D., Meikle, S. T., Whitby, R. L. D., & Mikhalovsky, S. V. (2009). The surface acidity of acid oxidised multi-walled carbon nanotubes and the influence of in-situ generated fulvic acids on their stability in aqueous dispersions. *Carbon, 47*(1), 73-79. doi:http://dx.doi.org/10.1016/j.carbon.2008.09.038

Wintterlin, J., & Bocquet, M.-L. (2009). Graphene on metal surfaces. *Surface Science, 603*(10), 1841-1852.

Wu, P., & Fokin, V. V. (2007). Catalytic azide-alkyne cycloaddition: reactivity and applications. *Aldrichimica Acta, 40*(1), 7-17.

Wu, Y., Tsui, W., & Liu, T. (2007). Experimental analysis of tribological properties of lubricating oils with nanoparticle additives. *Wear, 262*(7), 819-825.

Xiao, L., Jia, X., Liao, L., & Liu, L. (2014). Chemical Modification of Graphene Oxide by Copper Compound. *Chem. Rapid. Communic, 2*, 2325-9906.

Yu, B., Shi, Y., Yuan, B., Liu, L., Yang, H., Tai, Q., . . . Hu, Y. (2015). Click-chemistry approach for graphene modification: effective reinforcement of UV-curable functionalized graphene/polyurethane acrylate nanocomposites. *RSC Advances, 5*(18), 13502-13506.

Zhang, L., Chen, X., Xue, P., Sun, H. H., Williams, I. D., Sharpless, K. B., . . . Jia, G. (2005). Ruthenium-catalyzed cycloaddition of alkynes and organic azides. *Journal of the American Chemical Society, 127*(46), 15998-15999.

Zhang, W., Zhou, M., Zhu, H., Tian, Y., Wang, K., Wei, J., . . . Zhang, P. (2011). Tribological properties of oleic acid-modified graphene as lubricant oil additives. *Journal of Physics D: Applied Physics, 44*(20), 205303.

Zhang, Z. J., Simionesie, D., & Schaschke, C. (2014). Graphite and hybrid nanomaterials as lubricant additives. *Lubricants, 2*(2), 44-65.

Zhao, F., Bai, Z., Fu, Y., Zhao, D., & Yan, C. (2012). Tribological properties of serpentine, La (OH) 3 and their composite particles as lubricant additives. *Wear, 288*, 72-77.

Zheng, W., Shen, B., & Zhai, W. (2013). *Surface functionalization of graphene with polymers for enhanced properties*: INTECH Open Access Publisher.

Zhu, C., Guo, S., Fang, Y., & Dong, S. (2010a). Reducing sugar: new functional molecules for the green synthesis of graphene nanosheets. *ACS nano, 4*(4), 2429-2437.

Zhu, Y., Murali, S., Cai, W., Li, X., Suk, J. W., Potts, J. R., & Ruoff, R. S. (2010b). Graphene and graphene oxide: synthesis, properties, and applications. *Advanced materials, 22*(35), 3906-3924.

LIST OF PUBLICATIONS AND PAPERS PRESENTED

ISI paper

1. **Ismail, N. A.**, & Bagheri, S. (2017). Highly oil-dispersed functionalized reduced graphene oxide nanosheets as lube oil friction modifier. Materials Science and Engineering: B, 222, 34-42.